CHALMERS
UNIVERSITY OF TECHNOLOGY

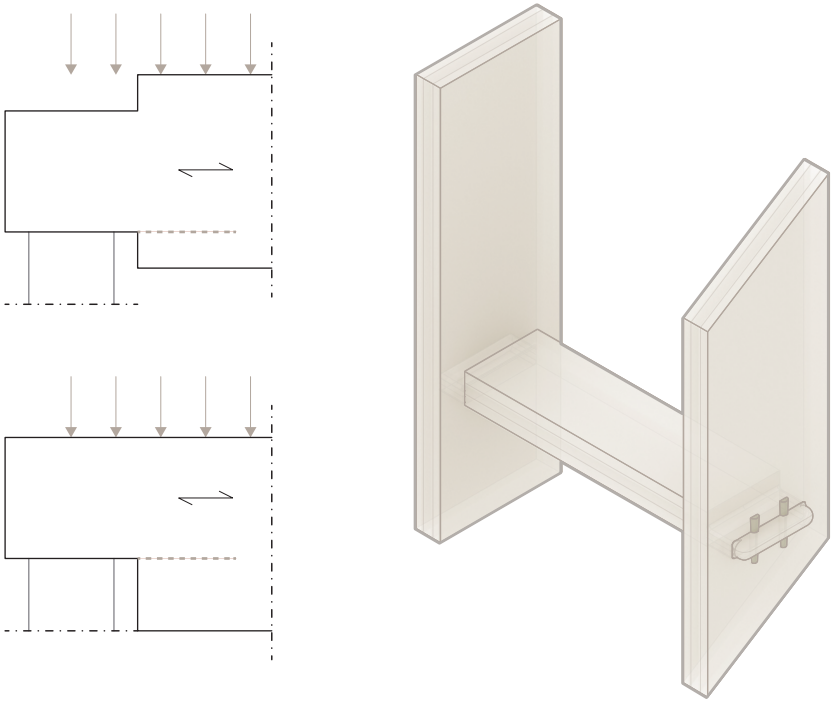

Conceptual design and development of a preliminary calculation method for wood-wood connections

Through design of two visible connections

Master's thesis in Master Program Structural Engineering and Building Technology

Sara Eidenvall & Erica Samuelsson

Department of Architecture and Civil Engineering
Chalmers University of Technology
Gothenburg, Sweden 2021
www.chalmers.se

Master's thesis ACEX30

Conceptual design and development of a preliminary calculation method for wood-wood connections

Through design of two visible connections

Sara Eidenvall
Erica Samuelsson

Department of Architecture and Civil Engineering
Division of Structural Engineering
Research Group for Light-Weight Structures
Chalmers University of Technology
Gothenburg, Sweden 2021

Conceptual design and development of a preliminary calculation method for wood-wood connections

Through design of two visible connections

Master's Thesis in the Master's Programme Structural Engineering and Building Technology

Supervisor: Robert Jockwer (CTH), Elzbieta Lukaszewska (Sweco AB) and Eric Rundqvist (Sweco AB)
Examiner: Robert Jockwer

Department of Architecture and Civil Engineering
Division of Structural Engineering
Research Group for Light-Weight Structures
Chalmers University of Technology
SE-412 96 Göteborg
Sweden
Telephone: + 46 (0)31-772 1000

Department of Architecture and Civil Engineering
Gothenburg, Sweden, 2021

Cover. *Illustration of one analysed failure mode and a resulting connection.*

Conceptual design and development of a preliminary calculation method for wood-wood connections

Through design of two visible connections

Master's thesis in the Master's Programme Structural Engineering and Building Technology

SARA EIDENVALL
ERICA SAMUELSSON

Department of Architecture and Civil Engineering
Division of Structural Engineering
Research Group for Light-Weight Structures
Chalmers University of Technology

Erica Samuelsson

Chalmers University of Technology
August 2019 - January 2021
Msc, Structural Engineering and Building Technology

Buro Happold Engineering
January 2018 - July 2018
Industrial placement

Chalmers University of Technology
January 2017 - January 2019
Msc, Architecture and Urban Design

École Nationale Supérieur d'Architecture de Lyon
August 2016 - January 2017
Msc, Architecture and Urban Design

Chalmers University of Technology
August 2013 - June 2016
Bsc in Architecture and Engineering

Sara Eidenvall

Chalmers University of Technology
August 2019 - January 2021
Msc, Structural Engineering and Building Technology

DTU - Technical University of Denmark
January 2020 - July 2020
Msc, Structural Engineering and Building Technology

Kungsbacka Municipality
Plan and Construction
May 2019 - September 2019
Internship

Sweco Architects
June 2017 - October 2017
Internship

Chalmers University of Technology
August 2015 - April 2019
Bsc in Architecture and Engineering

ABSTRACT

Timber structures get more and more common in the Swedish context of construction. With an increasing interest in new ways of building sustainably, and with structures getting a more relevant role in the visual architecture of a building, the connection of structural members hold an important role.

By constructing these connections of only wood instead of more commonly with metal screws, nails and plates, a more sustainable solution can be achieved. This also gives way for new solutions with a different architectural appearance, similar to the more traditional carpentry joints.

Despite many advantages of using these types of connections, both due to the technological progress of manufacturing and the interest due to sustainability, amongst others, they are very rarely used in a building context today. One of the main problems that cause this is the lack of information as well as the lack of calculation methods and guidelines.

Carpentry connections are today referred to as an historical connection. By designing two carpentry joints the aim is to investigate a method of design and open up the possibility of using these types of connections in a modern context.

The method is designed by a literature review of current methods for carpentry joints. Different designs are compared against each other and evaluated to specify the method for the two specific connections. By using the construction of a timber building in Borlänge the method and thesis is narrowed down to a Swedish context. The method itself is, due to this, adapted for modern construction even more by utilizing the timber engineered materials glulam and CLT, which are the structural materials used in the building.

The calculation method in the end is transformed to illustrate a more general approach. Where it can be used for more connections than the two utilized in this study. The method is a good starting point for increasing the interest in using carpentry connections as simple and tangible results can be calculated. Although for an holistic approach, and as a future step, more elements of construction need to be regarded for the connections to be fully plausible in design.

Key words:

Wooden joinery
Timber
Carpentry joints
Connections
EC5
Preliminary calculation method
Glulam
CLT (Cross-laminated timber)

INDEX

LIST OF FIGURES

LIST OF TABLES

PREFACE

In this study two carpentry connections have been designed with the intent of developing a general calculation method for carpentry joints in modern construction. The study was performed from September 2020 to January 2021.

The work has been carried out at both the Division of Structural Engineering, Department of Architecture and Civil Engineering at Chalmers University of Technology, Sweden and at Sweco AB, Structures division in Gothenburg, Sweden.

We would like to thank our three supervisors in the project. Robert Jockwer, Assistant Professor at the Division of Structural Engineering at Chalmers University of Technology and Elzbieta Lukaszewska and Eric Rundqvist at Sweco AB. Your feedback and expertise within the subject of timber construction has been greatly appreciated and this thesis would not have been possible without your guidance.

We would also like to thank AIX Arkitekter who together with Sweco AB let us use their project in Bältartäppan 7 as a reference project to carry out the study on.

Finally we would like to thank our fellow students who has helped us with reading through drafts giving us feedback during our process, with special thanks to Alexander Angrén and Ola Sjöberg.

Sara Eidenvall och Erica Samuelsson

Gothenburg, January 2021

ABBREVIATIONS

avg.	*Average*
b.c	*Boundary condition*
b.f.	*Bottom fibre*
b.n.	*Bottom notch*
b.t.	*Bottom tenon*
C1	*Connection one*
C2	*Connection two*
c	*Centred*
c-c	*Center-centered*
c.f.	*Centred fibres*
c.t.	*Central tenon*
CLT	*Cross Laminated Timber*
CNC	*Computer Numerical Control*
DT	*Dovetail joint*
EC5	*Eurocode 5*
eq.	*Equation*
LC1	*Load Combination 1*
LC2	*Load Combination 2*
l.t.	*Lower tenon*
N1, 2	*Notched joint, 1, 2*
min.	*Minimum*
max.	*Maximum*
m.f.	*Middle fibre*
n.c.	*Notch corner*
P1, 2	*TM with a peg joint, 1, 2*
PD1, 2	*Plate dovetail joints, 1, 2*
perp.	*Perpendicular*
RD1-5	*Rounded dovetail joint, 1-5*
s-s	*Side-side*
S-ZZ	*The stress on the z-face in the z-direction*
t.f.	*Top fibre*
t.n.	*Top notch*
TM	*Tenon and Mortise joint*

1. INTRODUCTION

"A structure is a constructed assembly of joints separated by members"

- McLain, 1998

THESIS BACKGROUND

Timber is an increasingly used material for the construction of buildings, both large and small. Despite its decline over the last centuries with the immersion of new materials, such as steel and concrete, and its relationship to fire, it has now taken an upswing due to its many environmental advantages and aesthetics. Architects and engineers are becoming more and more conscious of the structure of a building as something to show rather than hide which opens up the discussion of joints as both structural elements and architectural features.

For many years fire has been the main issue when using timber as a construction material and it was not until the mid 90's that laws for functional requirements in fire regulations were instituted to help increase the use of wood once more. Today, few engineers are not aware of the advantages of building with wood, as it is the only main construction material that stores the amount of CO_2 in the air during its service life. When it comes to the question of sustainability though a main issue is that of how it affects deforestation. For many countries this is an issue that needs to be evaluated, but by looking into the Swedish local context the forest industry is continuously increasing with a yearly net growth of forest mass. Therefore, by sourcing timber locally, wood as a construction material is not likely to harm the forest sustainability in Sweden *(Gustafsson et al., 2019)*.

The amount of built timber structures is increasing in Sweden as the demand and resources exists *(Trähusbarometern, 2020)*. Although, when it comes to the joining of structural members a lot of steel is still used in timber construction.

By trying to reduce this steel one can decrease the CO_2 emissions substantially since the amount of energy it takes to produce a ton of steel is 24 times as high as for a ton of wood *(Mayo, 2015)*.

When looking into the historic examples of carpentry joining, many of the ancient timber structures using these still stand today which is a perfect example of the durability of this material when cared for *(Gustafsson et al., 2019)*. There are also a few modern examples where the amount of steel in joints have been reduced to a minimum, such as the Tamedia office building in Zurich. The technological development of manufacturing is also a resource which introduces many possibilities of using new materials, such as CLT and glulam. Creating geometrical connections using for example CNC machinery is one of these advancements. For many cases though, the guidelines for connections that uses very little or no steel are very few and does not promote the use of these connections.

Today's technology and market for timber, especially in Sweden, brings a lot of possibilities and so far is not fully utilized. By embracing the old ways of carpentry jointing in a modern way and clarifying preliminary calculation methods, these resources can be used in a way to promote building in wood even further.

THESIS QUESTION

How can a modern carpentry design approach be developed?

How can a preliminary calculation method be designed for carpentry joints?

How can this be adapted for glulam and CLT?

AIM AND OBJECTIVES

The aim of this master thesis is to present a possible preliminary calculation method for timber joints only made of wood. This is made to elevate the living and renewable material of wood and hopefully increase the use of these types of carpentry connections within construction.

Some of the objectives to be able to fulfil this aim are:

- Compiling a resource library of possible carpentry joint techniques.
- Compile design proposals for two wood-wood connections.
- Investigate the important failure modes of the calculation method through the use of simple FE-models.
- Propose a preliminary calculation method for these designed connections by investigating existing calculation methods.
- Discussing future features of the design of carpentry connections apart from the calculations, to fulfil a holistic view of the design.

DELIMITATIONS

How to structurally solve two visible wood-wood connections for the ongoing project in Borlänge, is the main focus in this project. The structural aspects are limited for the load cases and initial stresses for the chosen design proposals. The calculation method will be created for the designed connections and similar connections for future work. The live load is specifically designed for the building's purpose. Wind loads are based on the location, Borlänge.

The characteristics of moisture, acoustic and fire are certainly important and must be further described and examined in a next research step to meet all demands and requirements. These factors will be briefly mentioned, how they affect the connection design in general, and to some extent the designed connections, but will not particularly be part of this study nor calculated.

METHOD

GENERAL

The main method of the thesis is to design two wood-wood connections for an office building in Borlänge. This will be done first with a research step of historical ways of solving these types of connections. This will also include modern ways of solving these as well as research into methods of manufacturing and calculations. The second part of the thesis is the design phase and the development of a preliminary calculation method that will go hand-in-hand as the design will work as a basis for the calculation method and the method will work as a process step in iterating the design solutions. The preliminary design will be evaluated in simple FE-models to distinguish important failure modes of the design before finally designing the general calculation method.

RESEARCH

The research phase include mainly the research of historical carpentry connections as references for the design. It also includes some references of contemporary projects where carpentry joints have been used as a support for the design as well as the background of the thesis question. Other relevant parts of the research is the information on modern timber connections that normally use steel reinforcement or connectors as well as research into how the built structure is influenced by the wood-wood connections with regards to moisture, fire and acoustics.

DESIGN PHASE

Preliminary design of the connections are developed by using references and by sketches of the design. The iterations of the designs are preliminary made by evaluating how reasonable they are and their grading with regards to certain factors. From this grading two types of designs from each connection is brought into the next phase of developing a preliminary calculation method.

ANALYSIS

In this phase the designed connections are analysed in simple FE-models in Abaqus in order to identify possible failure modes. In this analysis minor modifications are made to the designs (to create several options for one connection type) in order to investigate the influence of geometry as well.

PRELIMINARY CALCULATION METHOD

From the literary review and the analysis the general calculation method is developed. The method is then used in order to analyse the chosen connections in a final step.

CHOICE OF PRELIMINARY DESIGN

As a final design step prototypes are made of some selected connections to identify possible weaknesses of the connections beside the structural verifications. Together with these and results from calculations two different solutions are selected for the preliminary design of each connection.

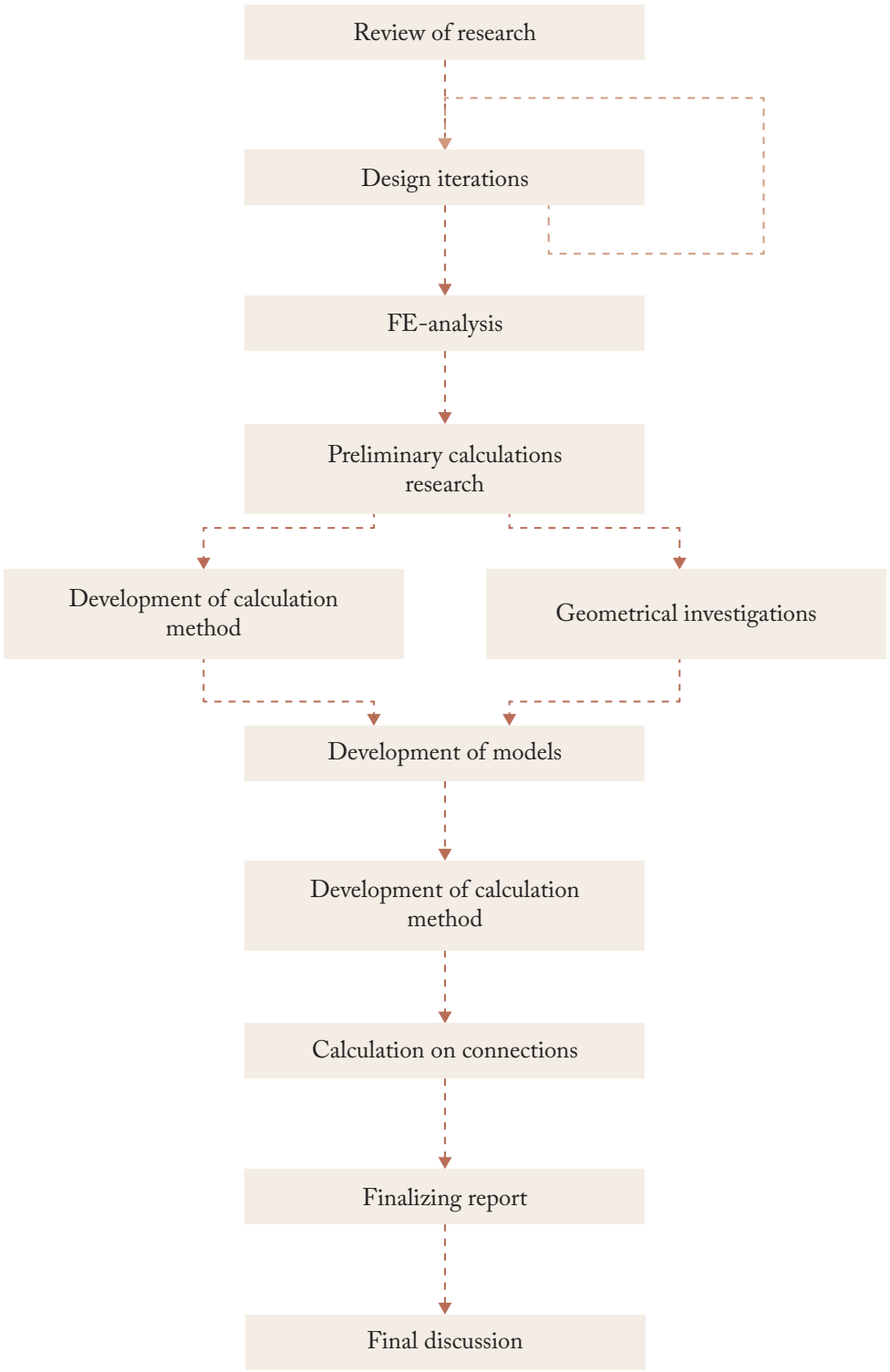

Figure 1.1. *Illustrative scheme of project method.*

READING INSTRUCTIONS

With regard to references and chapter numbering Chapter 6 which is the preliminary calculation method has its own index and numbering to be able to stand on its own outside of this report. For all references outside of Chapter 6 that refer to a chapter or equation stated within Chapter 6 will be explicitly put. The same works for referencing inside Chapter 6 to other parts of the report. The reference will then mention the report. If nothing explicit is mentioned the reference is to the same part as one is in. For example:

Reading in Chapter 5:
- The text refers to "eq. (5)" → eq. is found in the report.
- The text refers to "eq. (5) in the general calculation method" → eq. is found in Chapter 6.

Reading in Chapter 6:
- The text refers to "Chapter 5.2" → Chapter is found in Chapter 6.
- The text refers to "Chapter R.5.2" → Chapter is found in Chapter 5 in the report.

Regarding page numbering, Chapter 6 also includes an internal page numbering in order to be able to stand on its own outside of the report. The internal page numbering is illustrated in black and the corresponding report page numbering on the same page in round brackets and grey, as illustrated below.

	(Report nr.)	Internal page nr.
Ex.		
	(58)	3

2. PROJECT BACKGROUND

In this chapter the project utilized in the thesis is presented briefly together with the chosen connections. The connections are presented with their location in the building, their loads, materials and data that is needed for the preliminary calculation method.

PROJECT BACKGROUND

CONTEXT

Sweco AB are currently planning and designing the structural system for an ongoing project based in Borlänge. They are working together with the architectural office AIX Arkitekter. The project is called Bältartäppan 7 (BT7) and consists of residences and offices divided into three volumes A, B and C as seen in the situation layout plan in Figure 2.1.

FOCUS

The challenge is to focus on two visible connections in the open and public areas. This is also made with a goal that the design solution of the connection should display that the connection is only made out of wood. This was decided with the intent to market the possibility of these type of connections as an architectural element as well as functional.

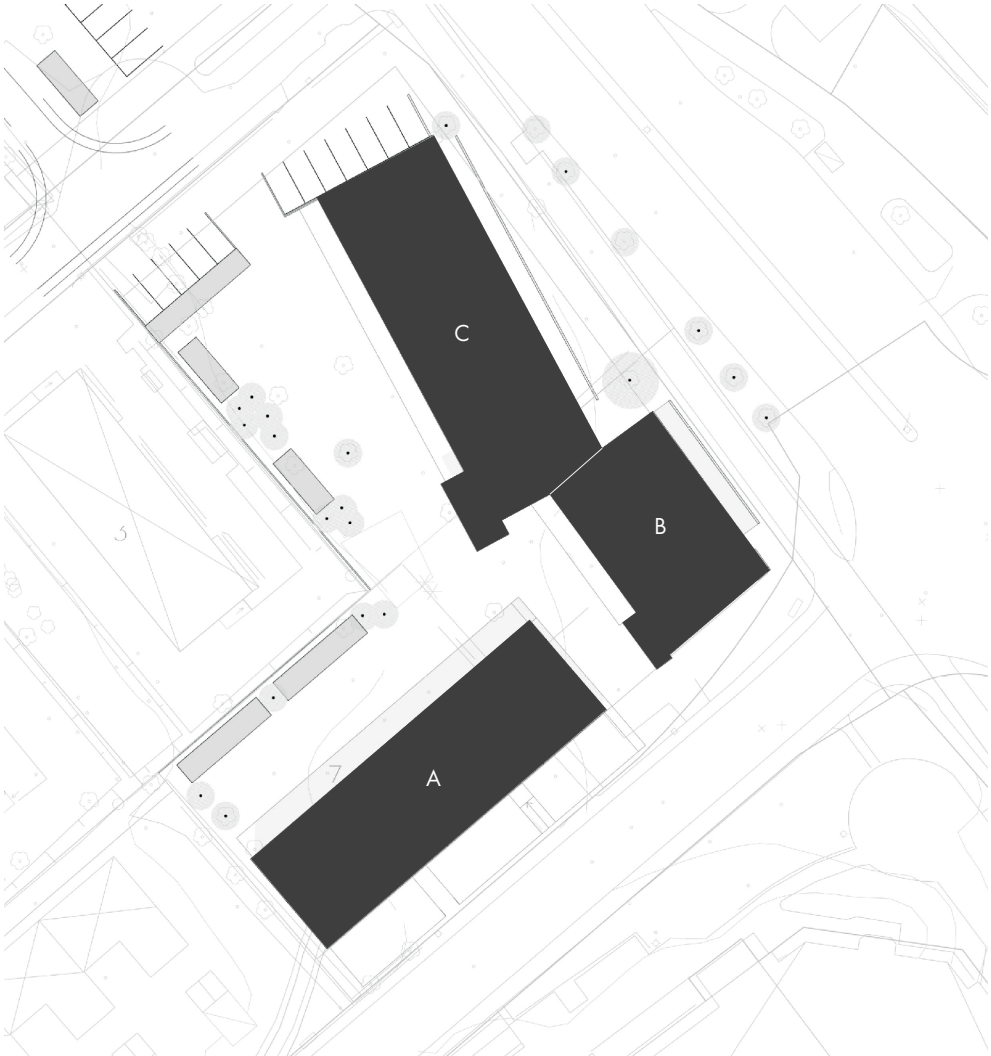

Figure 2.1. *Situation plan, scale 1:500 with building index (Drawing credit: AIX Arkitekter).*

Figure 2.2. *Floor plan, Level 1, Building B and C, Scale 1:400 (Drawing credit: AIX Arkitekter).*

The location of the two selected connection locations can mainly be seen in building complex B and C in the entrance halls, as marked red in Figure 2.2.

CONNECTION ONE, C1

The first connection, *C1*, investigated is a glulam – glulam connection between a beam attached sideways to a pillar. These are the load-bearing slats inside the glass panes of the entrance halls of building B and C as seen in Figure 2.2. The horizontal slats are inserted at different heights in every other pillar opening. This makes the assembly easier as the joists can be attached

to the pillar from the outside.

An illustration of how the beams are connected to the glulam pillars and in relation to the rest of the building can be seen in Figure 2.3 and a zoomed in illustration of the connection can be seen in Figure 2.4.

GEOMETRY

The base cross-section for the glulam can be seen in Table 2.1.

The geometry used for calculating the load is the approximate geometry of building B, these values can be seen in Table 2.1 and their referred locations can be seen in Figure 2.2.

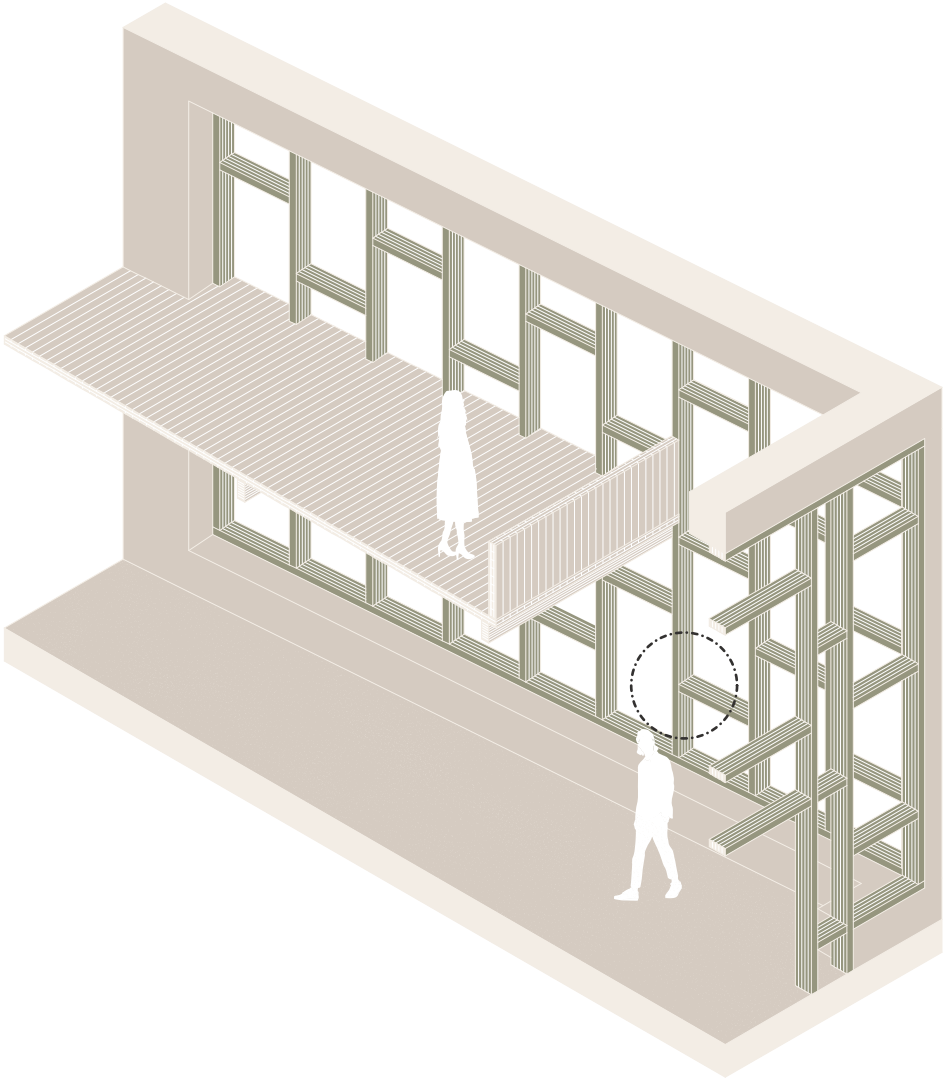

Figure 2.3. *Illustration of window geometry for connection, C1.*

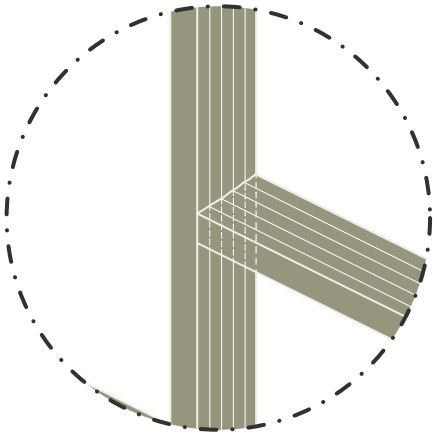

Figure 2.4. *Zoomed in illustration of location for C1.*

Table 2.1. *Geometry C1.*

Variable (relevance)	Value
Height (wind load)	11.5 m
Width Volume B	13.7 m
Length Volume B	21.4 m
Width, beam and pillar	90 mm
Depth, beam and pillar	225 mm
$cc_{distance}$, pillars	1000 mm
$cc_{distance}$, beams	1780 mm
l_D (wind load)	≈ 2.76 m
l_E (wind load)	≈ 2.23 m

LOADS

The window slats used for the calculation of the loads are the slats on the short side of the facade. As this is a load bearing wall it is assumed to have the most critical loads.

It is assumed that the full load on the outer walls are divided 50% - 50% between the two load bearing walls of the entrance. The load division and load bearing walls are marked in Figure 2.5.

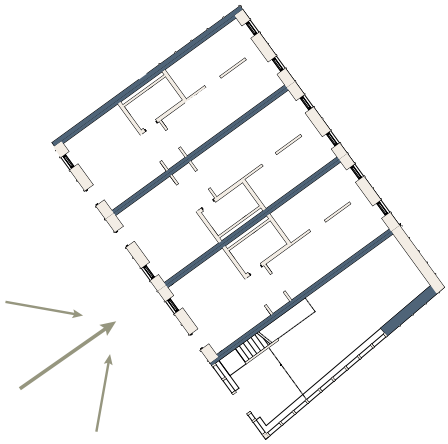

Figure 2.5. *Illustration of main wind load direction and load-bearing walls (Drawing Credit AIX Arkitekter).*

Some of the loads are received from Sweco AB. Both the calculated loads and given loads can be seen in Table 2.2. The full load calculations for connection 1, *C1*, and connection 2, *C2*, can be seen in Appendix B.

Table 2.2. *Loads C1.*

Load	Value
Self-weight glulam	4.3 kN/m^3
In-plane wind load	2.44 kN/m
Out-of-plane wind load	-1.09 kN/m^2

MATERIAL

The material used in this connection is glulam and the material class is chosen as GL30c with material values according to Gustafsson et al. *(2019)*.

CONNECTION TWO, C2

The second connection is the joint between the step of the stair and the railing. Both members are made from CLT. This type of stair can be seen in building B and C as seen in Figure 2.2, but also in building A. An illustration of the connection area can be seen in Figure 2.6 and a zoomed in illustration in Figure 2.7.

GEOMETRY

The base cross-section of the CLT is assumed to be a 3-layer CLT plate and the thickness and layer thickness is decided on based on the selection from Martinsons *(2020)*. The thickness's and other geometrical data used can be seen in Table 2.3.

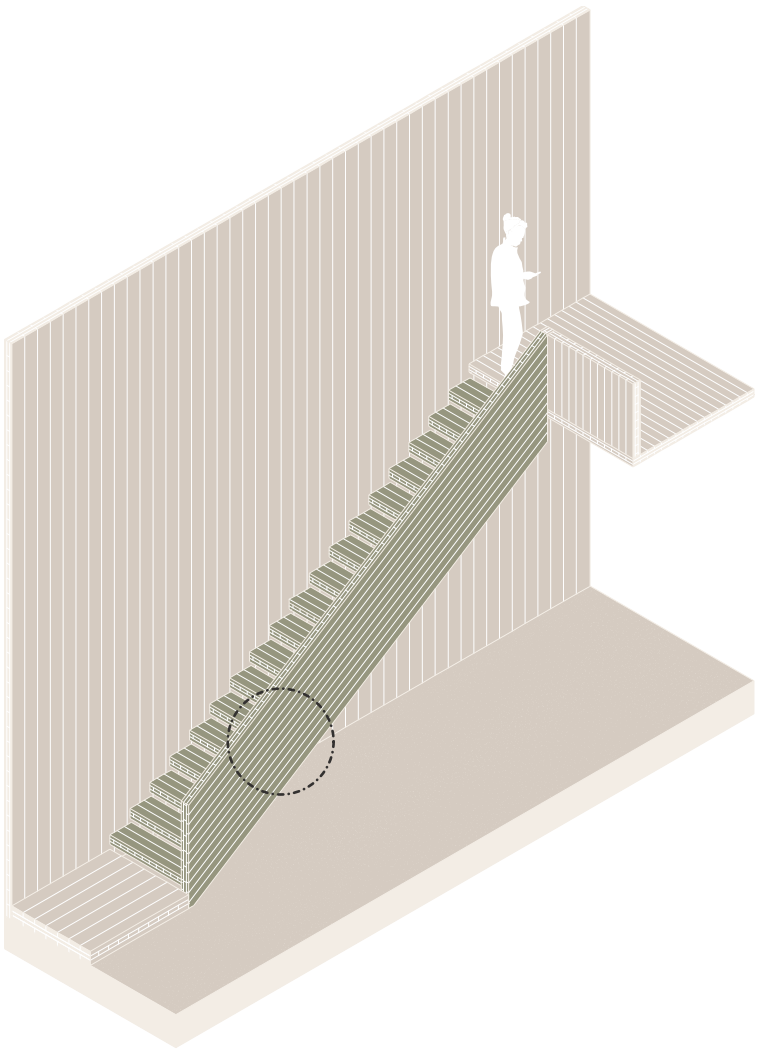

Figure 2.6. *Illustration of stair geometry.*

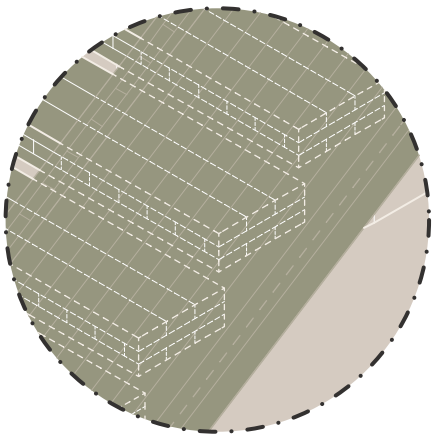

Figure 2.7. *Zoomed in illustration of location for C2.*

Table 2.3. *Geometry C2.*

Variable	Value
Thickness Step	120 mm (40+40+40)
Thickness Railing	100 mm (30+40+30)
Length, step	1000 mm
Depth, step	300 mm

LOADS

Any loads that might act on the railing are excluded from the calculations. The railing is assumed stiff enough and the connection is through this put more in focus in the calculations. The loads acting on the step is self-weight of the CLT and imposed loads taken from Swedish Standards Institute [SIS] *(2008)*. These can be seen in Table 2.4.

Table 2.4. *Loads C2.*

Load	Value
Imposed Point load	2 kN
Imposed horizontal load	0.5 kN/m
Self weight, CLT	4.5 kN/m^3

MATERIAL

The material used in this connection is cross laminated timber with internal strength classes given from Martinsons *(2020)* for the chosen thickness.

3. REVIEW OF RESEARCH

Timber has been used in construction for a very long time and whilst newer materials, such as concrete and steel, has many structural advantages it is important to remember that timber does too. This will be presented shortly in this chapter as an introduction to the thesis question and background for the design of connections.

WOOD AS A MATERIAL

BUILDING WITH WOOD

Timber as a construction material has been given an upswing in the past decade due to mainly its environmental impact. It is our belief that this increased the positive view on using timber as an architectural element as well. Timber is the only renewable building material so far with the advantage of storing CO_2 during its service life.

A great advantage of timber products is its weight-to-strength ratio which is very low in comparison to other materials. With further development of engineered timber products it is possible to incorporate timber in larger and larger projects where it is not yet possible today.

When it comes to timber in building most failures are caused in the connections which is therefore one of the most important aspects to consider in timber design. There are many advantages in doing these connections of solely wood when it comes to for example moisture, fire and acoustics which is described more further on.

Still, the European design standard rules gives very little guidance to design of carpentry joints and only about 20 % of the current Eurocode 5, *EC5*, is about connections *(Sandhaas, 2018)*. This is why the main focus of this thesis, to develop a calculation method, has arisen.

ENGINEERED TIMBER PRODUCTS

Many attempts are ongoing today with trying to minimize the orthotropic qualities that makes timber a difficult material to handle construction wise. The second goal of these attempts are to be able to create timber products not limited in size by the log itself.

Glulam

Glulam is a material built up of board lamellae with the grain oriented in the same direction for all boards. The main structural qualities of this is the freedom in dimensions and that using smaller timber pieces reduces the likeliness of defects such as knots.

Cross laminated timber

CLT is, as glulam, built up of boards but where every other layer of boards is oriented across from the one before, hence "cross-lamination". This greatly minimizes the effect on moisture movements which is a difficulty in timber construction.

MODERN MANUFACTURING

A main advantage of today's fast technological advancement is the increasing number of production methods when it comes to building materials.

With regard to carpentry joints the robotic technology increases the possibility of using these type of designs, as the manufacturing no longer need to be done by hand. By the use of a five-axis CNC (Computer Numerical Control) machine, for example, both the angle and direction of cutting and drilling as well as the cutting tool itself can be controlled.

The interaction between the design, which is today mainly done in a computer, and the manufacturing increases the accuracy of production and reduces production errors. When also taking into account the possibility of assembling a structure automatically also this step of the production can eliminate errors by fast assembly and precise positioning in the future (*Dedijer, 2016*).

WOOD ANATOMY

When it comes to the structure of wood there are two vital distinctions of types. This is softwood and hardwood. Softwood generally comes from conifer trees like spruce or pine. These are trees that grow faster than hardwood trees and therefore tend to be less dense. Hardwood is derived from deciduous trees such as ash, beech, birch and oak *(Middleton & Middleton, 2020)*. Figure 3.1 illustrates the different wood types.

Softwood is generally used as a main structural material due to its faster growth and its lighter weight. Hardwood is a good material to use in minor connections because it is a more homogeneous material and has a higher compression capacity both parallel and perpendicular to the grain.

MOISTURE, FIRE AND ACOUSTICS

These three properties are vital for the design of timber structures. They will be taken into consideration mainly in discussion in this thesis.

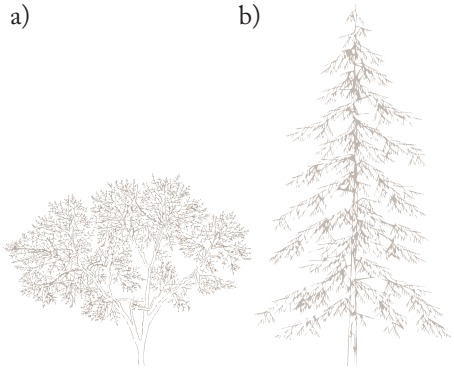

Figure 3.1. *Illustration of trees* a. *deciduous,* b. *coniferous.*

Moisture

Wood's moisture content regulates quite a lot of the other properties of the material. This becomes especially clear when the material goes below its fibre saturation point. With an increasing moisture content the stiffness and strength decrease *(Blaß & Sandhaas, 2017)*. Table 3.1 shows the impact on the mechanical properties with a changing moisture content level.

With regards to designing connections in solely wood this might give an advantage in that the whole connection deforms with a changing moisture content instead of just the main timber members when for example steel is used within the connection. This hypothesis would require more investigation though, as it is very dependant on the grain direction of the concerning members as is visible in Table 3.1.

Fire

Historically fire has always been a main problem for timber constructions and has discouraged many from using wood in this purpose.

Whether a fire develops or subsides depends on the heat generation during a current fire situation. If a fire is set on a visible wooden surface the combustion will proceed in constant speed inwards the material. Due to a covered layer of carbon on the surface the penetration is slow usually about 0.6 – 1.1 mm/minute. Through this the carbon layer wood protects itself and its inner parts and works as a heating-insulation. It counteracts the heat flow to the pyrolysis zone and is a favourable property of the wood. The fire penetration zones can be seen in Figure 3.2.

Table 3.1. *Change in the properties with a one percent change in wood moisture. The benchmark figure is the properties at a moisture content of 12 % (Blaß & Sandhaas, 2017).*

Property	Change (%)
Compression || to the grain	6
Compression ⊥ to the grain	5
Bending strength	4
Tension || to the grain	2.5
Tension to ⊥ the grain	2
Shear	2.5
E-modulus || to the grain	1.5

Metallic fasteners such as nails, screws and steel dowels increase the burning and make connections the most critical part when considering fire for buildings. An efficient way to obtain fire protection in the connections when steel embraces the timber elements, is to cover it with either wood dowels, wood wedges or glulam or plywood board. Therefore, excluding steel components in the connections entirely with the use of carpentry connections would be of great advantage to the fire protection of a construction *(Crocetti et al., 2016)*.

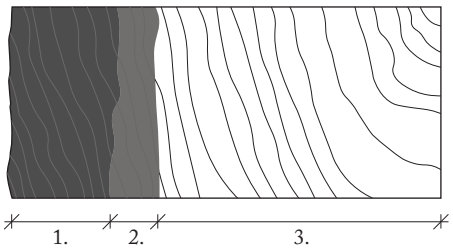

1. Charred wood, *the surface cracks and erodes.*
2. Pyrolysis zone
3. Unaffected wood

Figure 3.2. *Phenomenon of the charring process and fire penetration zones of wood.*

Acoustics

At an early stage, sound and sound insulation should be considered in the construction process. Sound will move through any cavities and connections are therefore especially important with regard to acoustics. By using timber connections that are properly manufactured difficulties in connections can be minimized as the timber geometries are closely assembled with no gaps. With regard to carpentry connections these might face a problem as they generally remove and cut more holes in the involved members, than a normal steel nail connection for example, therefore this is an important aspect to look into in further studies.

DESIGN OF CONNECTIONS

TYPES OF JOINTS

Timber joints affect the constructive behaviour of the elements by, for example, contributing moment resisting joints or hinged attachments and have to be joined together to function as a system. Two main types of joints can be distinguished depending on their working principle, either by transmitting the forces through a contact area or by transmitting the forces by a mechanical connector.

Joints can be divided into glued joints, carpentry joints and joints using various metal fasteners. In contemporary timber structures the most common connections are produced with steel plates and laterally loaded metal dowel-type fasteners. The ease of design, production, and assembly, as well as their high load-carrying capacity and ductility are advantages of these connections *(Palma et al. 2016)*. The following chapter will go through the most common traditional contact joints and their advantages in design.

TRADITIONAL WOODEN JOINERY AND LIBRARY OF CONNECTIONS

Traditional wooden joinery has a lot of interesting features that, with modern dowel type and metal reinforced joints, has disappeared from the profession today *(Branco, 2015)*. With modern manufacturing techniques, the possibility of bringing back these traditional joinery methods has increased, since the manufacturing is no longer a handmade issue. Important to try and incorporate in this thesis is the idea of these traditional joints but with modern manufacturing techniques and contemporary timber materials.

Traditional carpentry joints can be categorized into four different categories. These are *"Tenon and mortise joints"*, *"Lap joints"*, *"Notched joints"* and *"Scarf joints" (Branco, 2015)*.

The next paragraphs show some of the most common traditional wooden joints related to this thesis and a short description of their main features.

Below, a short summary of the main features of the category of tenon and mortise joints and notched joints are shown as well as images of some examples of such joints. More examples for each joint type can be seen in Appendix A1.

Tenon and mortise joints

The tenon and mortise joints normally connect members to form an "L" or "T" configuration. The two components consist of the tenon tongue and the mortise hole *(Branco, 2015)*. They can be locked by wedges or pinned into place and the connection can include shoulders to stabilize as well as different shapes of the tenon, such as rectangular or dovetail.

A few examples of such joints can be seen in Figure 3.3-3.5. A structural advantage is that they can generally take forces in many different directions due to the locking mechanisms. These could preferably be made of hardwood.

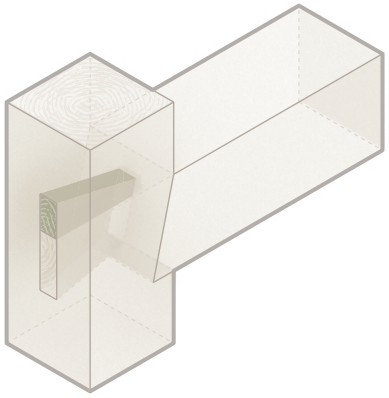

Figure 3.3. *Wedged dovetail joint with a half-shoulder.*

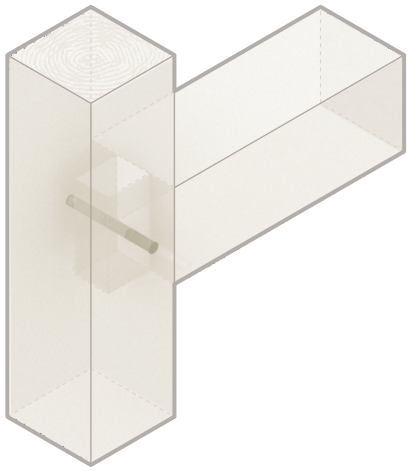

Figure 3.4. *Pinned tenon and mortise joint.*

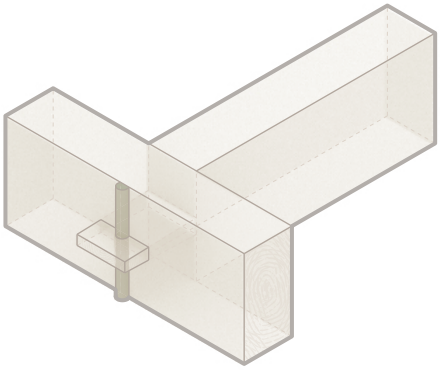

Figure 3.5. *Reverse dovetail through, pinned tenon and mortise joint.*

Notched joints

In order for this type of joint to work they need appropriate joinery at multiple locations for example tenons or pegs and pins. A notch is a V shaped groove most commonly cut perpendicular from the beam *(Branco, 2015)* as seen in Figure 3.6. The joints shown below can more commonly be rounded or notched out with a diagonal to reduce the number of sharp corners and the stress extremes in these points. Structurally a notch, similar to a tenon, can help hold two members in place whilst they are locked together with a peg or wedge. It prevents both rotation and translation.

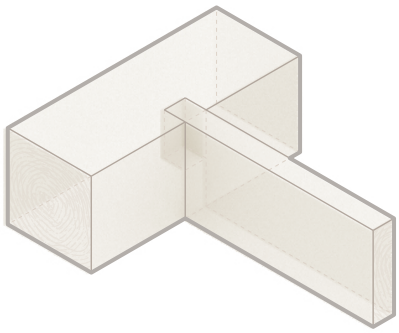

Figure 3.6. *Notched joint.*

The following two sections describe some common solutions for the two connections treated in this thesis. The goal is to create carpentry connections that are able to transfer the forces as these common connections show.

C1: GLULAM - GLULAM

To attach glulam frames of horizontal and vertical elements in front of a glass facade the same solution as for connecting beams and columns can be used. The connections in Figure 3.7 are designed so the compression of the beam is transmitted to the column by contact pressure between the end of the beam and the column. This type of joint is dimensioned on the basis that the beam's transverse force and normal force are transmitted by the wood screws, which are subjected to shear and tension.

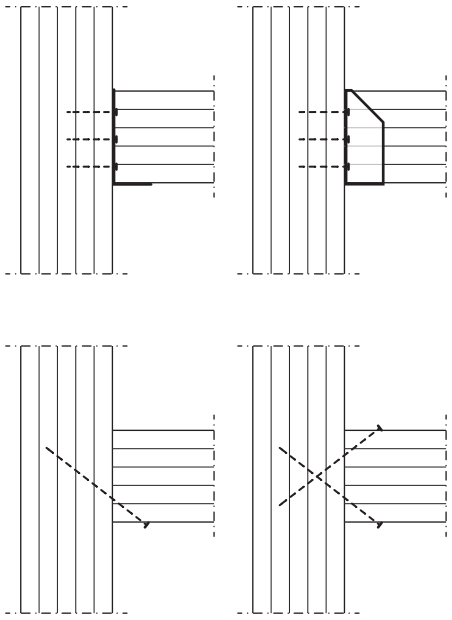

Figure 3.7. *Standard connections for glulam.*

C2: CLT - CLT

Long self-drilling wood-screws are today the most standard solution for connecting CLT members. This is seen in Figure 3.8a. This is done by placing the horizontal CLT plate on top of the vertical one. This helps transfer the vertical forces and reduces the shear forces that occurs in the connection as seen in Figure 3.8d. Figure 3.8b. shows how the same components can be joined using angle brackets or nail plate angles. Generally larger transverse forces can be taken, compared to merely screwing. Another, alternative is slotted fittings in Figure 3.8c. These reduce the visibility of the connecting parts.

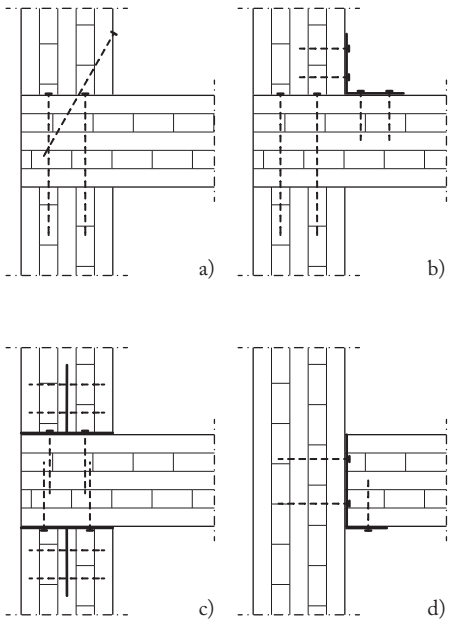

Figure 3.8a-d. *Standard connections for CLT members.*

REFERENCE PROJECTS

The following section includes a couple of reference projects to support the discourse of this thesis. These projects use both carpentry connections, computer controlled manufacturing and engineered timber materials.

VIDY THEATRE

Vidy Theatre is a timber pavilion in Lausanne, Switzerland. The structural support is completely made of double-layered timber folded plates. This holds its mechanical performance from the stiffness of its joints in a span of 20 m. The connections are double through tenon joints. Some metal connectors are used but have been greatly reduced by these connections. The tenon connections and structure can be seen in Figure 3.9a-b.

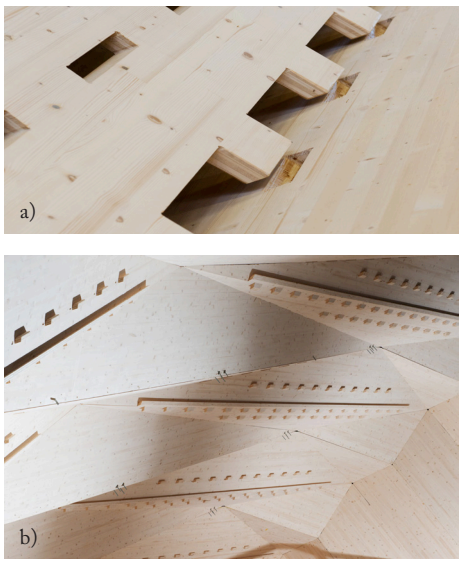

Figure 3.9a. *Structure details of Vidy Theater (EPFL, 2020)* b. *Assembly the roof to the building (EPFL, 2020).*

TAMEDIA OFFICE BUILDING

Tamedia office building is one of the most well known contemporary structures that uses carpentry joints. It was the first 7-storey timber construction in Switzerland so it is both known for its daring size and techniques. The free form connections hold a special hardwood filling that is precisely CNC milled *(Blumer-Lehmann, 2021)*. The beams and pillars are produced of glulam elements and can be seen in Figure 3.10.

Figure 3.10. *Structure of the Tamedia Office Building (Shigeru Ban Architects, 2014)*

SWG PRODUCTION HALL

The SWG production hall is another example of a timber construction that, to some extent, uses carpentry connections. The hall's most outstanding part is the highly stressed central joint. It involves notches which absorb and transmit large forces down to the ground from the 40 meters long roof trusses on both sides. This connection is illustrated in Figure 3.11. An advancement in this construction is that it mainly uses hardwood in its construction which made it possible to design very slender cross-sections.

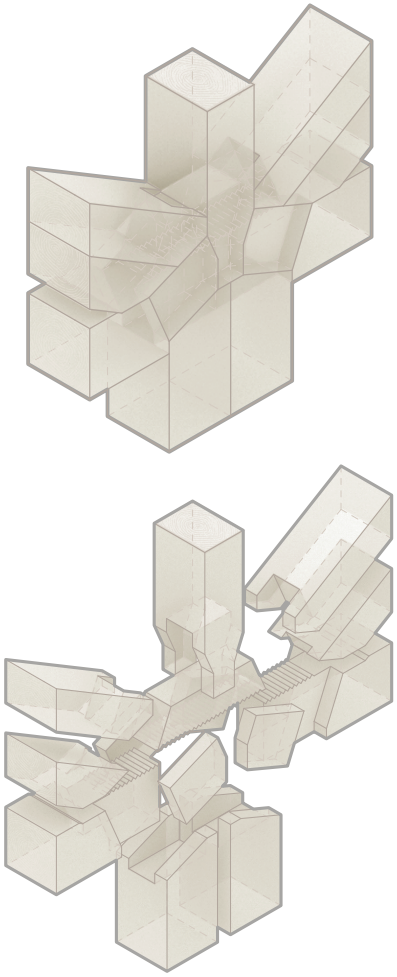

Figure 3.11. *Illustrations of the "Puzzle Connection" and carpentry joint in the framework system.*

X-FIX

X-fix is a produced timber-to-timber coupling system for joining CLT elements. This system is patented and proof that construction, at least CLT constructions, with only carpentry connections is feasible.

This system contains of two pieces of LVL with a double dovetail as can be seen in Figure 3.12. It is simple to assemble where the only on-site tool needed is a hammer *(X-fix, 2021)*.

Figure 3.12. *Two dovetail-shaped and tapered coupling strips, X-fix L (X-fix, 2021).*

TRADITIONAL CARPENTRY JOINTS IN SWEDEN

The pictures in Figure 3.12 show some simple traditional carpentry joints from Pelarne Church in Småland. This church which is believed to have been built in the 13th century still stands today showing both the durability of the carpentry joints as well as the tradition of constructing in timber in Sweden. The church's construction consist of a combination of tenon and mortise, notched and peg joints.

CHAPTER CONCLUSION

What is brought into the next phase of design is the library of historical connections. This will be a relevant starting point in the design. The implementations of carpentry joints in the reference projects are relevant to bring into a discussion in a later stage as a description of how the designed connections could be applied on larger construction parts and in more complex ways. The research about manufacturing and moisture, fire and acoustics is also a relevant discussion subject and are used in a later stage to grade the designed connections based on a few criteria. This is described more in Chapter 4.

Figure 3.13. *Connections Pelarne Church in Småland.*

4. ARCHITECTURAL DESIGN

Throughout this chapter the architectural design process from an early stage to the investigation phase (where the types will be studied as FE-models) will be shown for the two visible wood-wood connections.

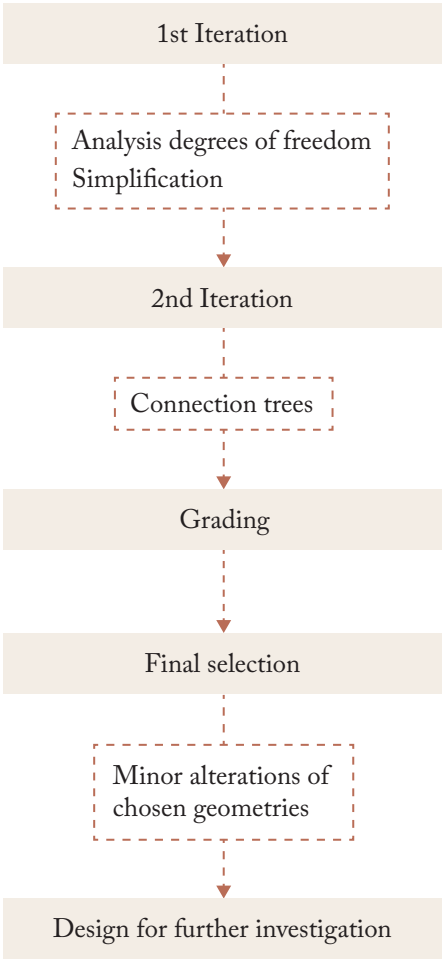

Figure 4.1. *Process illustration for the Architectural design.*

Figure 4.1 shows a more detailed illustration of the general development of the connections and of what is described in this chapter. Figure 4.2 illustrates the location for the two connections C1 and C2. For more detail into this, see Chapter 2.

FIRST ITERATION

A library was gathered of traditional carpentry connections in the research and listed into four main joint categories, Tenon and Mortise, Lap, Notched and Scarfed joints. This library introduce essential possibilities of what wood-wood connections can look like. By combining the historical connections from this library with ideas for the specific two connections in this project, different suggestions were implemented in schematic tables. These connection types were divided into degrees of freedom. In this phase both applicable and less applicable varieties are considered to keep the design open and to keep an easy comparison with the different degrees of freedom. The tables including these are shown in Appendix A2.

a)

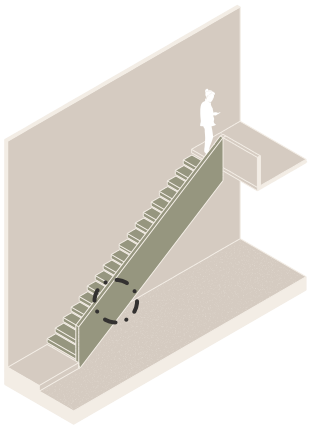

b)

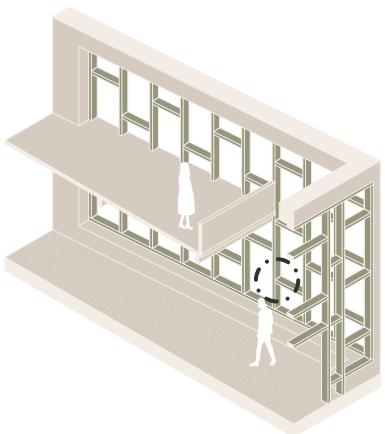

Figure 4.2a. *Location for C1.* b. *Location for C2.*

C1

Figure 4.3 show design examples that failed for their complex design and lack of functionality. The first can rotate thanks to a circular geometry and the circular hole in the plate inside of the pillar. A dowel connects the beam to the column. The second is characterized by its puzzle-components, where the first component consist of a dovetail inserted in the column, then a cut-out component connects the two elements and lastly two wedges which keep the beam in place. This connection is set as rigid, hence no arrows. The third consists of a cube with a dovetail, inserted from the side into the pillar which is not a reasonable geometry due to the high possibility of movement as indicated.

Alternatives which managed to solve the connection demands and at the same time represent simple and smart solutions continued on as interesting alternatives. Three examples of these are shown in Figure 4.4.

C2

All dynamic solutions were removed as this did not seem to be a likely connection solution for a staircase. Nor the solution with a single pin insertion which can rotate was reasonable as a stair step. Some examples of these solutions can be seen in Figure 4.5. A slight modification to this which could work instead would be to have two pins instead of one. These were all designed in this iteration but removed in the second iteration two.

After this first iteration the step height was also increased which rendered a few of the previous solutions unnecessary and to intricate for the next step.

The solid arrows explain the possible translations and the dashed grey arrows together with a solid red the possible rotations for the next coming figures.

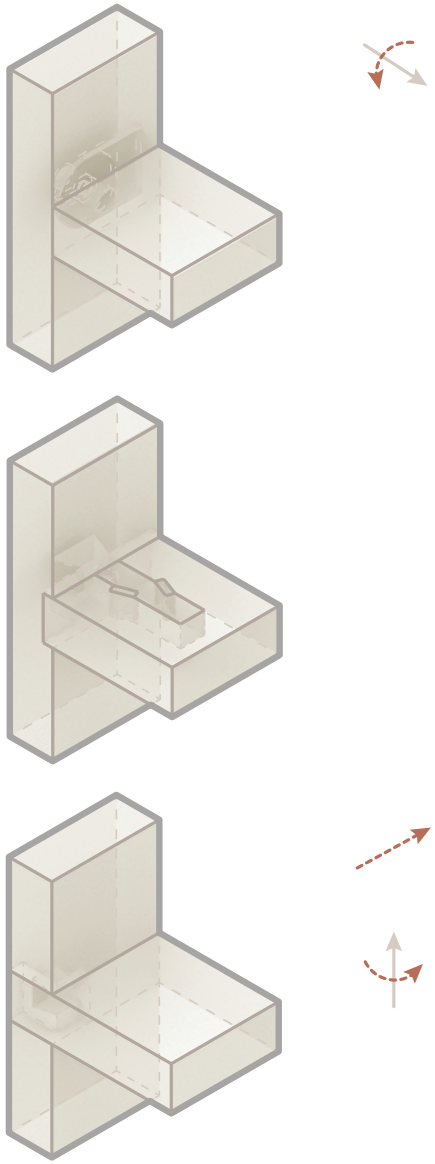

Figure 4.3. *Examples of excluded connections for C1 after the first iteration.*

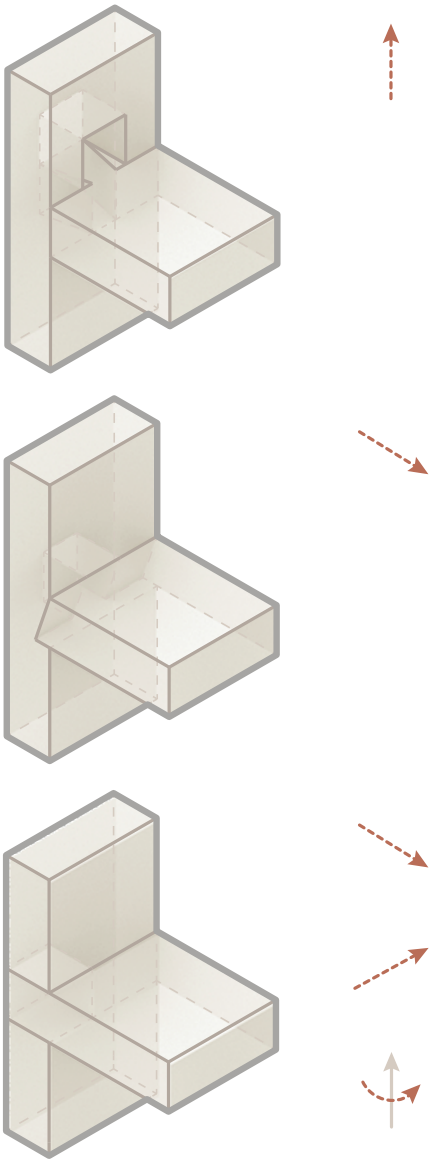

Figure 4.4. *Examples of some continued interesting alternatives for C1 after the first iteration.*

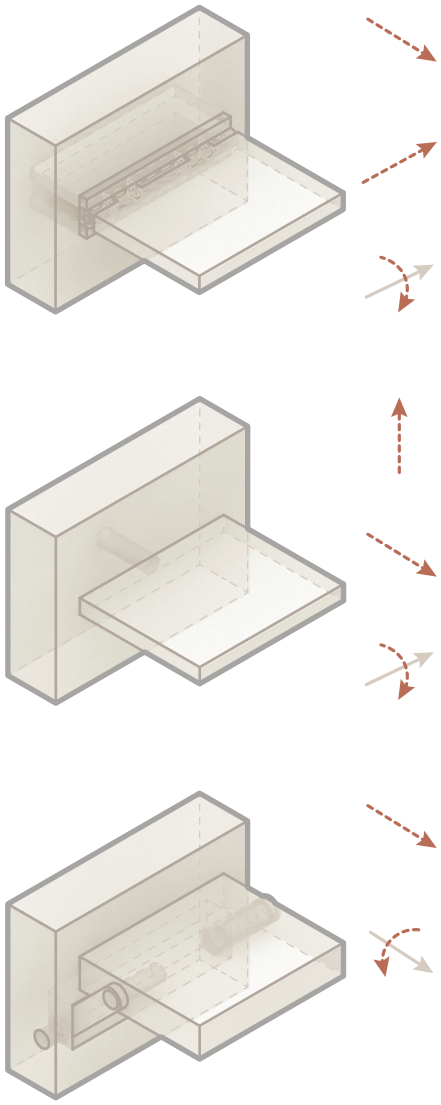

Figure 4.5. *Examples of excluded alternatives for C2 after the first iteration.*

For full tables of design proposals after the first iteration see Appendix A2.

Some of the remaining proposals for C2 can be seen in Figure 4.6. These seemed reasonable enough to be moved into the next iteration step.

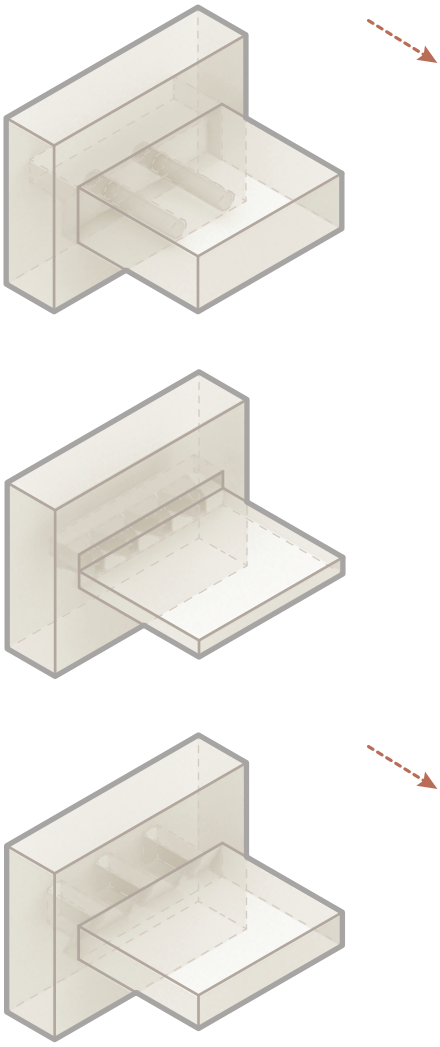

Figure 4.6. *Examples of some continued interesting alternatives for C2 after the first iteration.*

SECOND ITERATION

In the second iteration the connections are simplified as much as possible to, in step-by-step, add new more advanced features of the connections. Different examples were grouped into categories due to the insertion method, the joints geometry and position. Small advancements and differences of the connections were then made in a group from simple to more sophisticated design. This is found in Appendix A3.

This was done as a first step to categorize the connections and to not get too many extremely different solutions. This is also in order to be able to compare them more easily in the next step.

C1

A division of groups were named "Centred Insertion" with subclasses of rectangular and dovetail cross-sections. "Side insertion" is the other main group where the inserted part is visibly connected from the side of the pillar. An example of this is presented in Figure 4.7, where a rectangular cube is developed by adding cuts, amount of elements and insertion depth.

C2

The connections for C2 were divided into three different groups. The first one, “Full cross-section”, where the full cross-section of the step is inserted in the supporting CLT railing. The second, “Part cross-section”, where more tenon and mortise like connections are used. The last is “Dovetail tenon”, similar to a tenon and mortise joint but where the tenon includes a slanting of its edges to create a dovetail. In Figure 4.8 the tree structure of the part cross-section is shown as an example.

EVALUATION

The last step before finalising the chosen designs is an evaluation of the connections based on several criteria. These are designed to be as easily measurable as possible for a clear comparison of the qualities of each connection design.

CENTERED INSERTION

Part cross-section

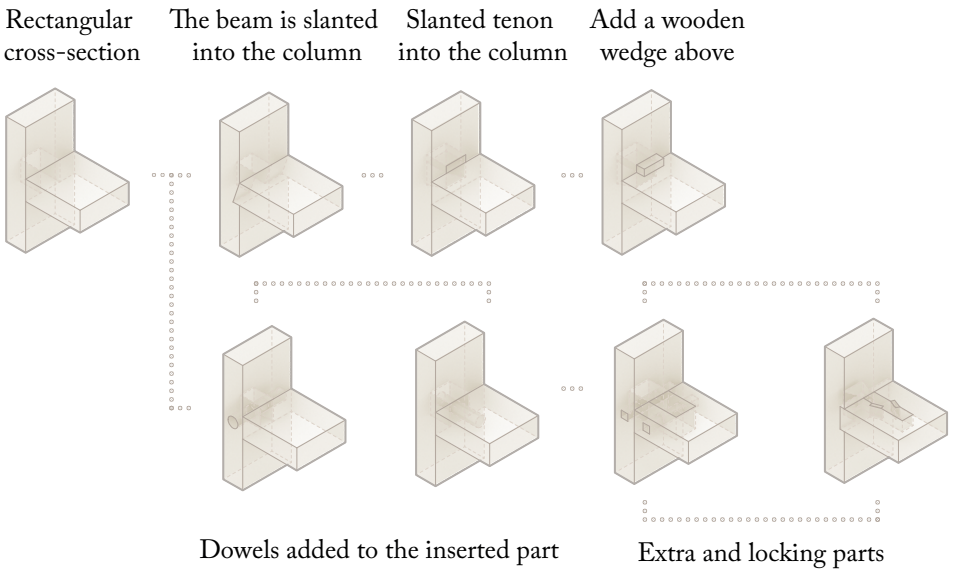

Figure 4.7. *Extract from Appendix - A3. Example of centred tenon connections for C1 with small differences.*

Part cross-section

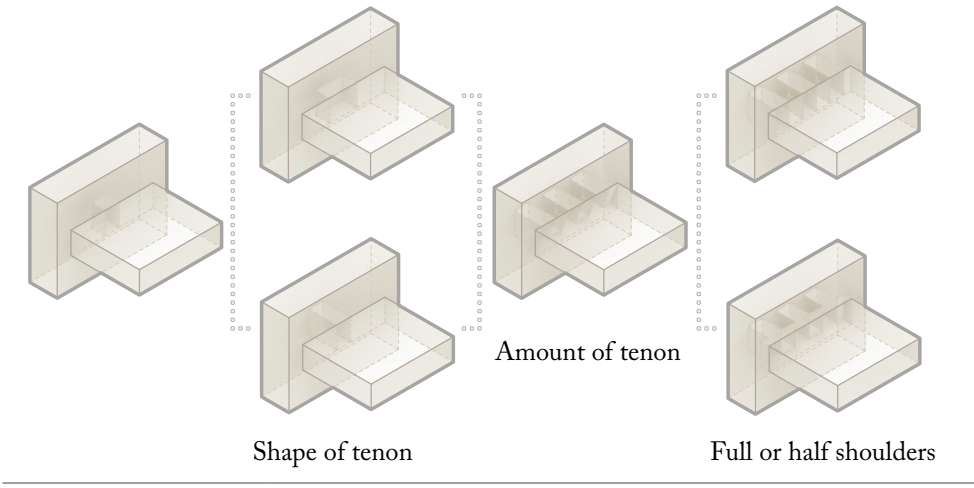

Figure 4.8. *Extract from Appendix - A3. Example of a part cross-section insertion connections for C2 with small differences.*

CRITERIA

Manufacturability

In all projects, manufacturability is an important aspect to consider since this often goes hand in hand with economy and how easy it is to assemble. For this category the connections are looked at based on how many cuts it would take to create the geometry. Dowels and the drilling holes are also counted as one cut.

Assembly

For future restorations, demolitions, re-usability as well as erection time and economy, assembly is an aspect to consider. This is measured for the connections by how many movements are needed for joining the connection.

Fire & Acoustics resistance

Influencing this criteria is depth of penetration for the connected members, the risk of gaps and cracks forming between the pieces and if the joining geometry is mostly covered (how many sides are exposed).

Regarding this one question that is considered is how likely is it that small gaps are created in the joining? Several angled sides (dovetails) increase the risk of gaps more than a block.

With regard to C1 and C2 the acoustical qualities are not considered in this step as these connections are within one room and will not open up for vibrations to move between rooms.

Architectonic qualities

For C1 and C2 this feature matters since these are two visible connections. One of the goals for these connections is that it is visible and the connection is shown as mentioned in Chapter 2. Therefore this criteria is taken into consideration. The questions to answer are how many sides are shown? As well as if these connecting pieces are separate (for example dowels) and can be made out of another type of wood and can make them more visible?

Structure

A measure of how well the connection is optimized for what the construction demands. If the connection takes forces in a lot more directions and moments than is actually needed the design could be too intricate.

Applicability

Applicability has to do with future intent of this thesis and the involving connections. At this point it is not an easily measurable category but for future reference it is important to think of how easily the connections could be applied to other situations.

This criteria also takes in the "essence" of some of the other criteria such as assembly, manufacturing, fire and acoustics. How it performs within these will in some part determine how easily it could be applied to other scenarios as well. This criteria is an important part of the discussion in Chapter 8.

Grading tables are found in Appendix A4 for full overview of the evaluation. A grading for all connection types is set, with respect to the mentioned parameters, between one to three dots. They are ranked in comparison to each other where one dot stands for good, two dots for better and three for the best concept concerning the different categories for the connections.

C1

From the evaluation phase, two major different concepts per connection were selected for further investigation and calculation comparisons. In Figure 4.9 the two selected options from the evaluation are shown with their grading result. One geometry is a plane dovetail tenon inserted from the side and the other is a rectangular tenon with a locking peg.

TYPE OF CONNECTION	MANU-FACTURING	ASSEMBLY	FIRE AND ACOUSTICS	STRUCTURE	ARCHI. QUALITIES	APPLICA-BILITY
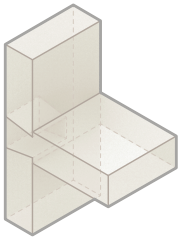	●●○	●●●	●○○	●●○	●●●	●●○
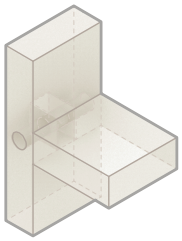	●●○	●○○	●●○	●●●	●●●	●●○

Figure 4.9. *An extract from Table 1 in Appendix A4 of the grading for C1.*

TYPE OF CONNECTION	MANU-FACTURING	ASSEMBLY	FIRE AND ACOUSTICS	STRUCTURE	ARCHI. QUALITIES	APPLICA-BILITY
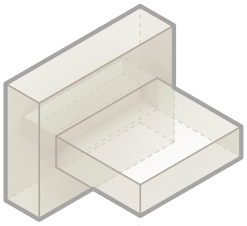	●●●	●●●	●●○	●○○	●●●	●●●
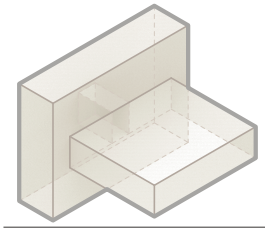	●●●	●●●	●●○	●●○	●●○	●●●

Figure 4.10. *An extract from Table 2 in Appendix A4 of the grading for C2.*

C2

The two major concepts brought forward from the evaluation phase was a notched geometry protruding the railing as well as a tenon and mortise geometry. A dovetail tenon is also chosen as a version of a notched geometry. Both kept alternatives for further studies are found in Figure 4.10.

CHAPTER CONCLUSION

From this chapter chosen options for C1 and C2 that will be further investigated, as a help to develop the preliminary calculation method, can be seen in Figure 4.11 - 4.14.

For C1 a side inserted plane dovetail and a centred tenon with a locked peg are analysed with two options each. These are variations of depth of the dovetail and a variation in peg size for the tenon and mortise as seen in Figure 4.11 and 4.12 with their respective shortened names. They are named "Plane dovetail 1", *PD1*, "Plane dovetail 2", *PD2*, "Peg 1", *P1*, and "Peg 2", *P2*.

For C2 the investigated geometries are three types of tenon and mortise joints where the position of the tenon differs and two different geometries are used. These different geometries are named "Tenon and mortise", *TM1*, "Upper notch", *N1*, and "Bottom notch", *N2*, as seen in Figure 4.13. For the dovetail joints five different models are investigated where the shape of the dove is taken into account as well as the number of doves in the connections. These are classified as "Round dovetail 1-5", *RD1 - RD5*. All varieties of the dovetail can be seen in Figure 4.14.

The different geometries are analysed in FE-models in the next Chapter as a further iteration before bringing a last selection into the hand calculation phase.

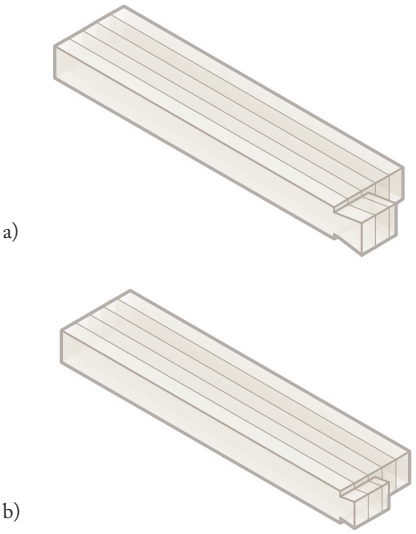

Figure 4.11a. *Plane dovetail full depth, PD1.* b. *Plane dovetail half depth, PD2.*

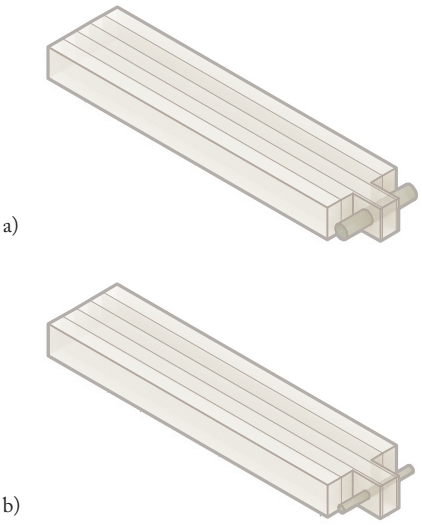

Figure 4.12a. *Tenon and mortise with thick peg, P1.* b. *Tenon and mortise with thin peg, P2.*

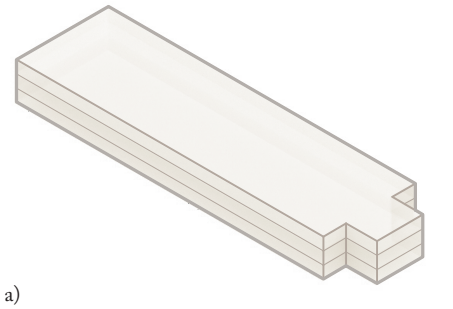

a)

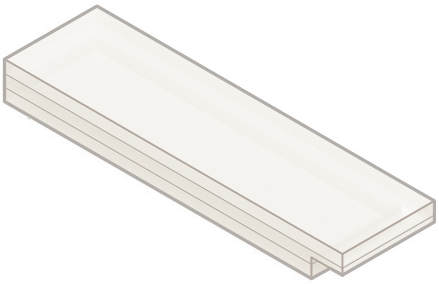

b)

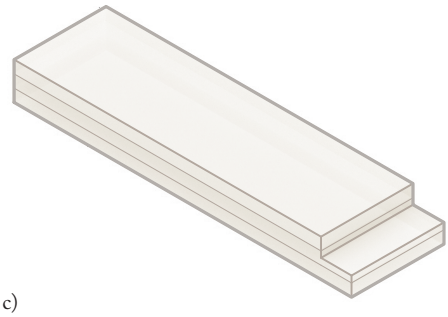

c)

Figure 4.13a. *Tenon and mortise, TM1.* b. *Top notch, N1.* c. *Bottom notch, N2.*

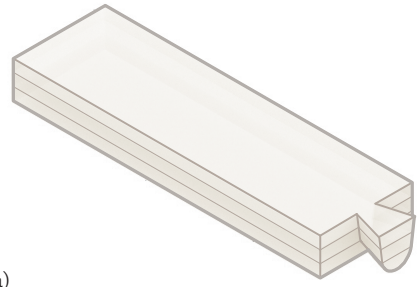

a)

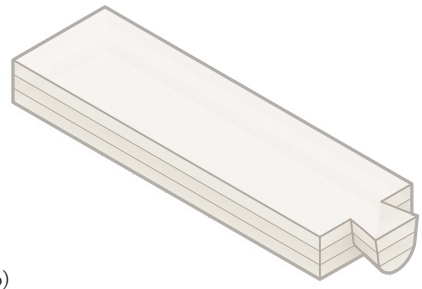

b)

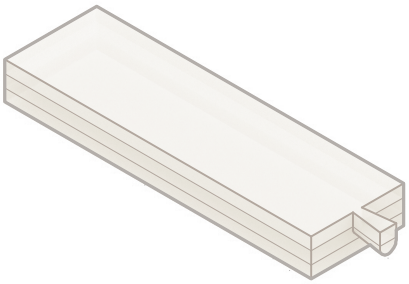

c)

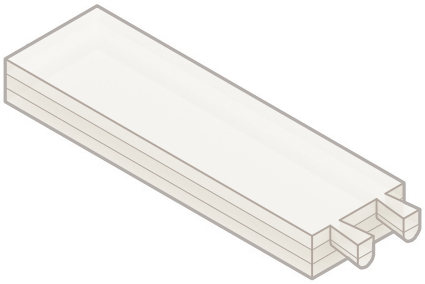

d)

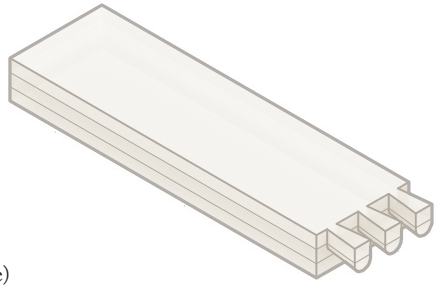

e)

Figure 4.14. *Rounded dovetails 1-5.* a. *RD1.* b. *RD2.* c. *RD3.* d. *RD4.* e. *RD5.*

5. ANALYSIS

The following chapter includes an analysis from the FEM-program, Abaqus, together with analytical calculations comparisons. In Appendix C more specific results are find from Abaqus.

FE-MODELLING

The FE-models in Abaqus are made to locate the most critical stress points and by this try to locate important failure modes. It is also used as a method to investigate the differences between the connections in both stress locations and magnitudes. Through a discussion on the differences between the connections a further iteration and choice can be made of which connections to perform hand calculations on. The first step of the FE-modelling was also utilized to identify the most critical load locations for the C2 connection.

INPUT C1

Loads

The loads are applied with two different load cases for the pinned connections but a conclusion was made that load case one is the most critical one. Therefore, the focus on the analysis are stress diagrams related to this load case. The loads are calculated and can be seen in Appendix B1.

Boundary conditions and Geometry

Regarding the geometry modelled for C1 and C2 it is important that enough of the model is considered to portray a reasonable stiffness with the chosen boundary conditions. Any other locking addition of nodes is merely made in order to prevent rigid body motion of the model. The mesh and boundary conditions for C1 can be seen in Figure 5.1. The end of the pillars are locked in translation in all directions. An additional boundary condition is used for the pinned connection where the connection is locked in one end in y-direction. This is to prevent rigid body motion which otherwise occurred.

The interaction added in the contact surfaces in the connection are simple normal force contact. No additional friction is added. This is to simulate that it is merely a contact connection and that no additional glue or joining mechanisms are used. This is the same for C2.

Material

The material values can be seen in Table 5.1 for glulam *(Atashipour ,2020)*.

Table 5.1. *Glulam engineering constants.*

Variable	Value
E1 (x)	12 600 MPa
E2 (y)	390 MPa
E3 (z)	700 MPa
υ12 (xy)	0.03 (-)
υ13 (xz)	0.04 (-)
υ23 (yz)	0.35 (-)
G12 (xy)	350 MPa
G13 (xz)	720 MPa
G23 (yz)	30 MPa

INPUT C2

Loads

The loads applied in the FE-models are the ones seen in Table 2.2 and 2.4 in Chapter 2 with minor differences in order to be applied in Abaqus. These differences are described below and calculated in Appendix B1 and B2. In order to eliminate as many singularities as possible and apply the loads upon the structures all line loads are divided by the area and applied as a positive or negative pressure.

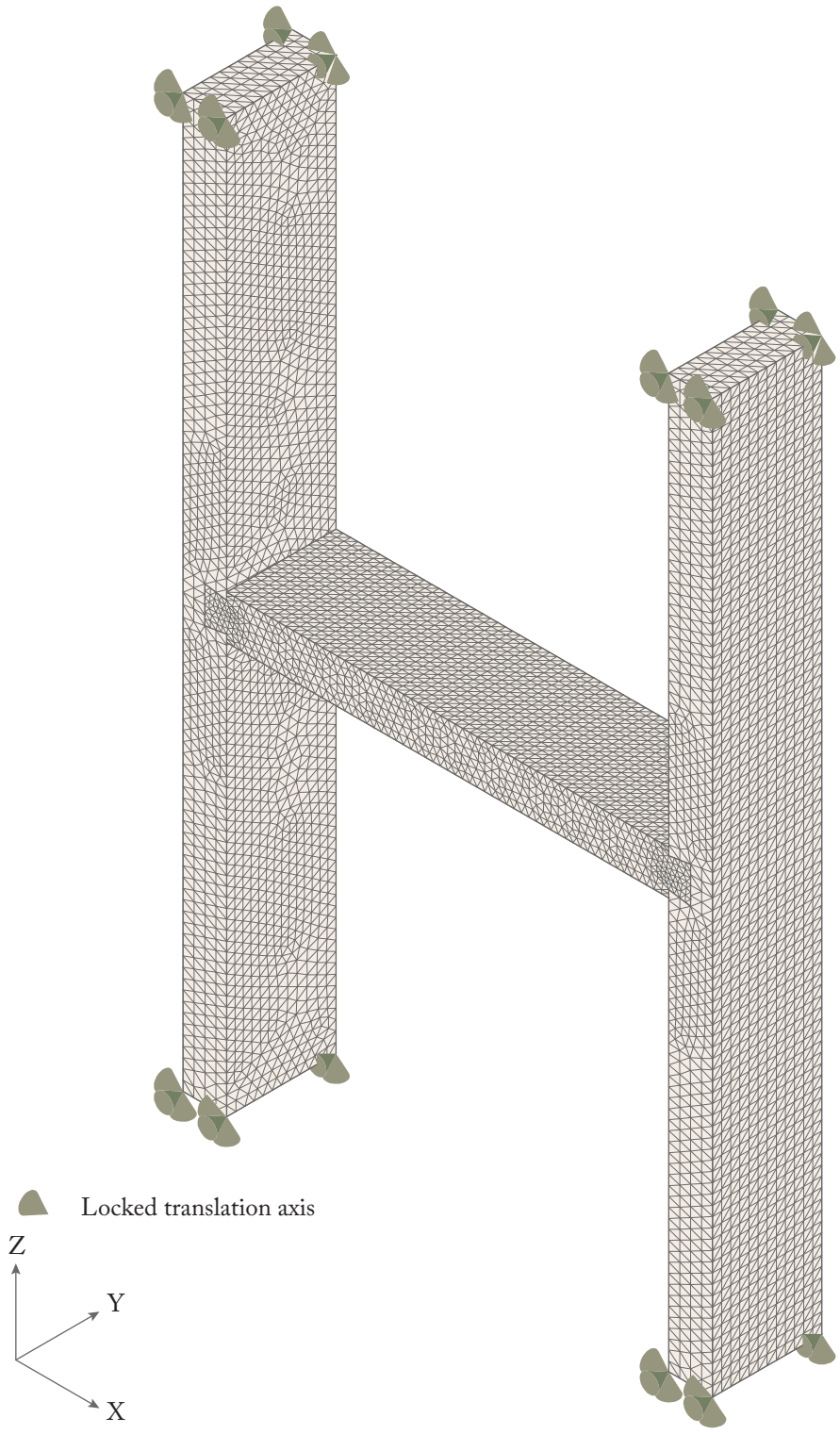

Figure 5.1. *Boundary conditions and mesh definition, Abaqus, C1.*

The point load acting on C2 is applied over an area of 100x100 mm instead of a single node. The values of the loads applied are calculated in Appendix B2.

Boundary conditions and Geometry

The boundary conditions, *B.C.*, applied to C2 can be seen in Figure 5.2. The B.Cs added on the railing are fully rigid with no translation or rotation. The B.C. added to the end of the step geometry where the connection toward the wall would have been has been kept unspecified and is therefore added as a symmetry condition and therefore locked in translation in x-direction and locked in rotation in y- and z-direction.

Material

The material values can be seen in Table 5.2 for CLT *(Al-douri & Hamodi, 2009)**.

Table 5.2. *CLT engineering constants.*

Variable	Value
E1 (x)	12 000 MPa
E2 (y)	600 MPa
E3 (z)	900 MPa
υ12 (xy)	0.015 (-)
υ13 (xz)	0.035 (-)
υ23 (yz)	0.558 (-)
G12 (xy)	600 MPa
G13 (xz)	600 MPa
G23 (yz)	50 MPa

* For C2 there was a mix-up in some of the material values in the modelling. This results in slightly different values than what should have been. A test was made using the proper values for some of the analysis and the conclusion was made that this only affect the magnitude of the stresses and not the location of the stress peaks. Therefore the discussion is not related to the size of the stresses which also is not the primary intention.

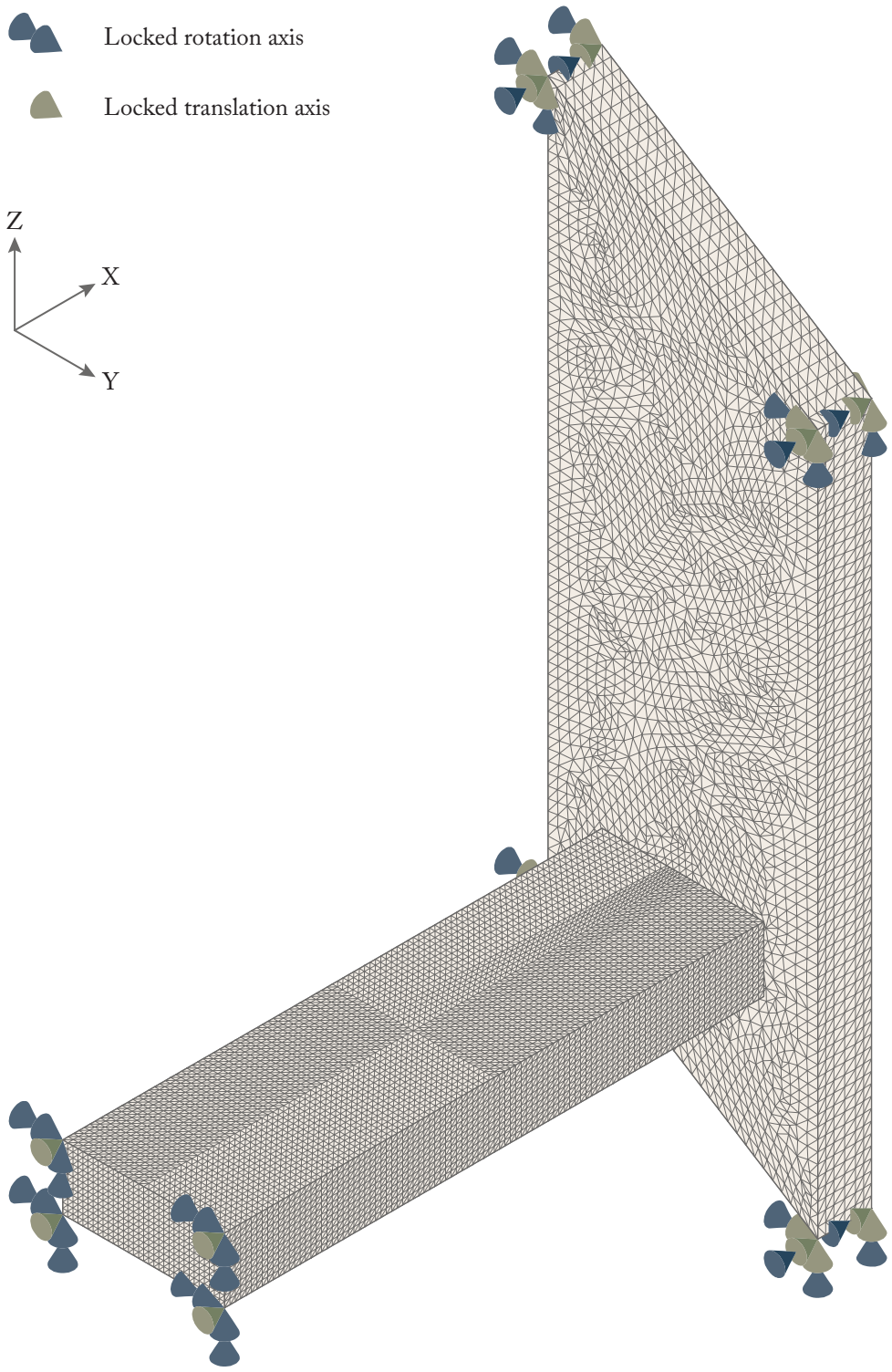

Figure 5.2. *Boundary conditions and mesh definition, Abaqus, C2.*

In this section the results of the FEM-analysis are presented. The stress results have been modified slightly to not account for stress singularities. This is done by applying a maximum, *max.*, and minimum, *min.*, magnitude of the stresses for each diagram. The analysed diagrams are taken from several locations surrounding the connections for shear, tension and compression stresses. Or on several locations along the step for the bending stress case . The analysed diagrams are an average of these stress lines.

Critical load case C2

The first iteration of the FEM-analysis was made on the most simple tenon and mortise joint for C2. The different load cases investigated for this can be seen in Table 5.3. For all of the cases a body load to simulate the self-weight was also added. The most critical location for the point load and the horizontal loads were then put together to give the most critical load case as seen in Figure 5.3. This load case is applied to the other connections as well as used in hand calculations.

Table 5.3. *Investigative load cases for C2*

Load	Illustration
Point load on centre-centre	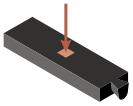
P.L. on centre-side	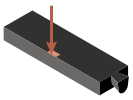
P.L. on edge-centre	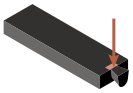
P.L. on edge-side	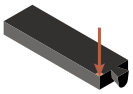
Horizontal length - Pressure	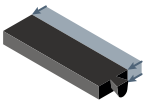
Horizontal length - Traction	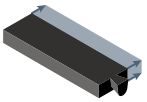
Side length - Pressure	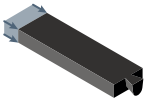
Side length - Traction	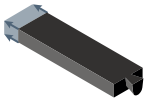

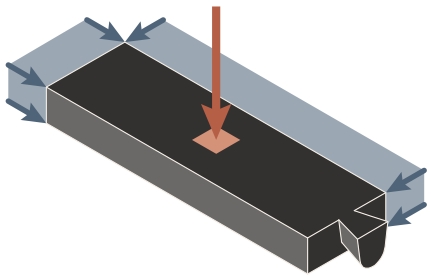

Figure 5.3. *Default load case for C2.*

C2 - Comparisons RD1, RD2 and RD3

This comparison focuses on the influence of the dovetail size on the bending stresses. The bending stresses, as an average along the length of the step, can be seen in Figure 5.4 for the top and the bottom fibres, *t.f.*, and *b.f.* In the graphs positive values represents tension and negative compression stresses. The graphs are taken along the x-direction of the step as illustrated in Figure 5.6. The geometries compared are seen in Figure 5.5.

The bending stresses are positive in the top of the connection, fibres in tension, and the b.f. are in compression around the connection. This has to do with the constraint of the railing and contact surfaces. This will differ in the hand calculations for the geometries as the step in C2 and beam in C1 are then assumed to be simply supported for the sake of the load calculations. Because of this, the tension in the t.f. around the connection will not be investigated in the calculation method. Although, verifying the compression stresses in the b.f. might be a relevant failure mode.

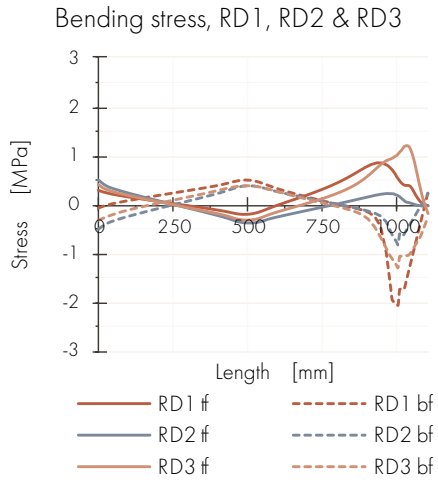

Figure 5.4. *Average bending stress for dovetail joints, RD1, RD2 and RD3 for tf and bf.*

Comparing RD1 with RD2 it is clear that a wider dovetail decrease the stresses. The highest stresses also seem to occur around the notch which is similar to the other geometries as well and indicates that this area is important to investigate for failure modes.

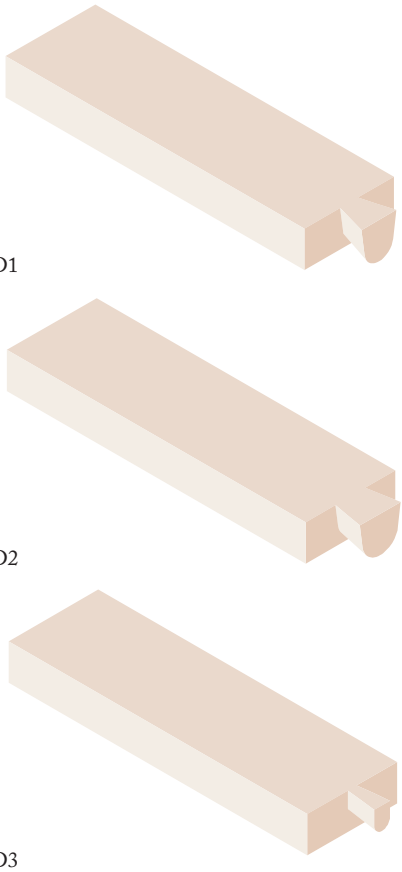

Figure 5.5. *Geometry comparison for RD1-RD3.*

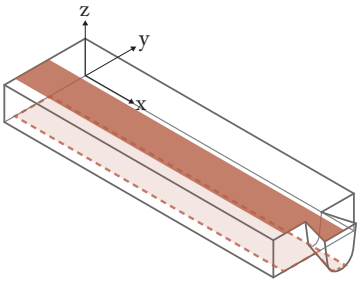

Figure 5.6. *Illustration of paths to consider bending for RD1. An average value are calculated from these paths.*

C2 - Comparisons TM1, N1 and N2

In general the bending graph for the three geometries shown in Figure 5.7 illustrates the same type of failure modes as for RD1-RD3.

The bending graphs for the t.f. shown in Figure 5.8 for TM1, N1 and N2 show that the stresses are less critical in tension for N2 around the notch than for the other two. This correlates to the theory on notches. When it comes to stresses around the notch, a notch at the same side as the support (N1) is generally a more critical solution.

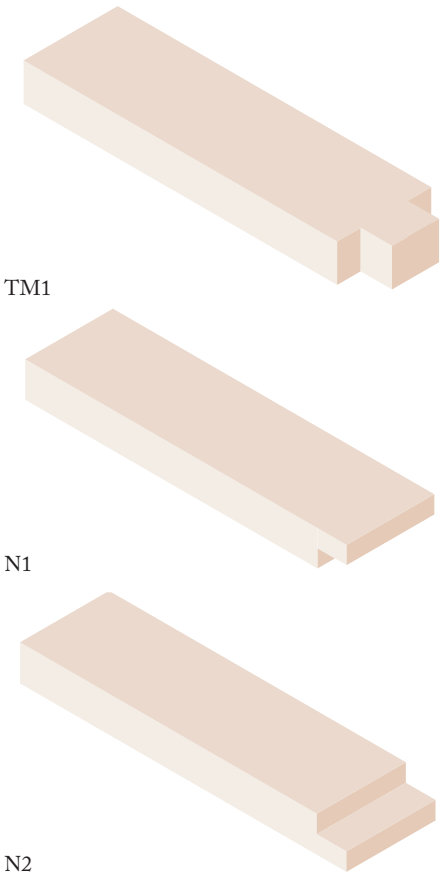

Figure 5.7. *Geometry comparison for TM1, N1 and N2.*

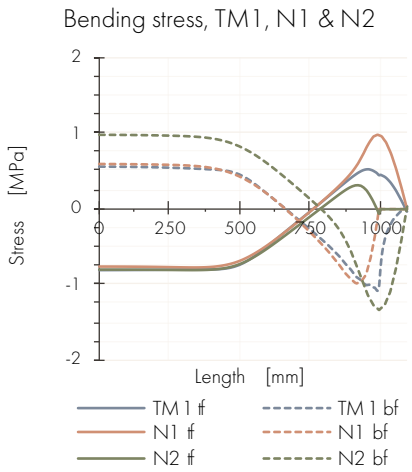

Figure 5.8. *Average bending stress for tenon and mortise, TM1, notches, N1 and N2 for tf and bf.*

The graphs in Figure 5.9 show the shear stresses along the height of the step around the connections. Figure 5.11 illustrate the area from which the stresses are taken for TM1. This is similarly done for N1 and N2. The shear stresses are generated when bending occur by loads perpendicular to the x-axis.

It is clear in the graphs in Figure 5.9 that the stresses are influenced by the layer properties of the CLT. This is therefore important to reflect on in the calculation method. For the two shear planes the layers with grain parallel to the plane take the highest stresses which reflects to the materials highest shear strength in panel shear as well.

In comparison to solid timber and glulam, where the grain runs parallel with the length of the beam for the full cross-section, it could be relevant to investigate the rolling shear strength for a CLT cross-section, since this is the weakest material property of timber.

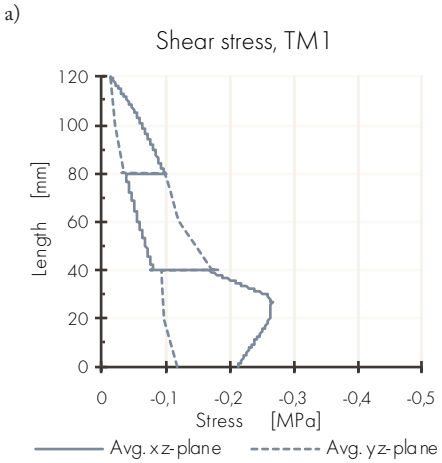

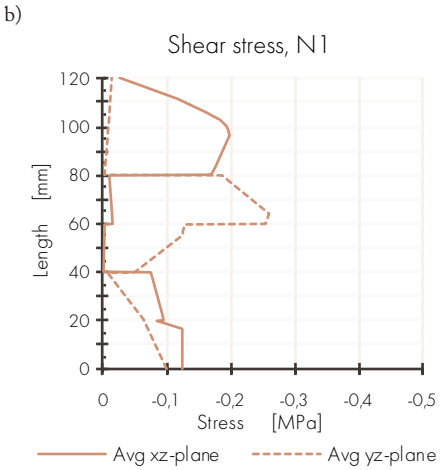

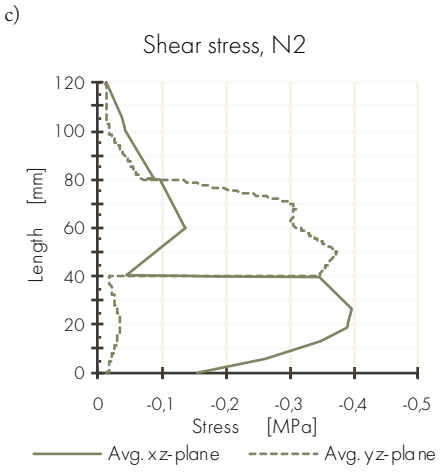

Figure 5.9. *Average shear stress in the tenon/notch for* a. *TM1*, b. *N1*, c. *N2*.

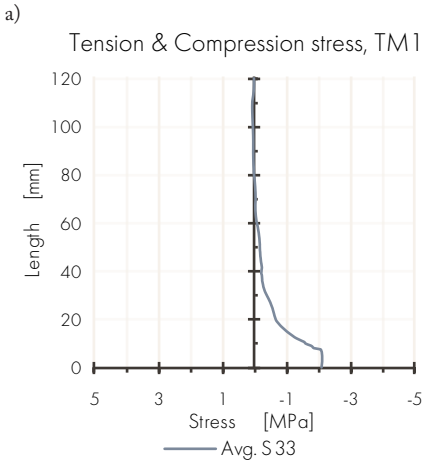

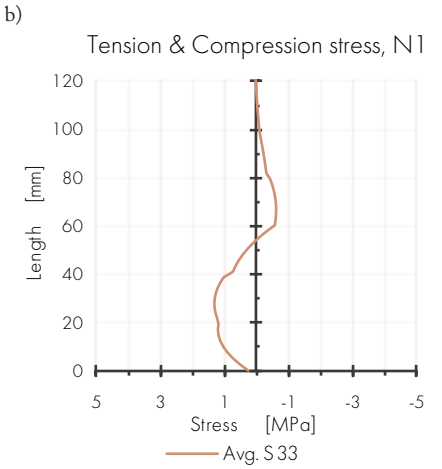

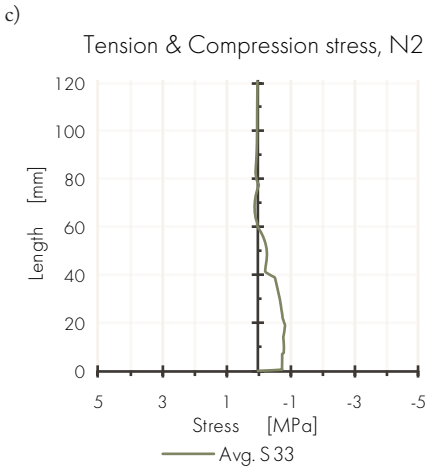

Figure 5.10. *Average axial stress in the tenon/notch for* a. *TM1*, b. *N1*, c. *N2 along the z-axis.*

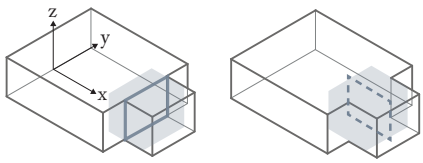

Figure 5.11. *Illustration of paths to consider shear for TM1 where an average value are calculated from these paths.*

With regard to critical stress points, it is visible in Figure 43b-c that high stresses occur in the notches and especially in the notch corner for N1.

Axial stresses in the tenon (z-direction, see Figure 5.11) are presented in Figure 5.10 for the same area from where the shear stresses are taken. Positive values define tension and negative compression. For this axis all stresses act perpendicular to the grain in all layers which is more critical than stresses parallel to the grain. Most critical of these are in tension which is illustrated in Figure 5.12 with a stress-strain relationship curve for timber.

Cracks primarily appear at the notch and tenon tip when having a combination of shear and tensile stresses. Such situations could rapidly happen without any markable deformation or visible signs *(Blaß & Sandhaas, 2017)* and is therefore a relevant failure mode. The axial stresses around the notch for N1 show tensile stresses under the notch. This could portray a likeliness of a combination with high shear stresses and a relevant failure mode especially for this type of notch.

The graphs in Figure 5.10 also show that a relevant failure mode might be compression perpendicular to the grain at the bottom surface of the notches and tenons as already mentioned from the bending stresses discussion as well.

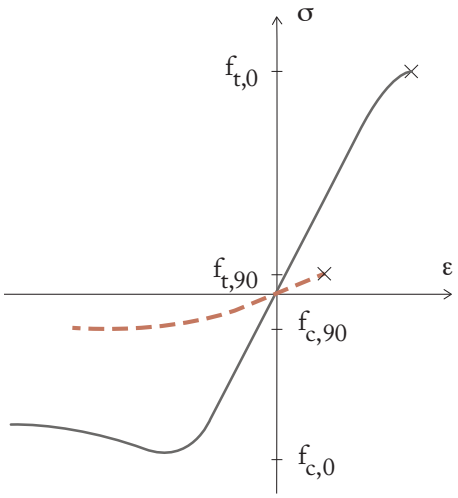

Figure 5.12. *Stress-strain-curve of clear wood, exposed to tensile and compression stresses (perp. to the grain - dashed line) and (parallel to the grain - solid line).*

C2 - Comparisons RD1 and N1

In many cases a dovetail can be approximated as a notch on the same side as the support, as both the geometries include the critical point of a notch corner at the bottom of the cross-section seen in Figure 5.13. When comparing the shear stresses for the two, as seen in Figure 5.14 and 5.15, as well as the axial stresses, as seen in Figure 5.16, it can be concluded that the highest stresses occur at similar points of the geometries. This would suggest that approximating the dovetail as a notch is not unreasonable for cases where verifications does not yet exist for dovetail geometries but for notches.

The shear stresses for RD1 are quite a lot larger than for N1. This is most likely mainly due to singularities in the model and since the width of RD1 is a lot smaller than for N1. This could also be due to the extra restraint in movement that the angled geometry of the dovetail entails. A main difference between the two geometries is the high rolling shear stresses in the bottom layer of the dovetail, which could relate to a failure mode only valid for this type of geometry. This might be due to the angled geometry of the dovetail and therefore the short fibres that are disconnected from the rest of the step which is a critical design point also in manufaturing.

N1

RD1

Figure 5.13. *Geometry comparison for RD1 and N1.*

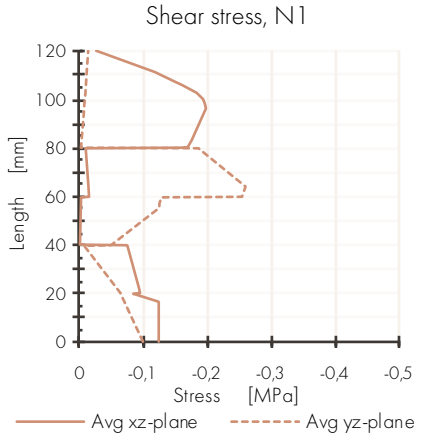

Figure 5.14. *Average shear stress for N1.*

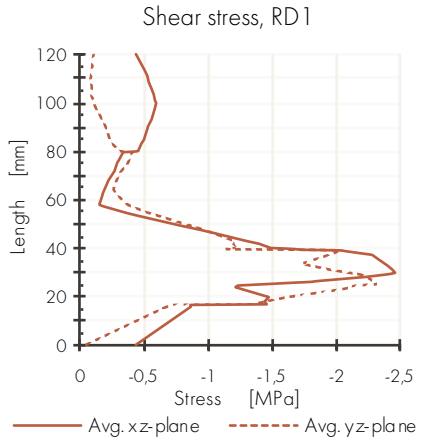

Figure 5.15. *Average shear stress for RD1.*

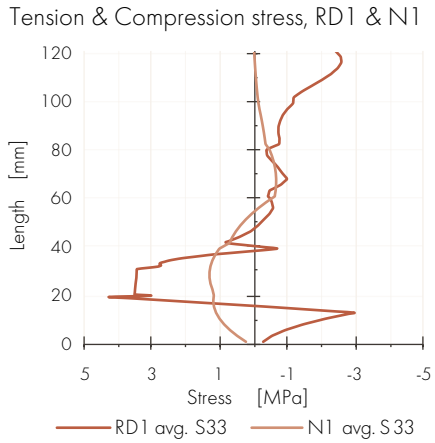

Figure 5.16. *Average shear, tension and compression stress for RD1 and N1.*

C2 - Comparisons RD3, RD4 and RD5

A comparison of affecting the number of dovetails (which could correlate to number of notches or tenons as well based on the previous discussion) is also made where the geometries are seen in Figure 5.17.

When comparing the shear stresses along the same line for the two dovetails in RD4, only minor differences occur, see Figure 5.18. It is therefore not a reasonable assumption that the load is divided equally between the used number of dovetails.

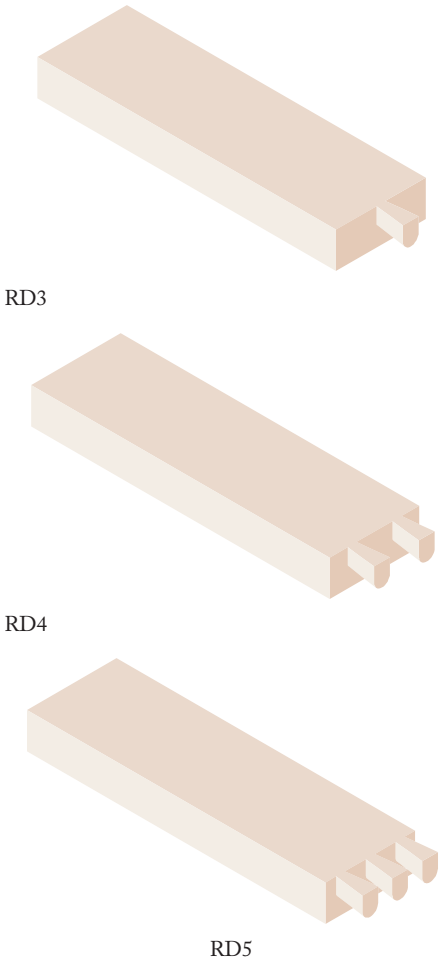

Figure 5.17. *Geometry comparison for C2, RD3-5.*

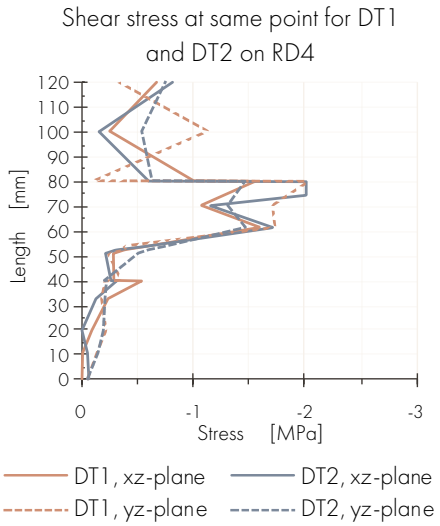

Figure 5.18. *Shear stress at the same location in DT1 and DT2 for the geometry of RD4.*

Comparisons C1, PD2 and C2, N2

A comparison between PD2 and N2, whose geometries can be seen in Figure 5.19, also means a comparison between the material glulam and CLT.

The main differences between the graphs shown in Figure 5.20 and 5.21 is that the glulam only take shear forces in one direction while the layer orientation of the CLT makes it possible for this to take the shear forces in both xz- and yz-plane.

Due to the orientations of the grains the failure mode of rolling shear will not be valid for the connections using glulam.

PD2

N2

Figure 5.19. *Geometry comparison for C1, PD2 and C2, N2.*

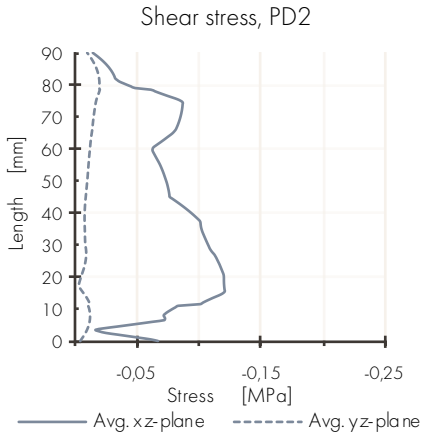

Figure 5.20. *Average shear stress for PD2.*

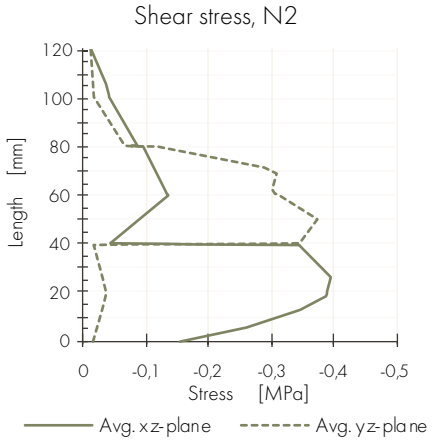

Figure 5.21. *Average shear stress for N2.*

PRELIMINARY CALCULATIONS

The analysis of the preliminary calculation method include two parts. The first part investigates different methods used for the same failure mode. The second part illustrate some geometrical effects that the chosen connections might have.

METHOD INVESTIGATION

Shear and tension perpendicular to the grain with a notch at the opposite side of the support

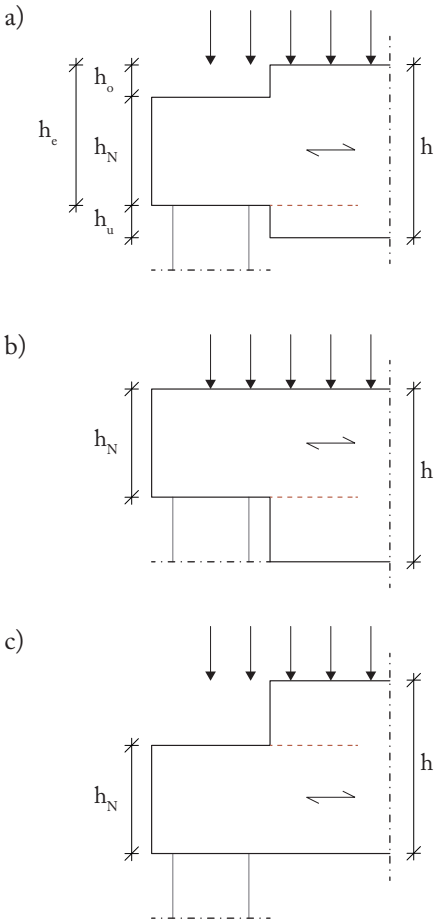

Figure 5.22. *Relevant geometry of Notched joint* b. *top notch,* c. *bottom notch and* a. *Tenon joist.*

The functions for notches and tenons are quite similar and verifies the same type of failure mode. Different sources state similar functions but with small changes.

Figure 5.22 show the relevant geometrical data for this comparison where the width of the beam, b, is same for all joint types.

The verification given in SIS *(2009)* for notches can be rewritten to a force capacity verification as seen in the equations below.

$$\tau_d = \frac{3}{2} \cdot \frac{V_d}{\alpha \cdot h \cdot b_{ef}} \leq k_v \cdot f_{v,d}$$

$$F_{v,Rd} = \frac{2}{3} \cdot \alpha \cdot h \cdot b_{ef} \cdot k_v \cdot f_{v,d} = \ldots \quad (1)$$

$$\ldots = \frac{2}{3} \cdot b_{ef} \cdot h_N \cdot k_v \cdot f_{v,d}$$

Different α's are used depending on if a notch function is used or a tenon function.

$$\alpha = \begin{cases} \frac{h_N}{h} & \text{for notch joint} \\ \frac{h_e}{h} & \text{for tenon joint} \end{cases}$$

In Müller et al. (*2016)* two different formulas are used for this verification depending on the position of the tenon in the cross-section.

$$F_{v,Rd} = \begin{cases} \frac{2}{3} \cdot b_{ef} \cdot h_e \cdot k_z \cdot k_v \cdot f_{v,d} & (2) \\ \frac{4}{9} \cdot b_{ef} \cdot h_e \cdot k_z \cdot k_v \cdot f_{v,d} & (3) \end{cases}$$

Equation (2) is used for lower tenons, *l.t.*, which also can be seen as a bottom notch, *b.n.*, when $h_e = h$. Equation (3) is used for central tenons, *c.t.*.

The first comparison seen in Figure 5.23 is made to determine which function should be used for a bottom notch, *b.n.*, (1) or (2). In equation (1) for b.n. k_v = 1.0 according to EC5. In equation (2) when using an $\alpha = 0.90$ (α is really 1 but then the k_v function fails as this means a division by 0) k_v still equals to 1.0 so this coefficient is the same for the two equations. The differences then comes down to the different heights h_N and h_e and the additional correctional coefficient k_z.

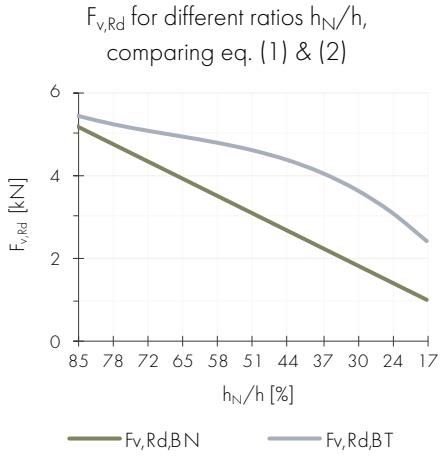

Figure 5.23. *Comparing the two functions that could be used for a bottom notch.*

The equations give a lower capacity the smaller the tenon or notch height is, which is reasonable. Comparing the two results, eq. (1) is more conservative and gives a lower capacity for a b.n. than eq. (2). Therefore, eq. (1) is used for all notched geometries.

The next comparison is made to see which equation should be used if the tenon centre of gravity doesn't correlate with the beam centre of gravity as seen in Figure 5.24.

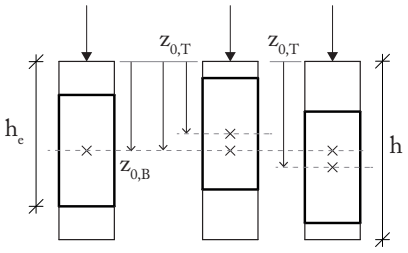

Figure 5.24. *Geometry for comparing the different positions of a tenon.*

The equations according to Müller et al. *(2016)*, eq. (2) and (3), are the functions to use for the tenon where $z_{0,T} > z_{0,B}$. Hence an underlying tenon as these functions give a requirement that $h_e \geq h_u$, as seen in Figure 5.22. For a central tenon, *c.t.* eq. (3) is used *(Müller et al., 2016)* but in other sources eq. (2) is used for both a l.t. and a c.t *(Blaß & Sandhaas, 2017)*. With the same reasoning as for a b.n. eq. (3) is used for a lower tenon as this gives the most conservative result.

When testing the different functions for a tenon where $z_{0,T} < z_{0,B}$, hence a higher placed tenon, this should most likely give a lower value for $F_{v,Rd}$ than a central tenon and a higher value than a top notch, *t.n.*, with the same height of the notch. This results in the use of eq. (3) as seen in Figure 5.25.

For most part the results in Figure 5.25 show that the capacity of the joint decrease with the height of the tenon. The only anomaly is that the capacity for a lower tenon is higher than that of a bottom notch since this equation uses h_e instead of h_N. This function also uses k_z but for this position of the tenon and geometry $k_z < 1.0$ and will therefore not increase the capacity any further. Given that this function for a lower positioned tenon is mentioned in several sources it is still considered to be a safe equation for the verification.

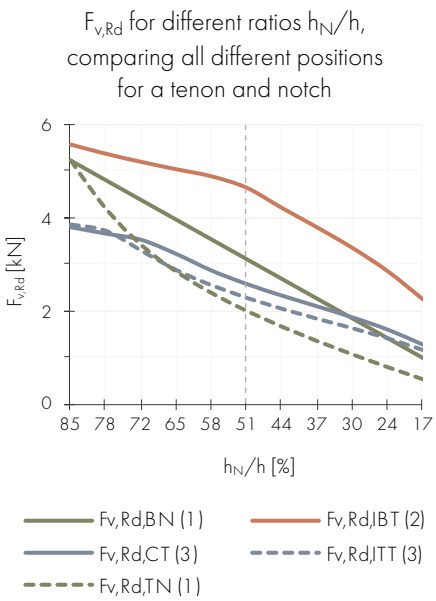

Figure 5.25. *Shear capacity for different positions of a tenon and a notch.*

Shear and tension perpendicular to the grain for a dovetail

For the typically used dovetail geometry seen in Figure 5.26 many different methods have been found to verify the cross-section for the same failure mode as for the top notch's bottom corner. The five methods used for comparison are summarized in Table 5.4.

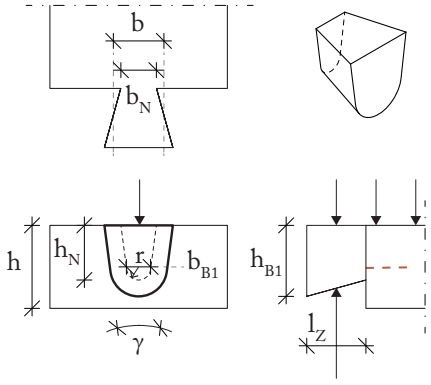

Figure 5.26. *Relevant geometry of Dovetail joint.*

The three equations used to calculate $F_{v,Rd}$ can be seen below. This is equations (4), (5) and (6).

$$F_{v,Rd} = \frac{2}{3} \cdot \left(b \cdot \left(h_N - r\right)\right) \cdot k_v \cdot f_{v,d}$$

$$F_{v,Rd} = \frac{2}{3} \cdot \left(b_{B1} \cdot \left(h_{B1} - r\right)\right) \cdot k_v \cdot f_{v,d}$$

$$F_{v,Rd} = \frac{2}{3} \cdot b \cdot k_{cr} \cdot h_N \cdot \frac{h_N}{h} \cdot \frac{f_{v,d}}{k_{cal}}$$

To note is a limitation on b. In these calculations. The limit is that $b_N \geq 0.8 \cdot b$ as mentioned in the sources. Hence:

$$b \leq \frac{b_N}{0.8}$$

This limitation, as well as other geometrical conditions given in the sources, is most likely based on the load-bearing capacity but also on common dimensions of these joints. For our case the width of the joist is wider than this in relation to the width of the dove. By using the "real" value of the joist the capacity in eq. (4) and (6) gets higher which is not reasonably the case if the geometry of the dove stays the same. For this reason the width of the joist is therefore limited in this calculation to get a conservative validation of the connection. The comparison of the shear capacity for the different methods with different heights of the dovetail can be seen in Figure 5.27.

Table 5.4. *Equations for verifying a dovetail joist in shear and tension perpendicular to the grain.*

	$F_{v,Rd}$	Area	k_v	
I	eq. (4)	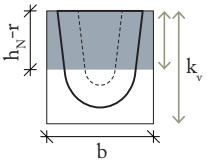	$k_v = \min \left\{ \begin{matrix} 1.0 \\ 6.5 \\ \frac{}{\sqrt{b} \cdot \left(\sqrt{\alpha - \alpha^2} + 0.4 \cdot \frac{l_Z}{b} \cdot \sqrt{\frac{1}{\alpha} - \alpha^2} \right)} \end{matrix} \right.$ $\alpha = \frac{h_N - r}{b}$	*
II	eq. (5)	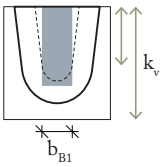	$k_v = \min \left\{ \begin{matrix} 1.0 \\ 6.5 \\ \frac{}{\sqrt{b} \cdot \left(\sqrt{\alpha - \alpha^2} + 0.4 \cdot \frac{l_Z}{b} \cdot \sqrt{\frac{1}{\alpha} - \alpha^2} \right)} \end{matrix} \right.$ $\alpha = \frac{h_N - r}{b}$	**
III	eg. (5)	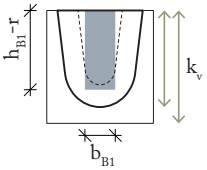	$k_v = \left(\frac{b_{B1}}{b} \right)^2$	**
IV	eg. (5)	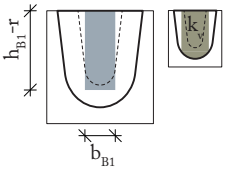	$k_v = \min \left\{ \begin{matrix} 1.0 \\ \left(\frac{3600}{A_B} \right)^{0.2} \end{matrix} \right.$ $A_B = \left(b_{B1} + 2 \cdot \tan\left(\frac{\gamma}{2} \right) \cdot \left(h_{B1} - \frac{b_{B1}}{2} \right) \right) \cdot \left(b_{B1} - \frac{b_{B1}}{2} \right) + \frac{\pi^2 b_{B1}}{8}$	**
V	eq. (6)	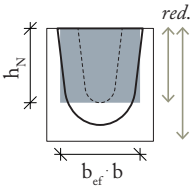	red. can be approximated to a reduction constant similar to k_v as it is a ratio of the notch height and the joist height in eq. (6).	***

* *(Blaß & Sandhaas, 2017)*

** *(CEN, 2019)*

*** *(CEN, 2017)*

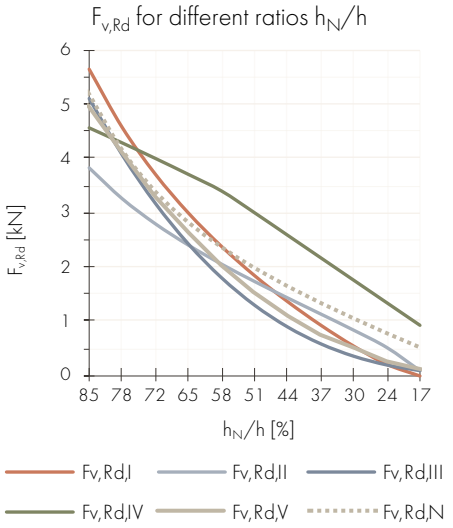

Figure 5.27. *Shear capacity at the notch for a dovetail with 5 different methods.*

The dotted line in this graph show the shear force of a regular notch in the top of the cross-section with a similar geometry of the dovetail.

Through this comparison the most conservative methods are either method II or III, depending on the ratio of the height of the dovetail to the height of the joist. Method III is more similar to the other curves and is the most conservative for the most critical ratios (smaller ratios, hence smaller dovetails). Therefore, this is chosen for the calculation of the capacity in the general calculation method for dovetail joints for this particular failure mode.

Shear and tension perpendicular to the grain for the header of a dovetail

For a dovetail header two different equations can be used for this verification. These can be seen as eq. (7) and (8). The comparison between these can be seen in Figure 5.28.

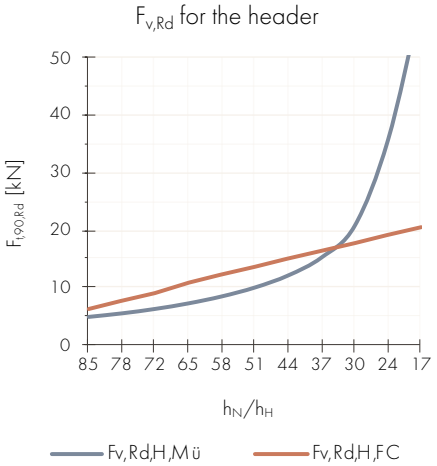

Figure 5.28. *Shear capacity for a dovetail header comparing two different methods.*

Eq. (7) is represented by the red curve from CEN *(2017)* and eq. (8) is taken from Müller et al. *(2016)* and includes more detailed geometrical variables. Both the equations give similar capacities for larger dovetails, hence where the height under the crack is smaller for a set total header height. Since eq. (7) shows quite a lot smaller capacity for the header where the values of the two equations start and then differ from each other, this equation is used for the most conservative solution.

$$\tau_{Ed} = \frac{3}{4} \cdot \frac{V_{Ed}}{b_H \cdot h_{H,u}} \rightarrow F_{v,Rd} = \frac{4}{3} \cdot b_H \cdot h_{H,u} \cdot f_{v,d} \tag{7}$$

$$F_{v,Rd} = \frac{h_N}{h_N - r} \cdot \left(6.5 + \frac{18 \cdot h_{H,u}^{\,2}}{h_H^{\,2}} \right) \cdot \left(l_z \cdot h_H \right)^{0.8} \cdot f_{t,90,d} \tag{8}$$

ADDITIONAL GEOMETRICAL EFFECT

This section investigates how the geometries and different calculation factors and formulas affect the load-bearing capacity. Some geometrical effects can be seen in the previous analysis as well, for example the effect of the tenon position and notch height on the load-bearing capacity.

Reduction factor, k_v (-)

The risk of crack growth in a notched and tenon member can be taken into consideration through a reduction factor k_v, which is found in EC5 *(SIS, 2009)*. A further definition for this reduction factor is found in Chapter 6.

Figure 5.29 shows how k_v changes depending on alpha (which is a geometry ratio), as defined above. The three geometries (one per graph) in this evaluation have different ratios of the depth of the tenon, l_z, divided by the height of the beam, h_B. In this test all curves has same height of the beam, set to 120 mm. Therefore it is the depth that changes between them. A low ratio between l_z and h_B gives a higher value of k_v. Hence, a smaller l_z gives a stronger notch.

Once alpha reach approximately 0.5 the blue curve (0.25) turns up and gives a higher value. Having a short length of the tenon or notch and at the same time a very small height of the tenon seems to give a stronger connection which could be misleading. Although taking into consideration the purpose of the connections it is highly unlikely that such a small notch or tenon is possible for the loads required in a construction. At least from a production point of view as well.

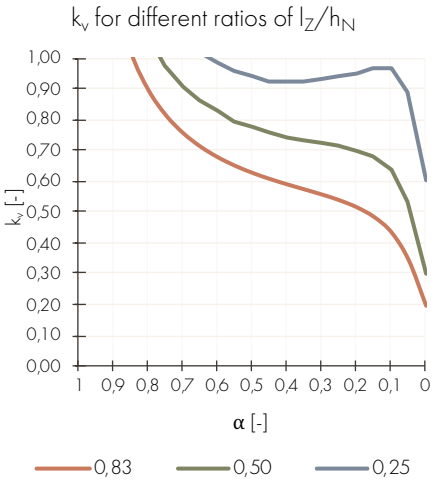

Figure 5.29. *Reduction factor, k_v for different ratio of l_z/ h_B depending on alpha.*

Geometry of the header

The height under the cut geometry of a header for a notch, tenon and mortise or dovetail header influences the strength in shear and tension perpendicular to the grain. This is shown in Figure 5.30. The geometry illustration and related failure mode can be seen in Figure 5.31.

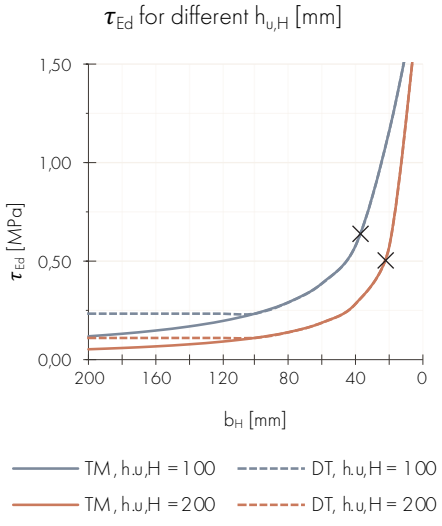

Figure 5.30. *Shear stress mortise depending on the width of the header b_{Hf}*

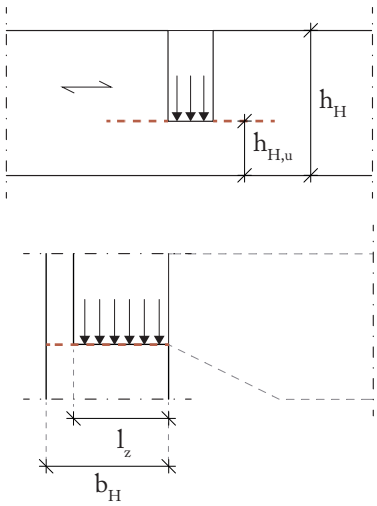

Figure 5.31. *Relevant geometry definitions of the header.*

The results are quite reasonable. If the height of the header underneath the crack is smaller the larger the stresses are. What can be seen is also that even though this height is doubled the difference in stress size is very small.

No clear correlation between height under the crack and width of the header can be deduced for when the geometry would be critical. Both the different heights show approximately the same width for when the stress increase dramatically towards a singularity, at 30 - 50 mm.

The equation used in this comparison from CEN *(2017)* includes a restriction on the width for a dovetail geometry. This is seen as the dashed lines in Figure 5.30. The influence of this is minor and this type of geometrical restriction is therefore not taken into consideration in the general calculation method.

CHAPTER CONCLUSION

As a conclusion of this chapter what seem to be important failure modes based on the FE-analysis are:
- Compression perpendicular to the grain at the bottom of the connection (notch).
- Shear stresses at the notch.
- Tension stresses at the notch (in combination with shear stresses).

It is also important to investigate the influence of layer orientation for the CLT connections. This would include rolling shear failure of the connection geometry.

Another important part that might be needed to consider in the calculation method are approximations of a dovetail geometry to a similar notched geometry.

Important to note is that the analysis in this chapter is focused on the joist geometry therefore research of similar failure modes for the header of the connection is needed for the development of the calculation method.

6. PRELIMINARY CALCULATION METHOD

This chapter includes the full general calculation method for the carpentry connections investigated for C1 and C2. This chapter has its own chapter index and numbering separate from the report.

INDEX

1. GENERAL INFO

The basic calculations with regards to material, loads and dimensioning of a cross-section the method in SIS (2009) should be followed. The calculation method in this report only include the parts that might differ from this standard or where additional verifications are made except from this.

When it comes to the preliminary calculation method for glulam and CLT the verifications made for solid timber are the same as for glulam but with given coefficients and changed material data.
For CLT depending on the orientation of the board some geometrical data is changed and verifications added due to the different grain directions of the material.

1.1. LOADS

Loads used for dimensioning are calculated from respective part of SIS *(2009)* for self-weight, imposed load, snow load and wind load.

The impact of load duration and service class is also stated in SIS *(2009)* .

1.2. VERIFICATION OF THE PARTIAL COEFFICIENT METHOD

1.2.1. Design values for material properties

The design values of the strength properties, X_d, used in this method is calculated according to equation (1) from SIS *(2009)*.

$$X_d = k_{\mathrm{mod}} \cdot \frac{X_k}{\gamma_M} \tag{1}$$

Where:

X_k	is the characteristic value of the load-bearing properties.
γ_M	is the partial coefficient for the material properties (Recommended values in Table 1).
k_{mod}	is the correctional factor with regard to load duration and moisture content (Recommended values in Table 3).

1.2.2. Partial coefficient

Table 1. *Partial coefficients.*

Material	Factor, γ_M	*Source*
Solid timber	1.3	*(SIS, 2009)*
Glulam	1.25	*(SIS, 2009)*
CLT	1.25	*(Gustafsson et al., 2019)*

2. LIMITATIONS

This calculation method is limited to CLT, glulam and solid timber although might be relevant and applicable, to some extent, for other timber engineered materials as well.

The calculation material is limited to verifications in ultimate limit state (ULS) and no consideration is taken for the connections in a service limit state (SLS).

The calculation material is based on moment free connections. The equilibrium equations are therefore limited to simply supported members or connections with moment free supports.

A geometrical constraint of this calculation method is that the geometry of the header follows the geometry of the joint (notch, tenon or dovetail). The header is the "inverted" shape and therefore the geometries of the two members are restricted by one another.

3. MATERIAL PROPERTIES

3.1. MODIFICATION FACTORS

Table 2 below includes all correctional and modification factors with small explanations of their purpose. It also states the equation number of the equation or equations including the factor.

Table 2. *Modification factors.*

Factor	Purpose	Equations	*Source*
k_{mod}	Correction factor with regard to load duration and moisture content. Found in Table 3.	(1), (25) & (26)	*(SIS, 2009)*
k_{cr}	Factor taking into account the risk of cracks.	(2), (6), (14), (18) & (20)	*(SIS, 2009)*
k_{n}	Proportionality constant established by testing	(3) & (7)	*(Blaß & Sandhaas, 2017)*
k_{v}	Reduction factor that takes into consideration the risk of crack growth in notched members.	(6), (7), (20), (23) & (24)	*(Blaß & Sandhaas, 2017)*
k_{k}	Correction coefficient to take into account the non-uniformly distributed tensile stresses.	(11)	*(Blaß & Sandhaas, 2017)*
$k_{c,90}$	Factor that take into consideration the fact that compression perpendicular to the grain is distributed over areas larger than the directly loaded area, here the support area of the connection.	(4), (5), (13) & (19)	*(SIS, 2009)*
k_{z}	Correction factor based on test results that takes into consideration influences of the tenon geometry.	(20) & (21)	*(Blaß & Sandhaas, 2017)*

3.1.1. Factor, k_{mod}

Table 3. *Modification factor, k_{mod}.*

Material	Climate class	Load duration class					
		Permanent	Long	Average	Short	Instantaneous	
Solid timber	1	0.60	0.70	0.80	0.90	1.10	*
	2	0.60	0.70	0.80	0.90	1.10	
	3	0.50	0.55	0.65	0.70	0.90	
Glulam	1	0.60	0.70	0.80	0.90	1.10	*
	2	0.60	0.70	0.80	0.90	1.10	
	3	0.50	0.55	0.65	0.70	0.90	
CLT	1	0.60	0.70	0.80	0.90	1.10	**
	2	0.60	0.70	0.80	0.90	1.10	
	3	0.50	0.55	0.65	0.70	0.90	*

** (SIS, 2009)*

*** (Gustafsson et al., 2019)*

3.1.2. Factor, k_{cr}

$$k_{cr} = \begin{cases} \dfrac{2.0}{f_{v,k}} & \text{Solid timber} \\ \dfrac{2.5}{f_{v,k}} & \text{Glulam} \\ 0.67 & \text{CLT *} \end{cases} \quad (2)$$

* For general CLT boards the cross lamination of the perpendicular layers mean that k_{cr} does not need to be taken into consideration and is therefore equal to 1.0 *(Blaß & Sandhaas, 2017)*. But for constructions with a small board width, such as a connection point, k_{cr} = 0.67 is used according to Gustafsson et al. *(2019)*.

3.1.3. Factor, k_n

$$k_n = \begin{cases} 5.0 & \text{Solid timber} \\ 6.5 & \text{Glulam} \\ 6.5 & \text{CLT *} \end{cases} \quad (3)$$

* The factor k_n is not specified for CLT so the value for glulam is applied as an approximation.

k_n is a proportionality constant established by testing which gave a range of constants for solid timber, glulam and LVL and simplified to the seen above to be used in the factor k_v *(Blaß & Sandhaas, 2017)*.

3.1.4. Factor, k_v

k_v is a reduction factor that takes into consideration the risk of crack growth in notched members. k_v must not exceed 1.0 to ensure no shear failure occur in the remaining cross-section. For beams with a notch at the opposite side of the support k_v = 1.0 can be used *(Blaß & Sandhaas, 2017)*.

Different functions are used for k_v depending on the geometry of the connection. The discussion of this can be seen in Chapter 5 in the Report. If different equations are used in the equations this will be stated.

3.1.5. Factor, $k_{c,90}$

This factor take into consideration the fact that compression perpendicular to the grain is distributed over areas larger than the directly loaded area. This is the support area for the joists with either a notch, tenon or dovetail in this method or the loaded area from the joist(s) for the headers. Therefore, this factor increases the compression strength perpendicular to the grain. This factor is given for discrete supports and for softwood *(SIS, 2009)*.

For a joist the compression zones will not interact with each other as the geometries for these does not interact. Although for a header with multiple joists this might be the case. Figure 1 and equation (5) display the conditions for such an interaction.

$$k_{c,90} = \begin{cases} 1.0 & \text{for all materials, } l_1 < 2 \cdot h_{H,u} \\ \text{eq. (5)} & l_1 \geq 2 \cdot h_{H,u} \end{cases} \quad (4)$$

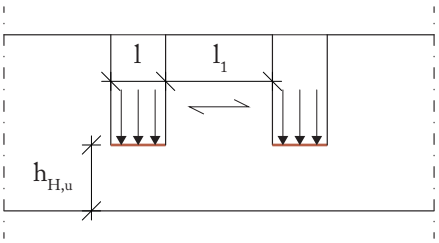

Figure 1. *Geometrical conditions for $k_{c,90}$.*

$$k_{c,\,90} = \begin{cases} 1.5 & \text{Solid timber} \\ 1.75 & \text{Glulam, } l \leq 400\ mm \\ 1.5 & \text{CLT } * \end{cases} \quad (5)$$

* This coefficient is only used for CLT orientation where compression perpendicular to the grain is acting upon all layers of the geometry *(Gustafsson et al., 2019)*. For CLT boards oriented in a different direction one or more layer would have grain parallel to the compression and this failure mode would seize to be relevant.

4. VERIFICATION OF NOTCHED JOINT

4.1. NOTCHED MEMBER

4.1.1. Geometry

All geometrical data for the verifications can be seen in Figure 2 for this member of the connection. The notch can be either on the opposite side as the support (referred to in this thesis as a bottom notch [b.n.]) or on the same side as the support (called a top notch [t.n.]). Figure 2.a. shows a top notch with two different cross-section possibilities. One where the width of the beam is larger than the width of the notch (this is also a possibility for the b.n. even though this is not visualized) and one where they are the same. For both of them it is the width of the notch that is used in the calculations. Figure 2.b shows a bottom notch.

The discussion on which equations to use with regards to a b.n. as seen in Figure 2.b. can be read in Chapter 5 in the report.

4.1.2. Shear and tension failure perpendicular to the grain at the notch corner

For notched beams one failure occur where a crack appear in the tip of the notch and propagate parallel to the grain, see Figure 3. These cracks are generally generated by a combination of shear and tensile stresses perpendicular to the grain.

Fracture mechanics is used to estimate the following formula for verifying the shear and tensile capacity of a notched beam. The formula is reduced to shear verification but this formula verifies the capacity for tension perpendicular to the fibres as well *(SIS, 2009)*.

$$\tau_d = \frac{3}{2} \cdot \frac{V_{Ed}}{\alpha \cdot h \cdot b_{ef}} \leq k_v \cdot f_{v,\,d} \quad (6)$$

Where:

V_{Ed} is the dimensioning shear force.

$b_{ef} = k_{cr} \cdot b_N$ is the width of the notch reduced to account for the negative influence of cracks (k_{cr} can be found in Chapter 3.1).

b_N is the width of the notch. May be modified for CLT see Chapter 4.1.2.1.

$$k_v = \min \left\{ \begin{array}{c} 1.0 \\ \dfrac{k_n \cdot \left(1 + \dfrac{1.1 \cdot i^{1.5}}{\sqrt{h}}\right)}{\sqrt{h} \cdot \left(\sqrt{\alpha - \alpha^2} + 0.8 \cdot \dfrac{x}{h} \cdot \sqrt{\dfrac{1}{\alpha} - \alpha^2}\right)} \end{array} \right. \tag{7}$$

is a reduction factor, see Chapter 3.1.

k_n is a proportionality constant, see Chapter 3.1.

i is the notch inclination, see Figure 2.

h is the joist height, see Figure 2.

$\alpha = \dfrac{h_N}{h}$ is the ratio between the notch height and the joist height. May be modified for CLT, see Chapter 4.1.2.1.

h_N is the height of the notch, see Figure 2.

x is the distance from the support reaction to the corner of the notch, see Figure 2.

$f_{v,d}$ is the design shear strength of the material.

4.1.2.1. Modifications for CLT

For cross laminated timber the verification in eq. (6) may need to be modified in order to account for the grain direction in the different layers. For a notched geometry of CLT where the load is applied perpendicular to the grain direction of all layers the height of the cross section in the calculation may need to be altered. This is done if the notch corner occurs in a layer where the grain is perpendicular to the crack propagation as seen in Figure 3. This type of connection can be seen in Figure 4.

This change will affect α and make it smaller than for a notched beam where all layers act parallel to the crack. This in turn will give a lower capacity through the calculations as $F_{v,Rd}$ decreases for a decreasing height of the notch.

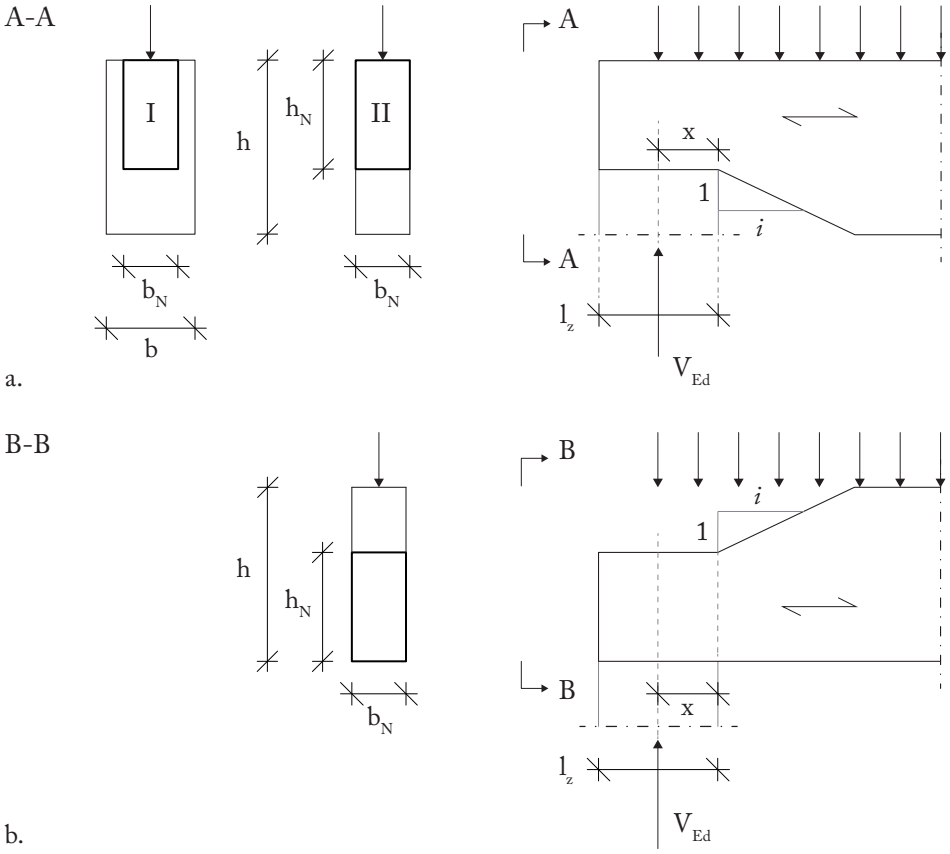

Figure 2. *a. Geometry of a top notch. b. Geometry of a bottom notch.*

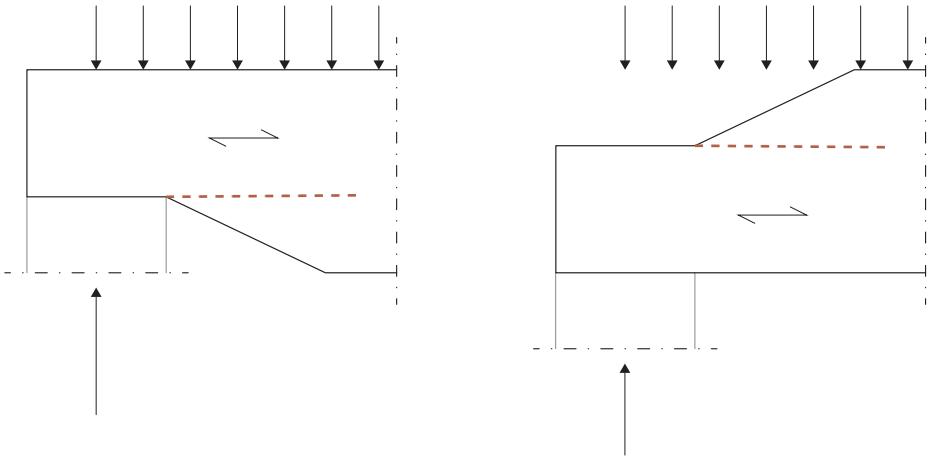

Figure 3. *Shear and tension failure perpendicular to the grain at the notch corner for the joist.*

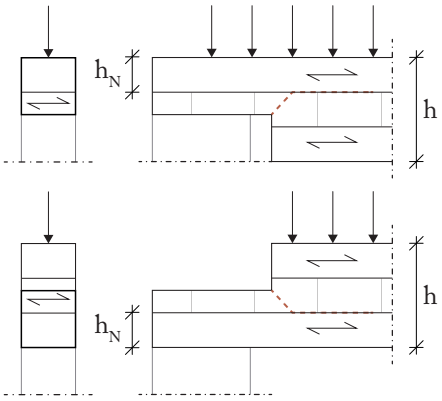

Figure 4. *Modification of height for CLT if notch at a layer perpendicular to the crack propagation.*

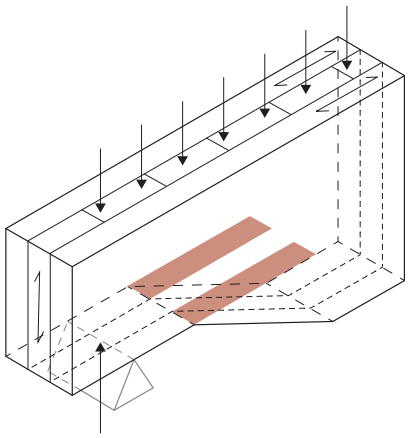

Figure 5. *Modification of width for CLT with not all layers parallel to the crack propagation.*

Depending on the layer orientation, one or more lamination layers may act as reinforcement of the cross section. This could for a possible tension failure perpendicular to the grain be proven sufficient to strengthen the cross-section against this type of failure, see Figure 5. For a layer to act as reinforcement the grain direction of the layer needs to be perpendicular to the tension failure.

When one or more layers act as reinforcement the shear stress calculated for verification of the crack propagation does not occur across the whole width of the cross-section, but only in the layers with a grain direction parallel to the crack. This is illustrated in Figure 5.

For verifying the cross-section for shear and tension failure perpendicular to the grain the same method as in Chapter 4.1.2. is used but with a reduced width of the cross-section.

$$b_N = \sum t_{i,\parallel} \tag{8}$$

Where:

$t_{i,\parallel}$ is the thickness of each layer with grain direction parallel to the crack.

By decreasing the width of the cross-section for shear verification the shear stresses increase and might result in failure of the cross-section. In this case it is therefore relevant to also verify the reinforcement layer which is the layer or layers parallel to the load and perpendicular to the crack propagation.

An approximation for this type of verification is done by using the formulas for externally glued on reinforcement plates on a similarly notched cross-section. The geometrical data for this type of verification can be seen in Figure 6.

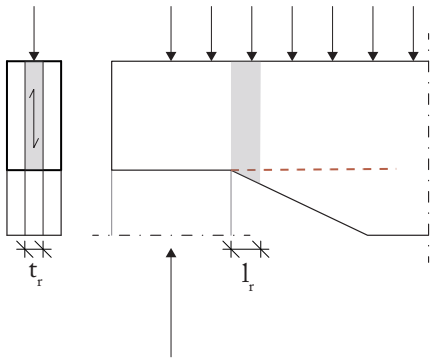

Figure 6. *Geometry for verifying one or several reinforcement layers for CLT.*

This reinforcement layer verification is generally only needed for notches at the same side as the support and tenons.

The generated force component for tension perpendicular to the grain can be calculated according the eq. (9) *(Blaß & Sandhaas, 2017)*.

$$F_{t,90,d} = 1.3 \cdot V_{Ed} \cdot \left(3 \cdot \left(1 - \alpha\right)^2 - 2 \cdot \left(1 - \alpha\right)^3\right) \tag{9}$$

Where:

V_{Ed} is the dimensioning shear force.

$\alpha = \frac{h_N}{h}$ is the ratio between the notch height and the joist height. May be modified for CLT see Chapter 4.1.2.1.

The factor 1.3 is approximated due to the fact that the stresses are not uniformly distributed at the notch corner, which results in peak stresses and an approximate increase of the tension force component by 30 % *(Blaß & Sandhaas, 2017)*.

For these reinforcement layers the bond line stress as well as the tensile stress is calculated and verified.

The effective bond line area taken into account is the area below the critical area of the failure (the area below the notch corner). The bond line is verified by calculating the stresses over the surface and verifying against the rolling shear strength of the material.

$$\tau_{ed,d} = \frac{F_{t,90,d}}{n_b \cdot \left(h - h_N\right) \cdot l_r} \leq f_{Rv,d} \tag{10}$$

The tensile stress in the reinforcement layers is then acting parallel to the fibres and verified as:

$$\sigma_{t,\,d} = \frac{F_{t,90,d}}{n \cdot t_r \cdot l_r} \leq \frac{f_{t,\,d}}{k_k} \tag{11}$$

Where:

$$n_b = \begin{cases} 2 \cdot n & \text{if only internal layers act as reinforcement} \\ 2 \cdot (n-1) & \text{if external layers are included as reinforcement} \end{cases}$$

is the number of bond-lines.

n is the number of reinforcement layers.

h is the joist height, see Figure 2.

h_N is the height of the notch, see Figure 2.

l_r is the effective width of the reinforcement, see Figure 6.

The effective width, l_r, of the reinforcement is limited to:

$$0.25 \cdot (h - h_N) \leq l_r \leq 0.50 \cdot (h - h_N) \tag{12}$$

Where the minimum value prevent crack development in the area accentuated in Figure 6 and the maximum value ensures that the area of the reinforcement taken into account is limited by the notch area subjected to tension perpendicular to the grain.

$f_{Rv,\,d}$ is the design rolling shear strength of the material.

t_r is the thickness of the reinforcement layer(s), see Figure 6.

$k_k = 2.0$ is a correction coefficient, see Chapter 3.1.

$f_{t,\,d}$ is the design tensile strength parallel to the grain of the reinforcement layer.

4.1.3. Compression failure perpendicular to the grain at the bottom of the notch

For tenon and mortise joints the compression perpendicular to the grain needs to be verified in the bottom of the tenon and as a notch can be compared to a tenon a similar verification can be made for this geometry *(CEN, 2017)*. The failure mode can be seen in Figure 7.

$$\sigma_{c,\,90,\,d} = \frac{V_{Ed}}{b_N \cdot l_{z,\,ef}} \leq k_{c,\,90} \cdot f_{c,\,90,\,d} \tag{13}$$

Where:

V_{Ed} is the dimensioning shear force.

b_N is the width of the notch.

$$l_{z,\,ef} = \min\begin{cases} l_z + 30\ mm \\ 2 \cdot l_z \end{cases}$$

is the effective length of the transverse compression [mm] (See Figure 8). In theory the effective area of the compression zone is extended depending on grain direction and on both sides of the support. $l_{z,ef}$ takes into consideration the distribution beyond the tenon length. The evaluated geometries in this thesis limit this zone to only be extended in one direction due to the interaction of the joist and its header.

$k_{c,\,90}$ is a correctional factor, see Chapter 3.1.

$f_{c,\,90,\,d}$ is the design compression strength perpendicular to the grain of the material.

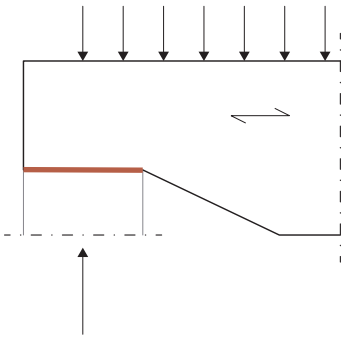

Figure 7. *Compression perpendicular to the grain at the bottom of the notch.*

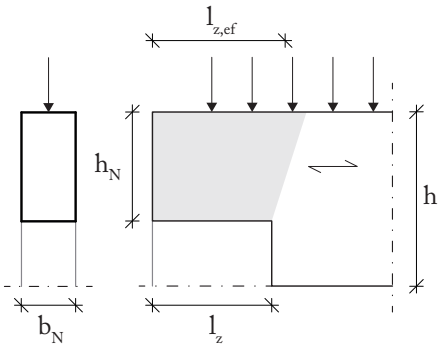

Figure 8. *Geometry of the effective compression length, $l_{z,ef}$*

4.1.3.1. Modifications for CLT

This failure mode is only possible when all layers are perpendicular to the load and therefore the compression surface.

The effective area is only extended in the direction of the fibres *(Gustafsson et al., 2019)*. Therefore, if the first layer closest to the compression surface has fibres oriented perpendicular to the grain as seen in Figure 8 then $l_{z,ef} = l_z$. This is illustrated in Figure 9.

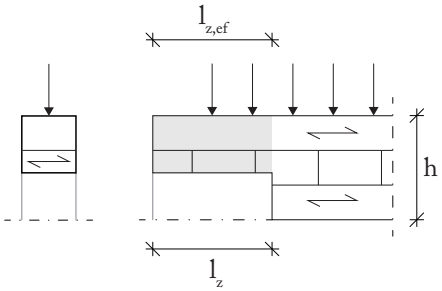

Figure 9. *Geometry of the effective compression length, $l_{z,ef}$ if surface in compression has grain perpendicular to the main grain direction of the beam.*

4.1.4. Rolling shear failure in the notch (only for CLT)

When a shear force is acting on a CLT member where all layers are perpendicular to the force one or more layers will act in rolling shear due to the bending of the member. This is verified by controlling the rolling shear stress specifically for the layers acting in rolling shear and verifying against the strength of the material. An example of what layers are concerned for a notched geometry is illustrated in Figure 10 with a bending around the y-axis.

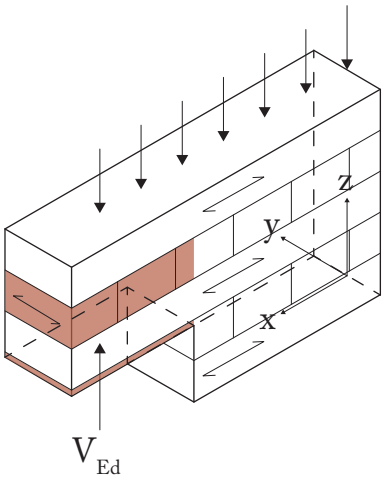

Figure 10. *Rolling shear failure of the layers with grain parallel to the bending axis.*

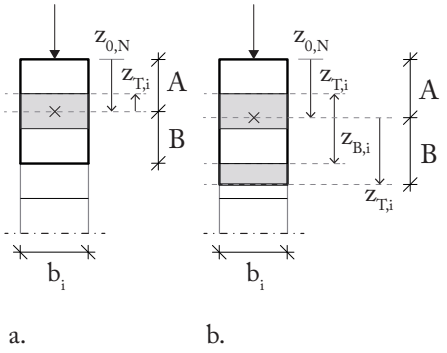

Figure 11. *Illustration of different cross-sections for the calculation of the first moment of inertia.*

$$\tau_{Rd} = \frac{V_{Ed} \cdot S_{R,x}}{I_{x,net} \cdot b_{ef}} \leq f_{Rv,d} \tag{14}$$

Where:

V_{Ed} is the dimensioning shear force.

$S_{R,x}$ is the first moment of inertia for the rolling shear layers, see Chapter 4.1.4.1.

$I_{x,\,net}$ is the second moment of inertia for the full cross-section of the notch, see Chapter 4.1.4.2.

$b_{ef} = k_{cr} \cdot b_N$ is the width of the notch reduced to account for the negative influence of cracks (k_{cr} can be found in Chapter 3.1).

$f_{Rv,\,d}$ is the design rolling shear strength of the material.

4.1.4.1. First moment of inertia for the rolling shear layers

For a symmetrical cross-section such as that seen in Figure 11.a. where the centre of gravity of the notched geometry as a solid member occurs at the same point as the centre of gravity for the same member in CLT. The first moment of inertia is the same for both part A and B and only one need to be calculated.

For a non-symmetrical cross-sections as seen in Figure 11.b. the first moment of inertia should be calculated for both the top and bottom half and the larger one should be used to verify the largest rolling shear stresses.

$$S_{R,\,x} = \max \begin{cases} S_{R,\,x,\,A} \\ S_{R,\,x,\,B} \end{cases} \tag{15}$$

Where $S_{R,z,A}$ and $S_{R,z,B}$ are calculated according to eq. (16).

$$S_{R,\,x} = \sum \left(\frac{E_{x,\,i}}{E_{x,\,ref}} \cdot b_i \cdot \int_{z_{B,\,i}}^{z_{T,\,i}} z \, \mathrm{d}z \right) = \sum \left(\frac{E_{x,i}}{E_{x,ref}} \cdot b_i \cdot \left(\frac{z_{T,\,i}^{\,2}}{2} - \frac{z_{B,\,i}^{\,2}}{2} \right) \right) \tag{16}$$

Where:

i is the index of each rolling shear layer in the notched cross-section on either side of the centre of gravity.

$E_{x,\,i}$ is the elasticity modulus for the rolling shear layers, which is the materials E_{90}.

$E_{x,\,ref}$ is a chosen reference value for the elasticity modulus in the x-direction, generally chosen as the strongest E-modulus of all the internal layers.

b_i is the width of each layer, see Figure 11.

$z_{T,\,i}$ is the distance from $z_{0,N}$ to the point of each layer that is furthest away from $z_{0,N}$, see Figure 11.

$z_{B,\,i}$ is the distance from $z_{0,N}$ to the point of each layer that is closest to $z_{0,N}$, see Figure 11. If the centre of gravity occurs in the layer $z_{B,i} = 0$.

4.1.4.2. Second moment of inertia for the notch

The second moment of inertia is calculated for the net cross-section of the notch with all layers included.

$$I_{x,\,net} = \sum \frac{E_{x,j}}{E_{x,ref}} \cdot \frac{b_j \cdot t_j^3}{12} + \sum \frac{E_{x,j}}{E_{x,ref}} \cdot b_j \cdot t_j \cdot a_j^2 \tag{17}$$

Where:

j	is the index of each layer in the cross-section of the notch.
$E_{x,j}$	is the elasticity modulus for each layer in x-direction. For layers with grain direction along x this is E_0 and for layers with grain direction along y this is E_{90}.
$E_{x,\,ref}$	is a chosen reference value for the elasticity modulus in the x-direction, generally chosen as the strongest E-modulus of all the internal layers.
b_j	is the width of each layer, see Figure 11.
t_j	is the thickness of each layer see Figure 11.
a_j	is the distance from the centre of gravity of each layer to the centre of gravity for the net cross-section.

4.2. HEADER MEMBER

4.2.1. Geometry

Two different geometries of the header is illustrated in Figure 12 and Figure 13 with the relevant geometrical notations for all verifications. Both of these geometries have the same failure modes. The force arrows display the load from the joist on the header.

4.2.2. Shear and tension failure perpendicular to the grain at the notch corner

For headers with a grain direction as shown in Figure 12 and 13 the header is loaded perpendicular to the grain and is therefore also subjected to shear stresses and tension stresses perpendicular to the grain at the notch corner similarly to the joist. This type of failure mode can be seen in Figure 14. In a similar way to eq. (6) the verification is reduced to control shear but through this verifies the tension perpendicular to the grain as well.

Note: This type of failure mode is only relevant when the header is not supported directly under the notch or if the height under the notch of the header is relatively large.

The failure mode is verified according to eq. (18) *(CEN, 2017).*

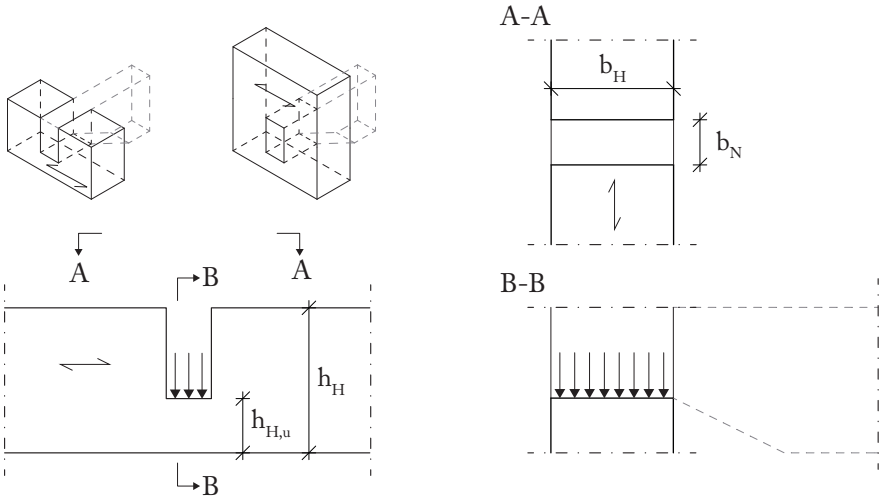

Figure 12. *Geometry of a header where the notch extends through the full width.*

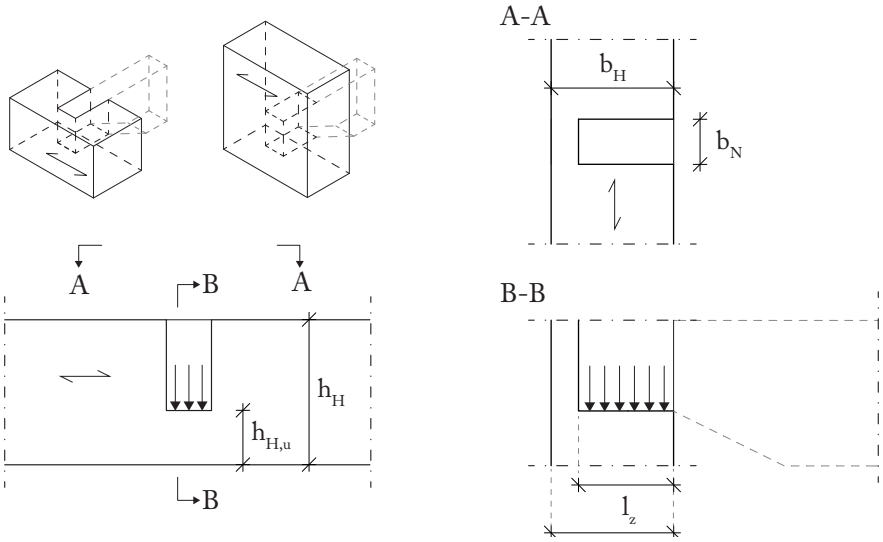

Figure 13. *Geometry of a header where the notch is embedded in the width of the header.*

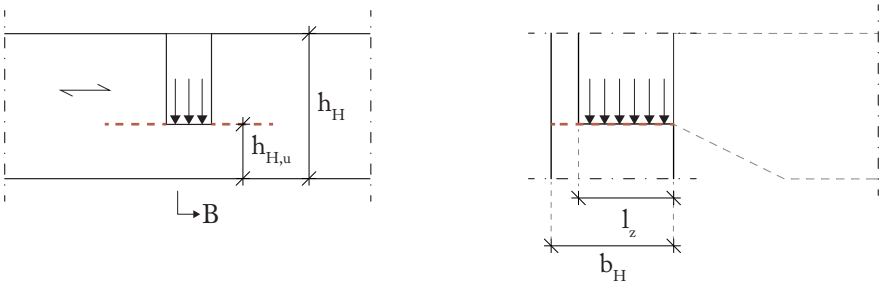

Figure 14. *Shear and tension failure perpendicular to the grain at the notch corner for the header.*

$$\tau_d = \frac{3}{4} \cdot \frac{V_{Ed}}{b_{H,ef} \cdot h_{H,u}} \leq f_{v,d} \quad (18)$$

Where:

V_{Ed}	is the dimensioning shear force.
$b_{H,ef} = k_{cr} \cdot b_H$	is the width of the header reduced to account for the negative influence of cracks (k_{cr} can be found in Chapter 3.1).
b_H	is the width of the header, see Figure 12 and 13.
$h_{H,u}$	is the height under the notch of the header, see Figure 12 and 13.
$f_{v,d}$	is the design shear strength of the material.

4.2.2.1. Modifications for CLT

In the case where CLT is used as the material of the header, where not all layers run parallel to the crack some modifications may be needed. For this type of failure the orthogonal grain patterns that may occur can be seen in Figure 15. This illustration shows the minor changes of the failure mode as well.

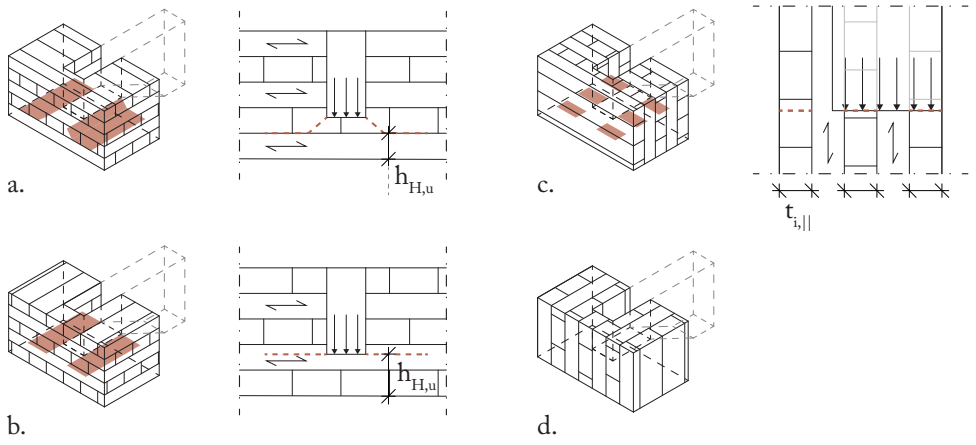

Figure 15. *Changes of the failure mode due to orientation of the CLT material of the header.*

For the orientation as shown in Figure 15.a and 15.b. The crack may occur in a layer with the grain perpendicular to the crack propagation which is a weaker grain direction. This results in a smaller height below the crack of the header similarly to the modification for the joist as seen in Figure 4. This result as mentioned in the reduced height of $h_{H,u}$ as seen in Figure 14.a.

For the layer orientation as seen in Figure 15.b. no changes need to be made for this verification.

For the orientation as that seen in Figure 15.c. not all of the layers have grain parallel to the crack propagation and one or more layers will act as reinforcement similarly to that explained for the joist in Chapter 4.1.2.1.

For the orientation as that seen in Figure 15.c. not all of the layers have grain parallel to the crack propagation and one or more layers will act as reinforcement similarly to that explained for the joist in Chapter 4.1.2.1. For this the width is similarly reduced to what is seen in eq. (8). Other than this the header and the reinforcement are verified according to eq. (18) and eq. (9), (10) and (11).

For eq. (9) some changes are made where the dimensioning shear force is divided in 2 since the crack appear on both sides of the notch in the header and therefore reinforcement layers act on both sides. Only one side is verified as the geometry is symmetrical around the notch.

$$V_{Ed} = \frac{V_{Ed}}{2}$$

and:

$\alpha = \frac{h_{H,u}}{h_H}$ is the α ratio of the header.

For eq. (10) the geometrical variables changed are:

$h = h_H$ the height of the joist is changed to the height of the header, see Figure 12 and 13.

$h_N = h_{H,u}$ the height of the notch is changed to the height under the notch of the header, see Figure 12 and 13.

The layer orientation of Figure 15.d. is only possible for a member with a support under the notch and this type of failure mode in the header will therefore not be possible.

4.2.3. Compression failure perpendicular to the grain at the bottom of the mortise

Depending on the grain direction of the header compression can occur in the header in the same way as for the notch geometry in Chapter 4.1.3. This type of failure mode can be seen in Figure 16. For this case if more than one joists are interacting with the header the compression zones can interact as explained in Chapter 3.1.5.
Other than this the same verification as for the joist in Chapter 4.1.3. is used with only $l_{z,ef}$ modified as seen in Figure 17.

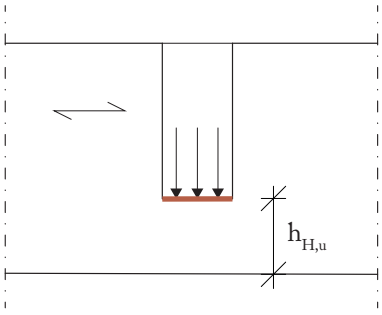

Figure 16. *Compression failure perpendicular to the grain at the bottom of the mortise of the header.*

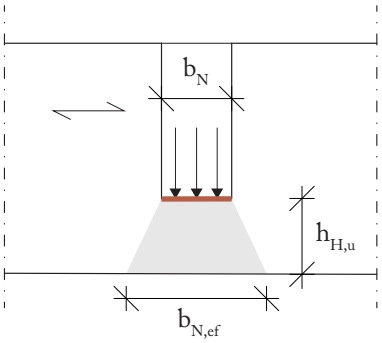

Figure 17. *Geometrical extension of the compression area b_N.*

For the header the geometrical variables changed for this method are:

$b_N = l_z$ — the width of the joist is changed to the depth of the compression area, see Figure 13.

$l_{z,ef} = b_{N,ef}$ — the effective depth of the joist is changed to the effective width of the compression area , see Figure 17.

$$b_{N,ef} = \min\begin{cases} b_N + 60\ mm \\ 2 \cdot b_N \end{cases}$$

$b_{N,ef}$ is extended in the direction of the grain and this will therefore be on both sides of the notch in the header, hence extension of 60 mm.

4.2.3.1. Modifications for CLT

This failure mode is only possible when all layers are perpendicular to the load and therefore the compression surface.

The effective area is only extended in the direction of the fibres *(Gustafsson et al., 2019)*. Therefore, if the first layer closest to the compression surface has fibres oriented perpendicular to the grain as seen in Figure 17 then $b_{N,ef} = b_N$ and l_z is extended to $l_{z,ef}$ instead in the same way as explained in Chapter 4.1.3. The only constraint to the extension of $l_{z,ef}$ is that it cannot exceed b_H. This modification is illustrated similarly for the joist in Figure 9.

4.2.4. Compression failure perpendicular to the grain due to an axial force in the joist

For an axial pressure on the header due to an axial force in the joist the compression perpendicular to the grain may be calculated for a decreased pressure area where the "hole" of the notch is removed as seen in Figure 18.

Depending on the geometry of the joist the pressure area might extend in width outside of the notch.

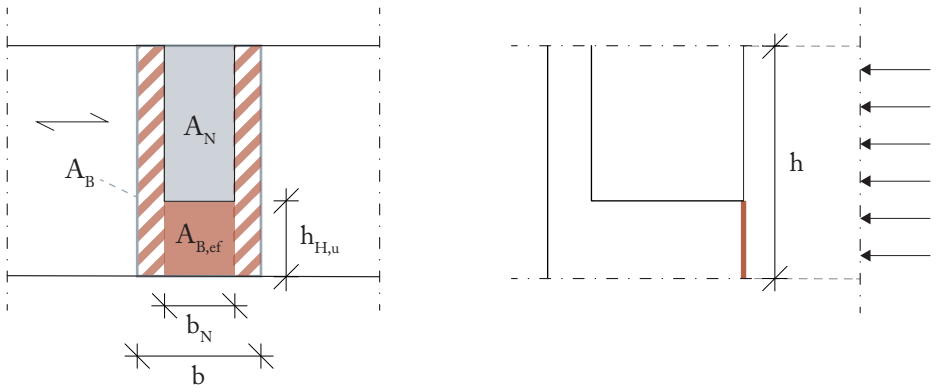

Figure 18. *Compression failure perpendicular to the grain due to an axial force in the joist.*

$$\sigma_{c,\,90,\,d} = \frac{F_{c,\,d}}{A_{B,\,ef}} \leq k_{c,\,90} \cdot f_{c,\,90,\,d} \tag{19}$$

Where:

$F_{c,\,d}$ is the dimensioning axial force.

$A_{B,\,ef} = A_B - A_N$ is the area of the header that is subjected to the pressure, see Figure 18.

A_B is the area of the joist, see Figure 18.

A_N is the area of the notch, See Figure 18.

$k_{c,\,90}$ is a correctional factor, see Chapter 3.1.

4.2.4.1. Modifications for CLT

For a CLT header with a grain orientation as seen in Figure 15.c. the verification should be performed in the same way as seen in Chapter 4.2.4.
For other orientations of the CLT part of this area will have grain direction parallel to the axial force and this type of verification is not needed.

5. VERIFICATION OF TENON AND MORTISE JOINTS

5.1. TENON MEMBER

5.1.1. Geometry

The tenon can be seen as a combination of a top notch and a bottom notch when it comes to the failure modes. Therefore, even though the tenon has two notch corners, it is the lower notch corner that is the most critical and the tenon is therefore, in most verifications, approximated as a top notch, see Figure 19.

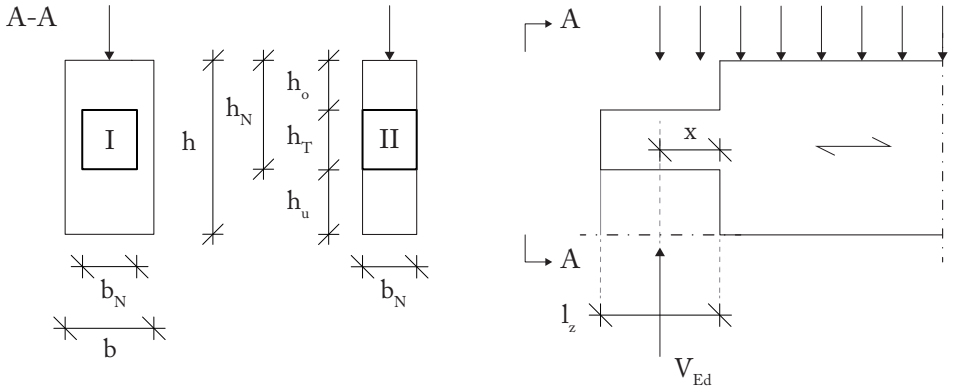

Figure 19. *Geometry of a tenon joist.*

5.1.2. Shear and tension failure perpendicular to the grain at the lower tenon corner

Similar to that of a notched member crack propagation in the grain direction at the height h_u is the major failure mode for the tenon member. The failure mode is illustrated in Figure 20.

This is verified in a similar way where the equation verifies the tension perpendicular to the grain but has been reduced to shear verification.
For the tenon joist different functions are used depending on the placement of the tenon. Compared to the equation for a notch (eq. (6)) the correctional factor k_z is also added *(Blaß & Sandhaas, 2017)*. The equations for this verification depend on the position of the tenon as explained in Chapter 5 in the report and this can be seen in Figure 21 where $z_{0,B}$ is the geometrical centre of gravity for the tenon and $z_{0,T}$ is the centre of gravity for the tenon.

$$F_{v,Rd} = \begin{cases} \frac{2}{3} \cdot b_{ef} \cdot h_N \cdot k_z \cdot k_v \cdot f_{v,d} \geq V_{Ed} & \text{for } z_{0,T} > z_{0,B} \\ \frac{4}{9} \cdot b_{ef} \cdot h_N \cdot k_z \cdot k_v \cdot f_{v,d} \geq V_{Ed} & \text{for } z_{0,T} \leq z_{0,B} \end{cases} \quad (20)$$

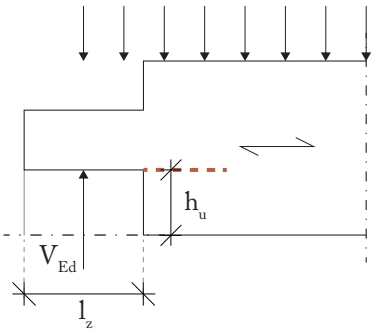

Figure 20. *Shear and tension failure perpendicular to the grain at the notch corner for the joist.*

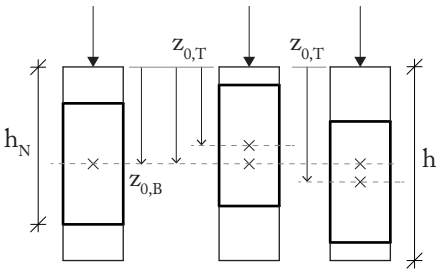

Figure 21. *Geometrical data for the positioning of the tenon.*

Where:

$b_{ef} = k_{cr} \cdot b_N$ is the width of the tenon reduced to account for the negative influence of cracks (k_{cr} can be found in Chapter 3.1).

b_N is the width of the notch, see Figure 19. May be modified for CLT see Chapter 5.1.2.1.

$$k_z = \frac{h_T}{h_N} \cdot \left(1 + 2 \cdot \left(1 - \frac{h_T}{h_N}\right)^2\right) \cdot \left(2 - \frac{h_N}{h}\right) \quad (21)$$

is a correction factor, see Chapter 3.1.

h_T is the tenon height, see Figure 19.

h_N is the height from the bottom of the tenon to the top of the beam, see Figure 20.

h is the joist height, see Figure 19.

k_v is a reduction factor according to eq. (7) and Chapter 3.1. with $\alpha = h_N/h$.

$f_{v,d}$ is the design shear strength of the material.

k_n is a proportionality constant, see Chapter 3.1.

V_{Ed} is the dimensioning shear force.

5.1.2.1. Modifications for CLT

The modifications with the use of CLT for this type of failure mode are the same as seen in Chapter 4.1.2.1. But with the modifications of applied to eq. (20) instead of eq. (6) in Chapter 4.1.2.

5.1.3. Compression failure perpendicular to the grain at the bottom of the tenon

For a tenon and mortise a possible failure of the tenon is also compression perpendicular to the grains in the tenon. This verification is similar to that of the notch under the same failure mode, see Chapter 4.1.3. and can be seen in Figure 22.

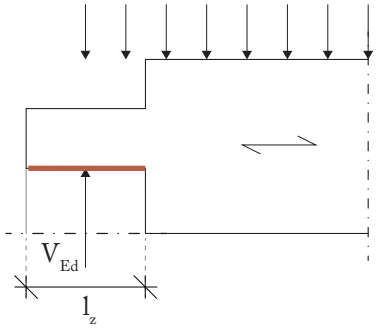

Figure 22. *Compression perpendicular to the grain at the bottom of the tenon.*

$$F_{v,\,Rd} = 1.7 \cdot b_N \cdot l_{z,\,ef} \cdot f_{c,\,90,\,d} \geq V_{Ed} \tag{22}$$

Where:

b_N is the width of the notch, see Figure 19.

$$l_{z,\,ef} = \min \begin{cases} l_z + 30\ mm \\ 2 \cdot l_z \end{cases}$$

is the effective length of the transverse compression [mm] (See Figure 8).

$f_{c,\,90,\,d}$ is the design compression strength perpendicular to the grain of the material.

V_{Ed} is the dimensioning shear force.

This formula is derived from tests and the factor 1.7 is derived from this. This factor corresponds to the coefficient $k_{c,90}$, as seen for notches, that takes into consideration the fact that compression perpendicular to the grain is distributed over areas larger than the directly loaded area, here the support area. Therefore, this factor increases the compression strength perpendicular to the grain with 70 %.

5.1.3.1. Modifications for CLT

See Chapter 4.1.3.1.

5.1.4. Rolling shear failure in the tenon (only for CLT)

The same method as in Chapter 4.1.4 is used but modified with the geometrical data of the tenon as seen in Figure 19.

5.2. MORTISE MEMBER

The geometry and verifications of the header for a tenon and mortise joint are the same as for the header of the notch and calculation method can be followed in Chapter 4.2.

6. VERIFICATION OF DOVETAIL JOINTS

In general a dovetail joint is very similar to a notched joint and is the reason why many of the failure modes and calculations are similar for the two but with modified geometrical data. The difference of the dovetail is that this joint can also handle axial tension between the dovetail and the header. This creates an additional failure mode.

6.1. DOVETAIL MEMBER

6.1.1. Geometry

This thesis include two different dovetail geometries with minor geometrical modifications between these. Figure 23 illustrate these geometries with their variables. The only difference between a. and b., and c. and d. is the orientation of the dovetail geometry. This is differentiated since the dovetail geometries are not symmetrical with regard to these two directions and this entail differences in the calculation methods for the two cases.

Figure 23.a2. and 23.b2. illustrates the geometry for when the dovetail is widened to more than the smallest width due to the radius as is shown in Figure 23.a1. and b1.

6.1.2. Shear and tension failure perpendicular to the grain at the lower dovetail corner

The point of failure is very similar to that of the notched member but the crack appears in the transition zone between the straight tenon and the fillet instead of at the notch corner for the geometry in Figure 23.a. *(Blaß & Sandhaas, 2017).*
For the geometry in Figure 23.b and d. the failure occurs in the notch corner. For the geometry in Figure X.c. the base of the dovetail is a straight notch and the failure occurs for this in the notch corner as well. All four failure modes can be seen in Figure 24.

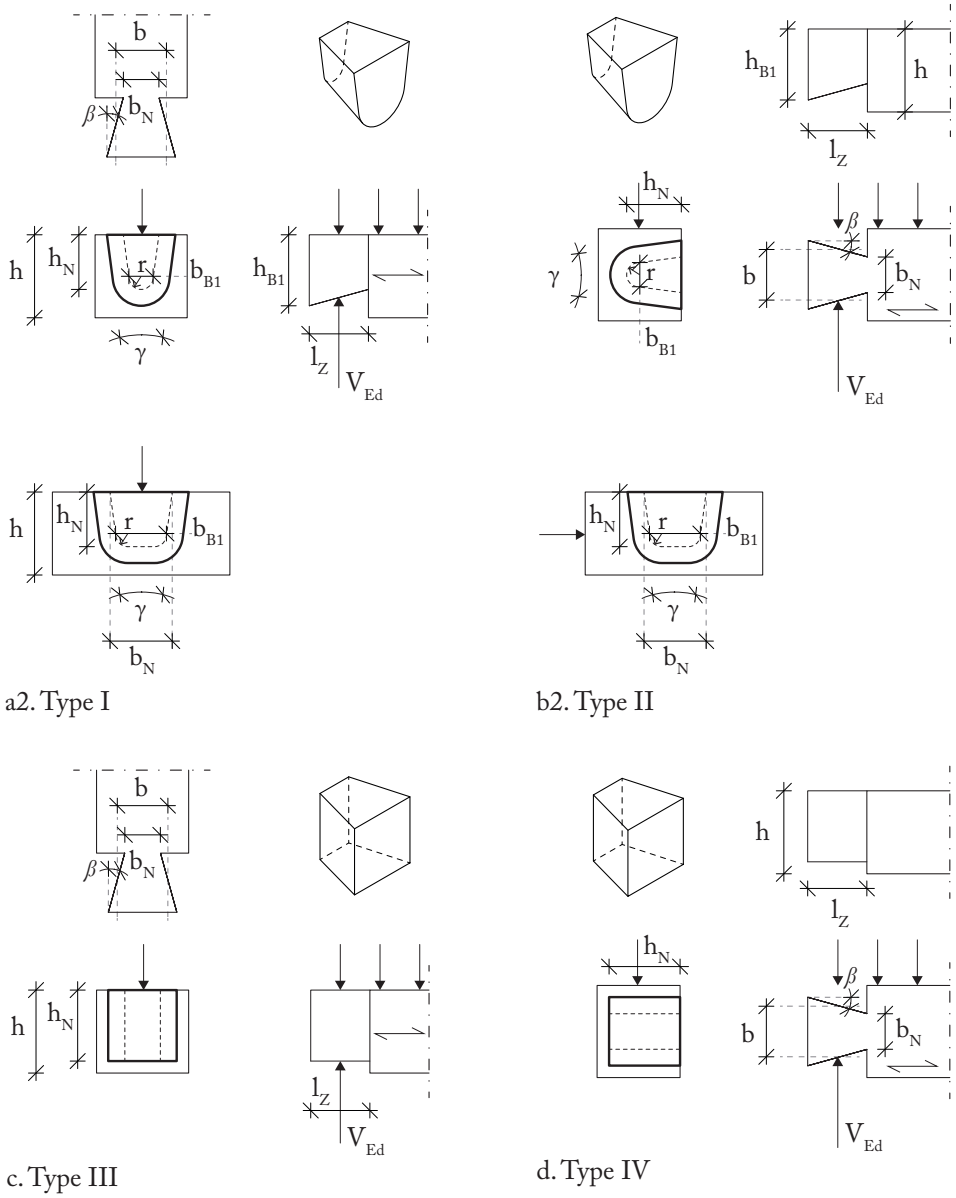

Figure 23. *a. and b. Geometry of a rounded dovetail for two different load cases. c. and d. Geometry of a straight dovetail for two different load cases.*

6.1.2.1. Dovetail type I

Dovetail type I is the most common geometry when it comes to calculations and could be found in several sources. The tension perpendicular to grain and shear stress verification for this is very similar as for a notch. A comparison with motivation of the choice of equation for verification of this failure mode can be seen in Chapter 5 in the report. The resulting equation is eq. (23) *(CEN, 2019)*.

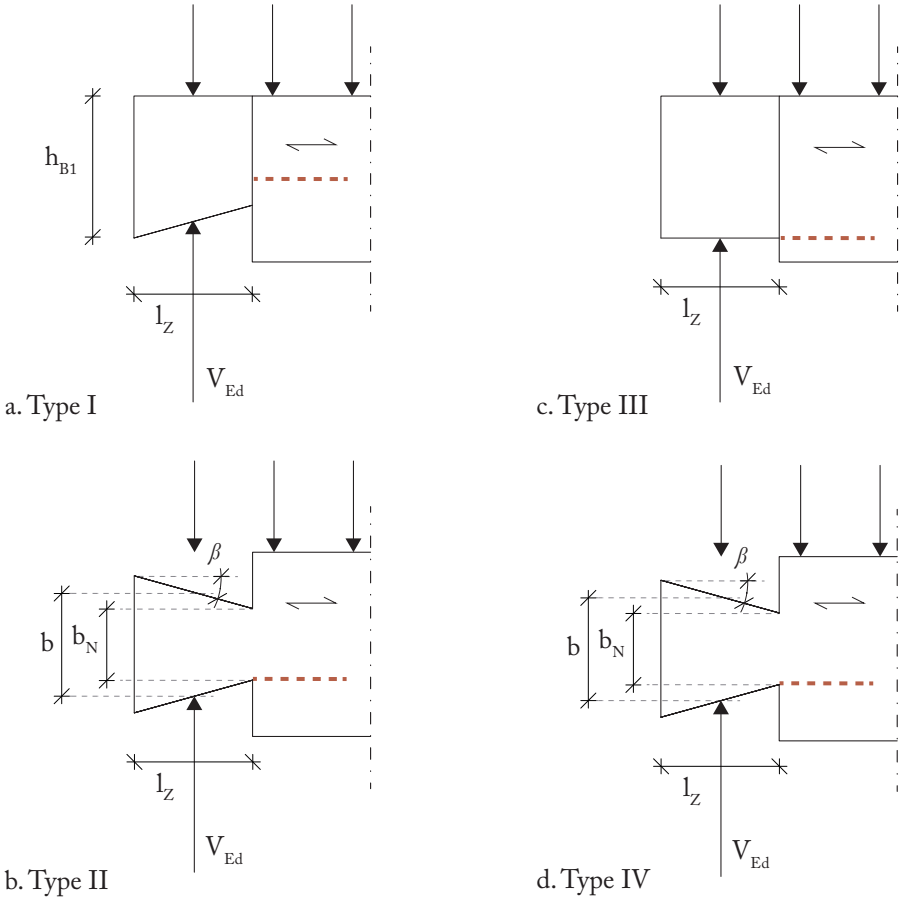

Figure 24. *Shear and tension failure perpendicular to the grain at the notch corner for the four different geometries shown in Figure 23.*

$$F_{v,Rd} = \frac{2}{3} \cdot \left(b_{B1} \cdot \left(h_{B1} - r \right) \right) \cdot k_v \cdot f_{v,d} \geq V_{Ed} \tag{23}$$

Where:

b_{B1} is the smallest width of the dovetail, see Figure 23.a.

h_{B1} is the largest height of the dovetail, see Figure 23.a.

r is the radius of the bottom fillet of the dovetail, see Figure 23.a.

$k_v = \left(\frac{h_{B1}}{h} \right)^2$ is the design compression strength perpendicular to the grain of the material.

$f_{v,d}$ is the design shear strength of the material.

V_{Ed} is the dimensioning shear force.

6.1.2.2. Dovetail type II

For the dovetail with the load as in Figure 23.b. the shear capacity is calculated according to DIBT *(2018)*. Where it is approximated that the reaction force is applied at the centre of the dovetail height. Even though the dovetail is not symmetrical over it's height, h_N, this is an approximation.

$$F_{v,Rd} = \frac{2}{3} \cdot b_{N,ef} \cdot h_N \cdot k_v \cdot f_{v,d} \geq V_{Ed} \tag{24}$$

Where:

$b_{N,ef} = b_N - h_N \cdot \tan\left(\frac{\gamma}{2}\right)$ is the approximated width of the dovetail.

b_N is the inner width of the dovetail, see Figure 23.b.

h_N is the smallest height of the dovetail, see Figure 23.b.

γ is the vertical angle of the dovetail, see Figure 23.b.

k_v is calculated according to equation (7) where:

$i = 0$ is the inclination of the notch corner.

$h = b$ is the width of the joist, this is limited to $\leq 0.8 \cdot b_N$ as explained in Chapter 5 in the report.

$x = \frac{l_z}{2}$ is the length from the reaction force to the notch corner.

and $\alpha = \frac{0.5 \cdot \left(b_N + b_{N,ef}\right)}{b}$

6.1.2.3. Dovetail type III

This type of dovetail and orientation in relation to the load is the same as a notched joint and the same verifications are performed according to Chapter 4.1.2.

6.1.2.4. Dovetail type VI

For the type of dovetail in Figure 23.d. the same verification is made as in Chapter 6.1.2.2. where the only difference is that there are no angles, γ and β, of the dovetail, hence:

$b_{N,ef} = b_N$ is the effective width of the dovetail.

h_N is the height of the dovetail, see Figure 23.d.

6.1.2.5. Modifications for CLT

The same modifications are made as for top notches or tenons according to chapter 4.1.2.1.

6.1.3. Compression failure perpendicular to the grain at the bottom of the dovetail

This is also a similar failure mode as that for a notched beam therefore this verification is made by following the method in Chapter 4.1.3. but where:

$$b_N = \begin{cases} b_N & \text{Dovetail type I and III} \\ h_N & \text{Dovetail type II and IV} \end{cases}$$

6.1.4. Rolling shear failure in the tenon (only for CLT)

This failure is the same as that shown in Chapter 4.1.4. but with minor modifications to better approximate the geometry of the dovetail. Depending on orientation of the dovetail and the load the geometry is approximated differently. See Figure 25.

For all of the dovetail types the rolling shear verification is simplified as much as possible by approximating each layer to a rectangular cross-section within the dovetail.

6.1.4.1. Dovetail type I

Very similar to the notched geometry but where $b_N = b_{B1}$ is used, which is the smallest width of the base of the dovetail. This is done to get the most conservative solution as can be seen in Figure 25.a.

6.1.4.2. Dovetail type II

For the rounded dovetail as seen in Figure 25.b. the cross-sections of each layer is limited by the smallest width b_{B1} and the smallest dovetail height h_N.

6.1.4.3. Dovetail type III and IV

For the straight dovetail in Figure 25.c. and d. the rolling shear layers are limited by the smallest width b_N and the height h_N.

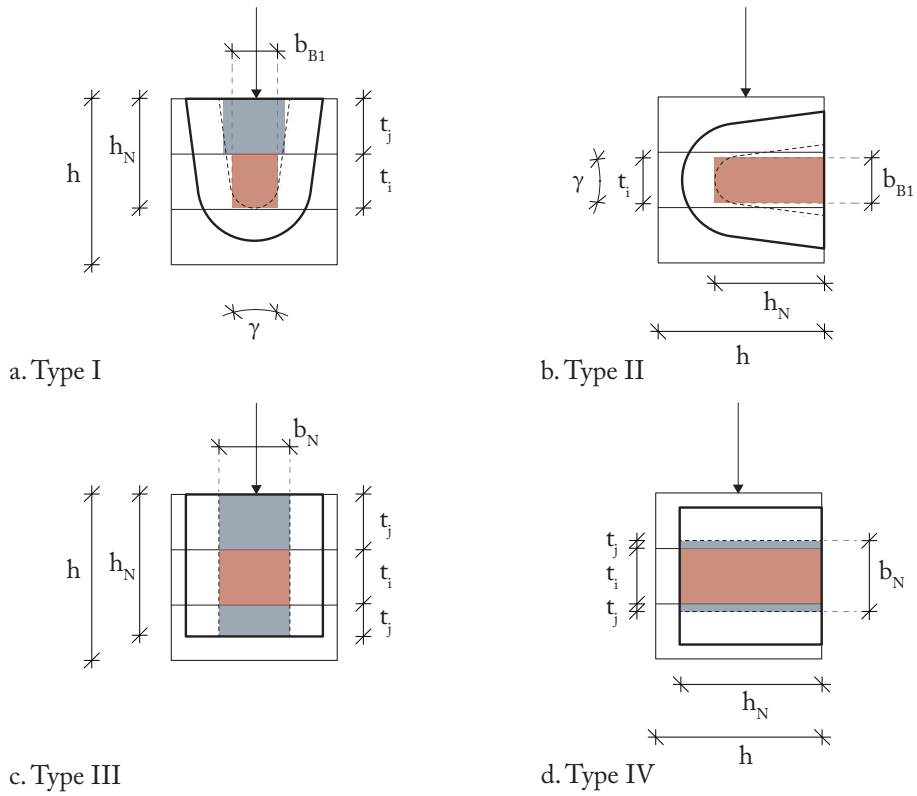

Figure 25. *Example of rolling shear layer approximation for the four dovetail types and load cases.*

6.2. HEADER MEMBER

The failure modes for the header of the dovetail are the same as for the header of the notched geometry seen in Chapter 4.2 with one additional failure mode for when an axial tension force is applied on the connection.

6.2.1. Geometry

The general geometry of the header corresponding to all four types of dovetails in Chapter 6.1 can be seen in Figure 26.

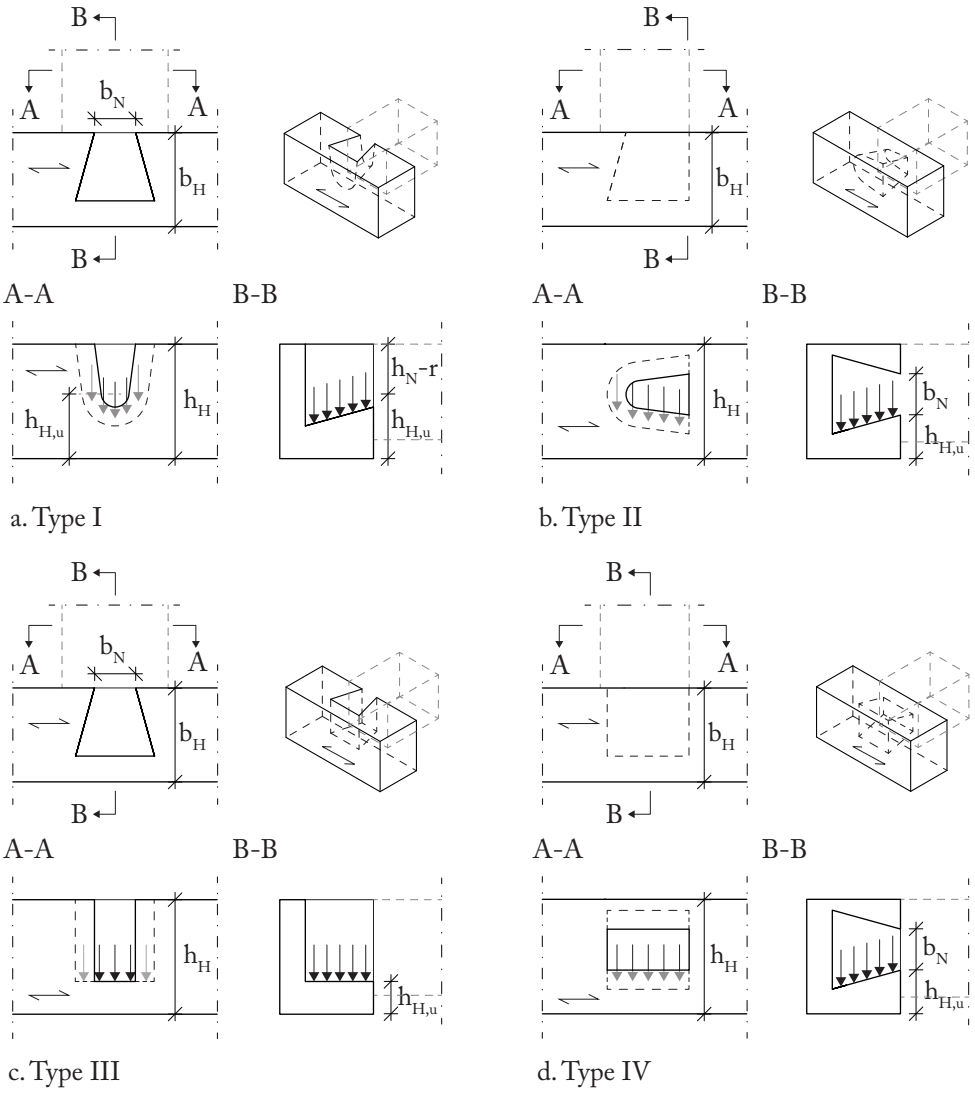

Figure 26. *Geometry of a header for the four different types of dovetail geometries.*

6.2.2. Shear and tension failure perpendicular to the grain at the notch corner

6.2.2.1. Dovetail type I

This failure is similar to that shown in Chapter 4.2.2. for a notch but where the crack propagation occur at the height of the transition between the straight tenon and the lower fillet similarly as for the joist with a dovetail *(Blaß & Sandhaas, 2017)*. This can be seen in Figure 27.

6.2.2.2. Dovetail type II

For these type of geometries of the header dovetail II is approximated to the geometry of dovetail IV by ignoring the slight angle, γ , of the dovetail and assume that the crack occurs at the height where the width of the dovetail is largest. This will give a $h_{H,u}$ as seen in Figure 27 and the verification can be performed by the method in Chapter 4.2.2.

6.2.2.3. Dovetail type III

The geometry of this dovetail does not affect the location of the crack or the verifications as the bottom surface of the dovetail is plane and horizontal the same as a regular straight notch and the same verifications as in Chapter 4.2.2. can be followed.

6.2.2.4. Dovetail type IV

For geometry type IV the crack is assumed to appear at the smallest width of the dovetail which gives the geometrical values as seen in Figure 27. By this the same verifications as seen in Chapter 4.2.2. can be followed.

6.2.2.5. Modifications for CLT

The same modifications as in Chapter 4.1.2.1. are made for all the different geometries of the dovetail but with the already made modifications of the height of the crack made in Chapter 6.2.2.1 - 6.2.2.4.

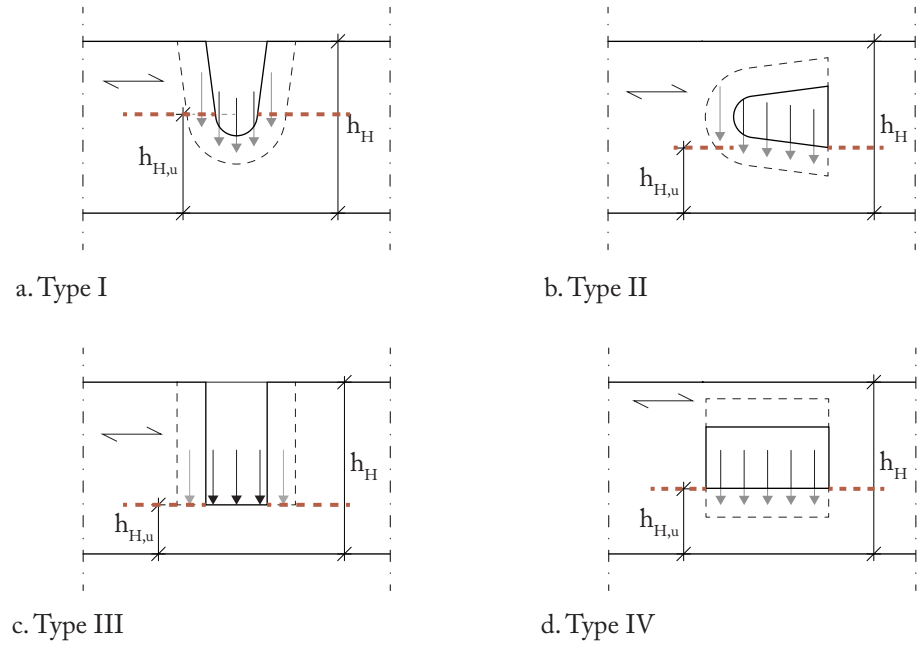

Figure 27. *Shear and tension failure perpendicular to the grain in the header for the four different geometries shown in Figure 26.*

6.2.3. Tension failure perpendicular to the grain due to an axial force in the joist

This failure mode is similar to the failure in shear and tension perpendicular to grain at the inner notched corner of the header. For that failure mode the vertical load acts perpendicular to the crack propagation. When treating the geometry of this failure mode in a similar way the tension force act perpendicular to the crack propagation and the failure can be verified in a similar way as described in Chapter 4.2.2.
This failure mode is not relevant for a dovetail that goes through the full header, hence where $l_z = b_H$, as the crack appears at the end of the dovetail as seen in Figure 28.

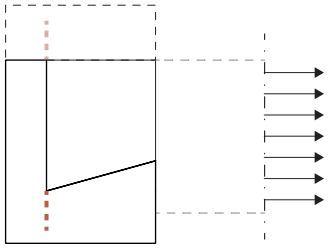

Figure 28. *Tension failure perpendicular to the grain in the header for an axial tension force acting on the joist.*

The only differences between the two verifications are minor geometrical differences where:

$b_{H,ef} = h_{H,ef}$ the height is used instead of the width of the header.

$h_{H,u} = l_z$ relates to the depth of the crack.

6.2.3.1. Modifications for CLT

For a header with a grain orientation as seen in Figure 15.c. the tension perpendicular to the grain should be verified for CLT headers in the same way as seen in Chapter 6.2.3. For other orientations of the CLT part of this area will have grain direction parallel to the axial force and this type of verification is not needed.

6.2.4. Compression failure perpendicular to the grain at the bottom of the mortise

Similar to a notch the compression perpendicular to the grain can be verified for the header of a dovetail joint. This is done by following the verifications in Chapter 4.2.3.

6.2.4.1. Modifications for CLT

The same modifications are made as in Chapter 4.2.4. but where $A_{B,ef} = A_{D,ef}$ as illustrated in Chapter 6.2.3.

6.2.5. Compression failure perpendicular to the grain due to an axial force in the joist

Similar to a notch the compression perpendicular to the grain can be verified for the header of a dovetail joint. This is done by following the verifications in Chapter 4.2.4 but where the area A_N of the dovetail can be approximated for simplicity. This should be done so that the outcome is a larger area than the true area for a conservative solution.

6.2.5.1. Modifications for CLT

The same modifications are made as in Chapter 4.2.4. but where $A_{B,ef} = A_{D,ef}$ as illustrated in Chapter 6.2.3.

7. VERIFICATION OF PEG JOINTS

The laterally loaded peg and it's supporting element is verified according to CEN *(2017)*.

7.1. PEG

7.1.1. Geometry

The geometry of the peg joint evaluated in this thesis can be seen in Figure 29 with its relevant variables.

7.1.2. Shear failure of a laterally loaded peg joint

This failure mode of the peg is illustrated in Figure 30.

$$F_{v,\,Rd} = \frac{9.5 \cdot n \cdot d^{2} \cdot k_{\mathrm{mod}}}{\gamma_M} \geq F_{Ed} \tag{25}$$

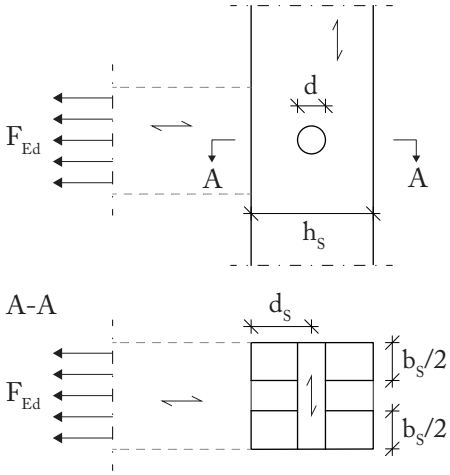

Figure 29. *Geometry of a peg joint illustrating both the peg and supporting member with relevant variables.*

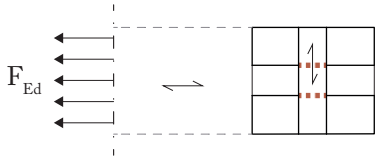

Figure 30. *Shear failure of a laterally loaded peg.*

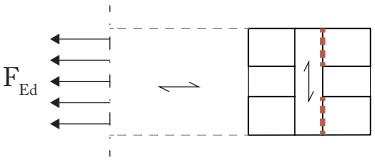

Figure 31. *Tension failure perpendicular to the grain in the supporting element.*

Where:

n	is the number of pegs in the joint.
d	is the diameter of the peg, see Figure 29.
γ_M	is the partial coefficient for the material properties (Recommended values in Table 1).

k_{mod} is the correctional factor with regard to load duration and moisture content (Recommended values in Table 3).

F_{Ed} is the dimensioning lateral force, see Figure 29.

7.2. SUPPORTING MEMBER

7.2.1. Geometry

The geometry of the supporting member of the peg is illustrated in Figure 29 with its relevant variables.

7.2.2. Tension failure perpendicular to the grain of the supporting member

This failure mode of the supporting member can be seen in Figure 31.

$$F_{90,Rd} = 14 \cdot b_S \cdot \sqrt{\frac{d_S}{1 - \frac{d_S}{h_S}}} \cdot \frac{k_{\text{mod}}}{\gamma_M} \geq F_{Ed} \tag{26}$$

Where:

b_S is the width of the supporting member, see Figure 29.

d_S is the distance from the centre of the peg to the end of the supporting element in the direction of the force, see Figure 29.

h_S is the full depth of the supporting member, see Figure 29.

γ_M is the partial coefficient for the material properties (Recommended values in Table 1).

k_{mod} is the correctional factor with regard to load duration and moisture content (Recommended values in Table 3).

F_{Ed} is the dimensioning lateral force, see Figure 29.

7. PRELIMINARY PROPOSAL

The preliminary selection of the joints for C1 and C2 is based on the results of hand calculations but also to some extent on the criteria from Chapter 4. A couple of chosen connections are made as prototypes in models which also better illustrate some strengths and weaknesses of each connection. This chapter presents the results of hand calculations, prototypes and the final selection of two possible connections for each joint.

DESIGN VERIFICATIONS

The full design verification is presented in Appendix B3 and B4 for the connections analysed for C1 and C2.

The results are presented as utilization rates where either the load capacity is compared to the applied load or a stress is compared to the strength of the material.

The failure modes not calculated, as shown in the tables, are not needed based on either the material used in the connection, grain orientation or due to the geometry of the connection.

C1

For the design verification see Table 7.1.

Table 7.1. *A summary of the utilization rate for the different connections for C1.*

Failure Mode	Load	Ratio			
		PD1	PD2	P1	P2
Joist					
1. Failure in shear and tension perpendicular to the grain.	Vertical	0.4 %	0.4 %	-	-
	Horizontal	11 %	10 %	8.0 %	8.0 %
2. Failure in compression perpendicular to the grain.	Vertical	0.2 %	0.1 %	0.2 %	0.2 %
	Horizontal	3.8 %	2.4 %	1.6 %	1.6 %
3. Rolling shear failure of the notch (only for CLT).	Vertical	-	-	-	-
Header					
4. Failure in shear and tension perpendicular to the grain.	Vertical	-	-	-	-
	Horizontal	2.3 %	2.3 %	3.0 %	3.0 %
5. Failure in compression perpendicular to the grain.	Vertical	-	-	-	-
	Horizontal	3.2 %	1.6 %	1.3 %	1.3 %
6. Failure in compression perpendicular to the grain due to an axial compression force on the joist.	Axial	10 %	10 %	19 %	19 %
7. Failure in tension perpendicular to the grain due to an axial force on the joist.	Axial	18 %	-	-	-
Peg					
8. Failure in shear of a laterally loaded peg joint.	Axial	-	-	40 %	**160 %**
9. Failure in tension perpendicular to the grain.	Axial	-	-	28 %	28 %

Based on the utilization ratio the only connection that fails in one regard is connection P2 with the thinnest peg.

C2

For the design verification see Table 7.2.

Table 7.2. *A summary of the utilization rate for the different connections for C2.*

Failure Mode	Load	Ratio		
		RD1	TM1	N2
Joist				
1. Failure in shear and tension perpendicular to the grain.	Vertical	88 %	-	15 %
	Horizontal	7.5 %	2.6 %	-
2. Failure in compression perpendicular to the grain.	Vertical	11 %	4.0 %	2.0 %
	Horizontal	-	-	-
3. Rolling shear failure of the notch (only for CLT).	Vertical	1.7 %	0.2 %	1.1 %
Header				
4. Failure in shear and tension perpendicular to the grain.	Vertical	7.3 %	8.6 %	8.6 %
	Horizontal	-	-	-
5. Failure in compression perpendicular to the grain.	Vertical	-	-	-
	Horizontal	-	-	-
6. Failure in compression perpendicular to the grain due to an axial compression force on the joist.	Axial	0.2 %	0.4 %	0.4 %
7. Failure in tension perpendicular to the grain due to an axial force on the joist.	Axial	-	-	-
Peg				
8. Failure in shear of a laterally loaded peg joint.	Axial	-	-	-
9. Failure in tension perpendicular to the grain.	Axial	-	-	-

PROTOTYPES

Model prototypes were designed in order to identify possible strengths and weaknesses with regard to manufacturing, architectural design and assembly. Four of the connections were selected for these prototypes, PD1 and P1 for C1, and RD1 and N2 for C2. The models are made in scale 1:2.5 and by using hand tools as well as a three-axis CNC-milling machine. The materials used are made to scale with lamellae size from Martinsons *(2020)*.

Photos of the prototypes can be seen in Figure 7.1 - 7.4.

Figure 7.1. *Model photography of connection PD1 for C1.*

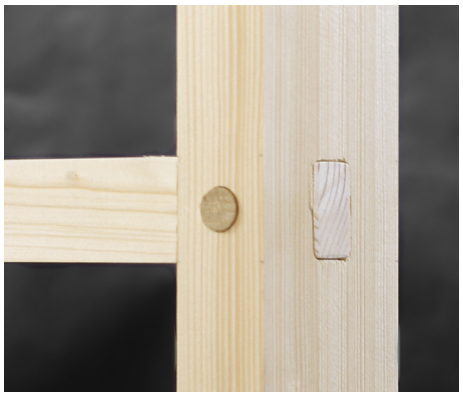

Figure 7.2. *Model photography of connection P1 for C1.*

Figure 7.3a-b. *Model photographies of connection RD1 for C2 in two different views.*

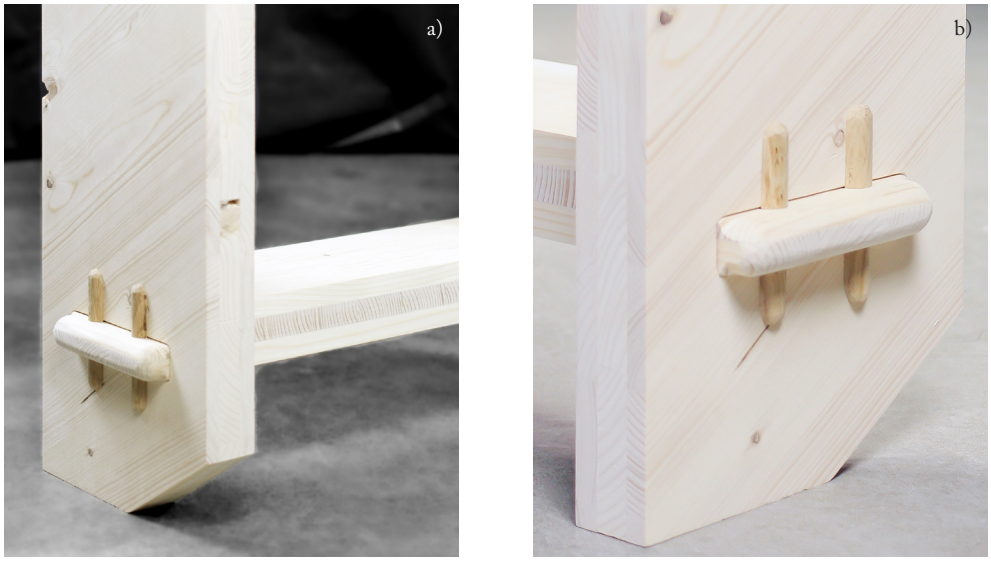

Figure 7.4a-b. *Model photographies of connection N2 for C2 in two different views.*

The manufacturing process itself is difficult to asses since the models are made using a three-axis CNC-machine. These would most likely be made in a five-axis machine with interchangeable tools in reality. This would therefore diminish the problems of manufacturing that occurred for these prototypes. What could be concluded from this are some geometrical difficulties, especially using CLT in the dovetail. It can be difficult to control that not too small pieces of single lamella occur, depending on where the lamellae and cuts end up.

The architectural design was mainly assessed by how clearly visible the connections are. The connections PD1, PD2 and TM1 look to be less visible since the prototype of PD1 only consist of two members with the same materiality.

With regard to assembly, connection P1 is the most difficult as the pillars need to be "moved" in order to assemble the system which would not be preferable. The strengths and weaknesses for each prototype can be seen in Table 7.3.

Table 7.3. *A summary of the strengths and weaknesses of each prototype.*

	Strengths	*Weaknesses*
PD1	Easy on-site assembly	Difficult geometry to manufacture Not very visible Not locked for loads in all directions
P1	Mixes different types of wood which increases visibility Locks in all load directions	Difficult assembly
RD1	Mixes different types of wood which increases visibility Locks in all load directions	Difficult geometry to manufacture
N2	Mixes different types of wood which increases visibility Locks in all load directions Easy to manufacture	Small pegs close to the edge could possibly lead to cracks

DESIGN SELECTION

Based on the calculations and conclusions from the prototypes four of the connections were selected, two for C1 and two for C2. Minor modifications are made to account for weaknesses.

A general difference between the geometries used for the hand calculations and the prototypes and selected designs are some small adjustments needed for manufacturing and assembly. This is for example the rounded corners that were made by the drill of the CNC-machine and the hardwood pegs and blocks for connection C2. The rounded corners will theoretically also improve the design by reducing stress increments in the corners. The pegs and blocks were added both to improve the visual impact and to permit the assembly of the members.

The assembly process for all selected connections is illustrated in Figure 7.9.

C1

PD1

Modifications for PD1 were made in order to lock the connections for all load directions and to make it more visual. In order to achieve this pegs are inserted on the outside of the header (pillar), see Figure 7.5. This will not affect the on-site assembly process substantially.

P1

Connection P1 is selected in comparison to P2 since this solution fails for the peg. Despite the slightly more difficult assembly process this is still regarded as a possible solution. An illustration of the connection can be seen in Figure 7.6.

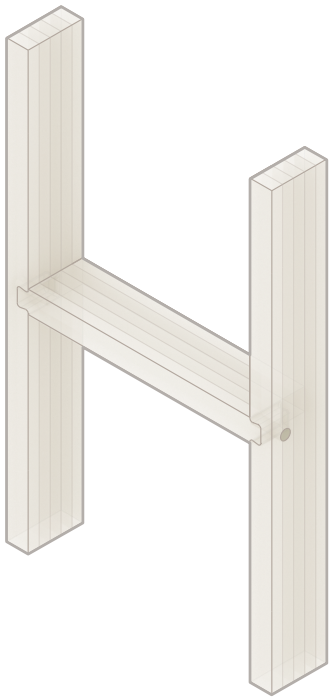

Figure 7.5. *Illustration of preliminary connection PD1.*

Figure 7.6. *Illustration of preliminary connection P1.*

RD1

No failures occur for connection RD1. As for many of the connections, a lot of the utilization ratios are well under their limit. The geometry of the connections are kept in order to simplify manufacturing and in order to look structurally sound for the users. The preliminary outcome of connections RD1 can be seen in Figure 7.7.

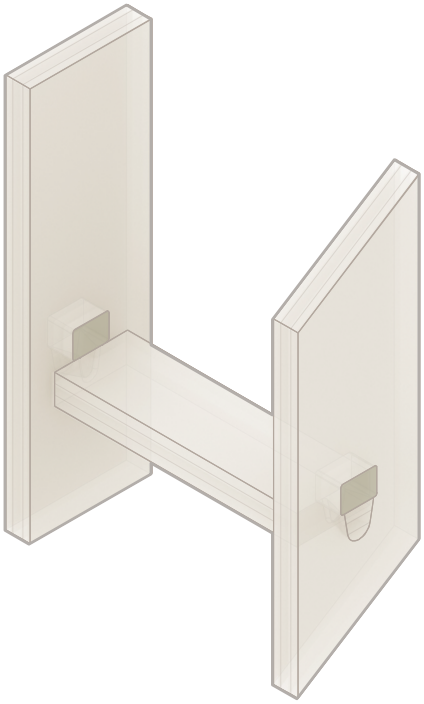

Figure 7.7. *Illustration of preliminary connection RD1.*

N2

Connection N2 shown in Figure 7.8 is selected mainly due to its strong structural capacity, simplicity to manufacture and visual impact. The added element of pegs on the outer side of the railing are verified in shear failure.

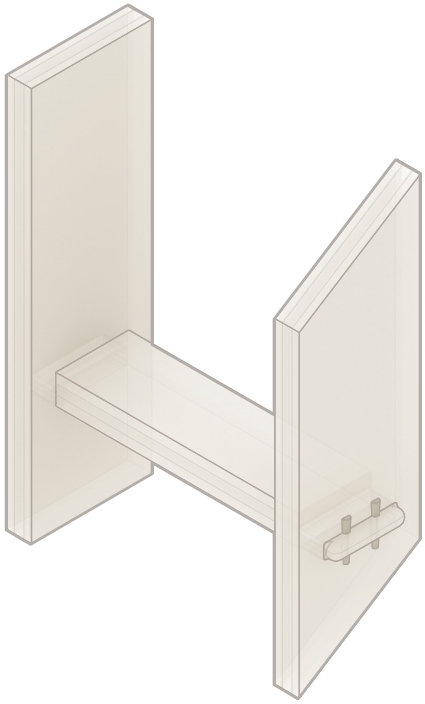

Figure 7.8. *Illustration of preliminary connection N2.*

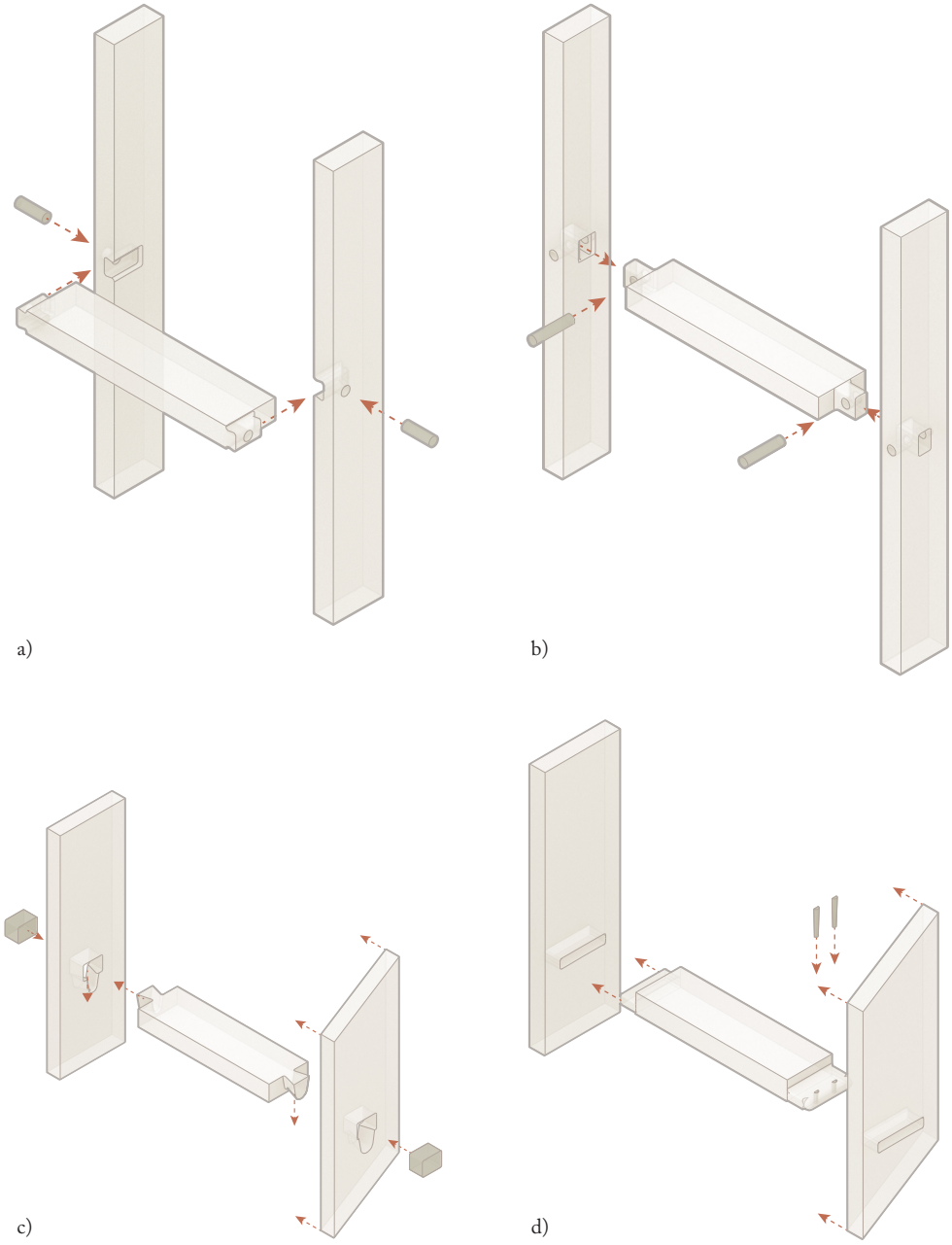

Figure 7.9. *Assembly of all four selected connections.* a. *PD1, C1*, b. *P1, C1*, c. *RD1, C2*, d. *N2, C2.*

8. DISCUSSION AND CONCLUSION

This chapter includes the final discussion of the results and analysis of the FE-modelling, calculation method and connection design. Discussed is also possible future studies relating to the thesis.

General calculation method

The primary result of this thesis is the general calculation method in Chapter 6. The main difference between this method and other standards published are the modifications for CLT and the comprehensive collection of different geometries and their respective failure modes. From the compiled research it can be concluded that most of the validated calculation methods that already exist rarely include many different types of carpentry joints and the correlation between these. Few of the sources utilized include as many failure modes for each connection type as the method in Chapter 6. For future reference it would therefore be interesting to investigate if all the possible failure modes within the calculation method actually need to be verified. It is our conclusion that the verifications analysed are needed in order to validate the connections for all different types of load application. An interesting future study with regard to the calculation method would be to include a moment in the connections.

With regard to the adaptation of the calculation method for different materials, glulam do not vary from the case of solid timber, except for the specific material constants. CLT, on the other hand, includes many modifications that would be interesting to validate with further studies and live testing. This is a material that is quite new within construction and very little material on the subject of connections in CLT exist today. This is for example the equation for validating one or several layers of CLT as reinforcement. This equation is adapted from the verification of external reinforcement of glued-on wooden plates. This might differ for CLT as this is both internal and might be adhered to the other layers differently.

The credibility of the method can be discussed based on the limitations of geometry that are not taken into account for many of the verifications. This was a choice in order to be able to adapt the method for larger connections since many of the limitations result in smaller proportions. It is likely that many of the limitations are established by the development of the verifications through testing. The geometrical limits are set based on the test geometries even though it is likely that the verifications hold for other sizes as well. Through this some constants in the equations could be needed to be modified in order to include other geometrical constraints. This could also be an interesting future investigation regarding this thesis.

One possible failure mode not included in the method or any of the found sources is the slipping of the dovetail and failure of the angled joist geometry in shear. For future iterations this would be relevant to investigate and add to the method. The validity of the results of the thesis are not assumed to be unreasonable, based on that the geometries do not differ extensively from the limits set in the sourced equations. Further improvements for the calculation method, might be the possibility of slight modifications to include even more geometries than what is already included. Similarly to the many small modifications made to the dovetail in order to approximate it as a notch. Another prospect of the method is to use it for other materials such as LVL and Plywood that are similar to the analysed materials but have slightly different grain structures and material properties.

Assumptions and modifications of the design

With regard to the preliminary design some assumptions and simplifications made within the verifications may result in non-conservative solutions. This is for example the simplification to disregarding the grain orientation of the railing in connection C2. This could be another iteration to implement in the calculation method, to consider grain orientations that differ from orthogonal solutions.

Another simplification made is the assumption of calculating the reaction forces for a simply supported beam for both connections. With analysing the FE-models it can be seen that this might not be the closest approximation to the real load case that can be made. Another load case would result in a moment in the connection which is why the simplification was made. It is rare to assume that a timber connection can take moments and it is concluded that this is a reasonable assumption to make for the hand calculations.

With this mentioned it could be relevant for future development of carpentry connections to use FE-modelling as a part of the design. In this thesis the FE-modelling was mainly used as a starting point of designing the hand calculation method. Within the design process FE-modelling is an important tool to use. In reality it would be preferable to use hand calculations as a preliminary design step and then finalize the design with the help of this type of analysing tool. This might then be able to validate the connection more thoroughly and together with the hand calculations give a strong motivation for the design.

Implementation

The aim of this thesis is to design a calculation method for some general carpentry joints. The objectives within this is to investigate the possibility of using carpentry joints in larger constructions.

This is made by an iterative process of designing several possible solutions for two different connections, one in CLT and one in glulam.

The connections chosen in this thesis are smaller connections excluded from the main load-bearing system of the building and therefore not exposed to larger loads. What can be concluded from the results of the hand calculations for the connections is that most of them are designed with capacities well above the applied load. They will therefore, most likely, be able to handle larger loads as in, for example, a connection between a timber roof member and outer wall member.

For further studies it would be relevant to implement the method in larger construction joints with higher applied loads in order to determine this explicitly. With regard to many coefficients used in the equations it would also be relevant to live test larger connections. To see if the results are proportional to the size and load or if the size would affect the equations themselves.

Summary

As a final review of this thesis the primary results with the general calculation method do include many interesting features of carpentry joints. The resulting designs from the research made and the verification based on the calculation method does suggest that carpentry joints are reasonable to use in construction. This was the main goal and hypothesis of this thesis. Further studies would be needed in order to validate this type of method in proper practice.

Although, what can be concluded from this study together with the reference projects, that are already using carpentry connections to some extent, is that using these type of joints in larger constructions are not an unreasonable idea and has many arguments promoting its case.

BIBLIOGRAPHY

AIX Arkitekter. (2020).*Drawings for BT7*. Drawing credit: architect Karin Löfgren.

Al-douri, H. and Hamodi, K. (2009). *Compression Strength Perpendicular to Grain in Cross-laminated Timber (CLT)*. (Master's thesisSchool of Technology and Design, Växjö University, Växjö, Sweden). Retrieved 2020 from https://www.diva-portal.org/smash/get/diva2:223627/FULLTEXT01.pdf

Atashipour, R. (2020). *Timber Engineering – FE Lab* [PDF]. Retrieved from Chalmers University of Technology, Timber Engineering, Canvas.

Blaß, H. J., & Sandhaas, C. (2017). *Timber Engineering – Principles for Design*. Karlsruhe: Karlsruher Institut für Technologie Scientific Publishing. Almere: Centrum Hout.

Blumer-Lehmann. *Tamedia office building: First seven-storey wood structure*. (n.d.). Retrieved January 08, 2021, from https://www.lehmann-gruppe.ch/en/holzbau/referenz/tamedia.html

Branco, J. (2015). *Analysis and strengthening of carpentry joints*. Construction and Building Materials Vol. 97, No. 30 October 2015, pp. 34-47

Comité Européen de Normalisation. (2017). French contribution for traditional carpentry joints (Standards No. CEN/TC 250/SC 5 - N 672).

Comité Européen de Normalisation. (2019). *Background Carpentry connections, Dove Tail* (Standards No. CEN/TC 250/SC 5 - N 1086).

Crocetti, R. (2016). *Limträhandbok Del 2*. Stockholm, Sweden. Skogsindustrierna Svenskt Trä.

Dedijer, M. (2016) *Shear Resistance and Failure Modes of edgewise multiple tab-and-slot joint (MTSJ) Connection with dovetail design for thin LVL Spruce Plywood KER-TO-Q Panels*. WCTE2016 World Conference on Timber Engineering.

Deutsches Institut für Bautechnik. (2018). *Allgemeine bauaufsichliche Zulassung/Allgemeine Bauartgenehmigung: Schwalbenschwanz-Verbindung in Bauteilen* [General building approval / general type approval: Dovetail connection in components] (Standards No. Z-9.1-649). Retrieved 2020 from https://www.lohn-abbund.de/wp-content/uploads/ABZ-Z-9_1-649-Juni-2018-high.pdf

EPFL. *Timber Pavilion of the Vidy-Lausanne Theatre*. Photo Credit: Ilka Kramer. Retrieved 2020 from https://www.epfl.ch/labs/ibois/projects/completed-projects/vidy-pavilion/

Gustafsson, A., Crocetti, R., Just A., Landel P., Olsson J., Pousette A., Silfverhielm M., Östman B. (2019). *KL-trähandbok*. Stockholm, Sweden. Skogsindustrierna Svenskt Trä.

McLain, T. E. (1998). *Connectors and fasteners: Research needs and goals*. Wood Engineering in the 21st Century: Research Needs and Goals, K. J. Fridley, ed, ASCE, Reston, Virginia.

Martinsons. (2020). *Materialguide för Martinsons KL-trä* [Brochure]. https://martinsons.se/byggnader-i-tra/limtra-och-kl-tra-for-byggnadsobjekt/kl-tra/

Mayo, J. (2015). *Solid wood: Case studies in mass timber architecture, technology and design*. London: Routledge.

Middleton, B., & Middleton, B. (2020, March 09). *Hardwood vs Softwood: What's the Difference?*. Retrieved October 09, 2020, from https://www.laver.co.uk/blog/hardwood-vs-softwood-whats-the-difference/

Müller, A., Vogel, M., Lang, S., Sauser, F. (2016). *Historische Holzverbindungen: Untersuchung des Trag- und Lastverformungsverhaltens von histori-schen Vollholzverbindungen und Erstellung eines Leitfadens für die Baupraxis*. [Historical Timber Connections: Investigation of the load-bearing and load deformation behavior of historical solid wood connections and creation of a guideline for building practice]. Bern Institute of Applied Sciences.

Palma, P. (2016). *Dowelled Timber Connections with Internal Members of Densified Veneer Wood and Fibre-Reinforced Polymer Dowels*. WCTE2016 World Conference on Timber Engineering.

Sandhaas, C. (2018). *Design of Connections in Timber Structures*. Germany. A state-of-the-art report by COST.

Shigeru Ban Architects. (2014). *Tamedia Office Building* Published 24 Feb 2014. ArchDaily. Retrieved January 08 2021.

a. Swedish Standards Institute. (2009). *Eurocode 5: Design of timber structures – Part 1-1: General – Common rules and rules for buildings* (Standards No. SS-EN 1995-1-1:2004).

b. Swedish Standards Institute. (2009). *Eurocode 1: Actions on Structures – Part 1-1: General actions – Densities, self-weight, imposed loads for buildings* (Standards No. SS-EN 1991-1-3:2005).

Swedish Standards Institute. (2008). *Eurocode 1: Actions on Structures – Part 1-4: General actions – Wind actions* (Standards No. SS-EN 1991-1-4:2005).

Trähusbarometern. (n.d.). Retrieved October 09, 2020, from https://www.tmf.se/statistik/statistiska-publikationer/trahusbarometern/

X-fix. *Fix Brettsperrholz BSP Verbinder / CLT Connectors*. (n.d.). Retrieved 2020 from http://www.x-fix.at/

APPENDIX A

Appendix A consists of material for the architectural design process.

APPENDIX A1

LIBRARY OF CARPENTRY JOINTS

Tenon and mortise joints

The tenon and mortise joints normally connect members to form an "L" or "T" configuration. The two components consist of the tenon tongue and the mortise hole. This joint is normally used when the adjoining pieces are at an angle of 45 to 90 degrees *(Branco, 2015)*.

They can be locked or pinned into place and the connection can include shoulders to stabilize as well as different shapes of the tenon, such as rectangular or dovetail.

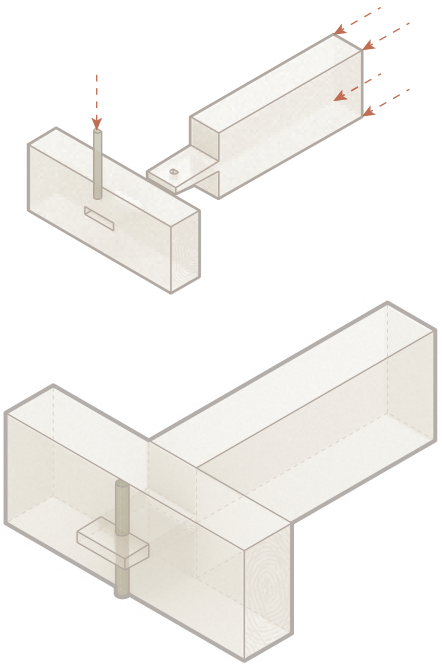

Figure 2. *Reverse dovetail through, pinned tenon and mortise joint.*

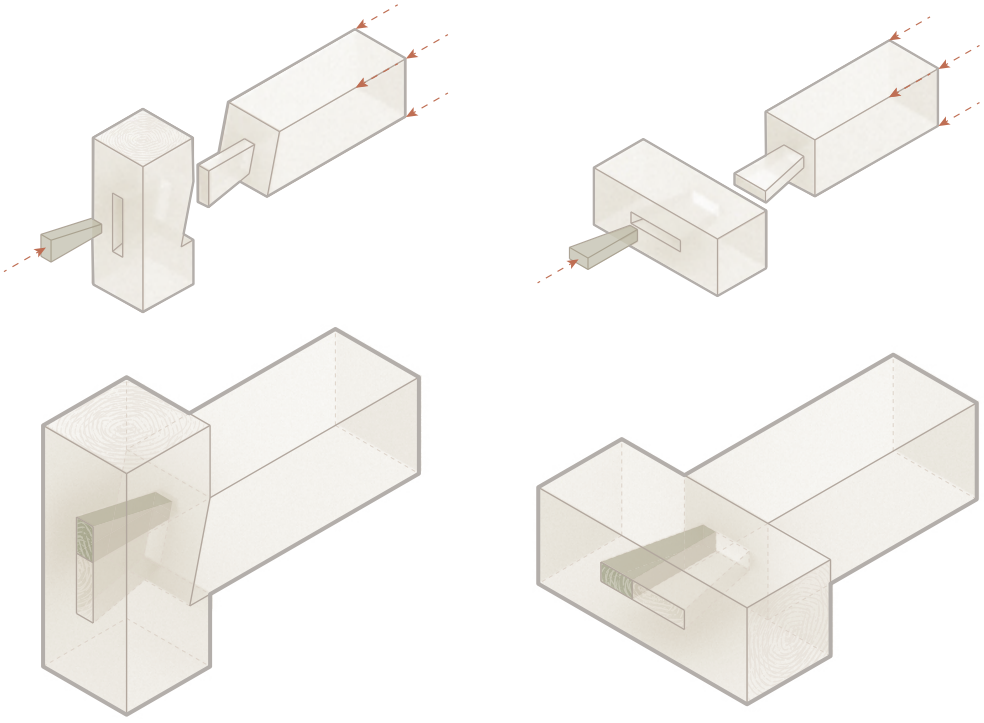

Figure 1. *Wedged dovetail joints with a half-shoulder.*

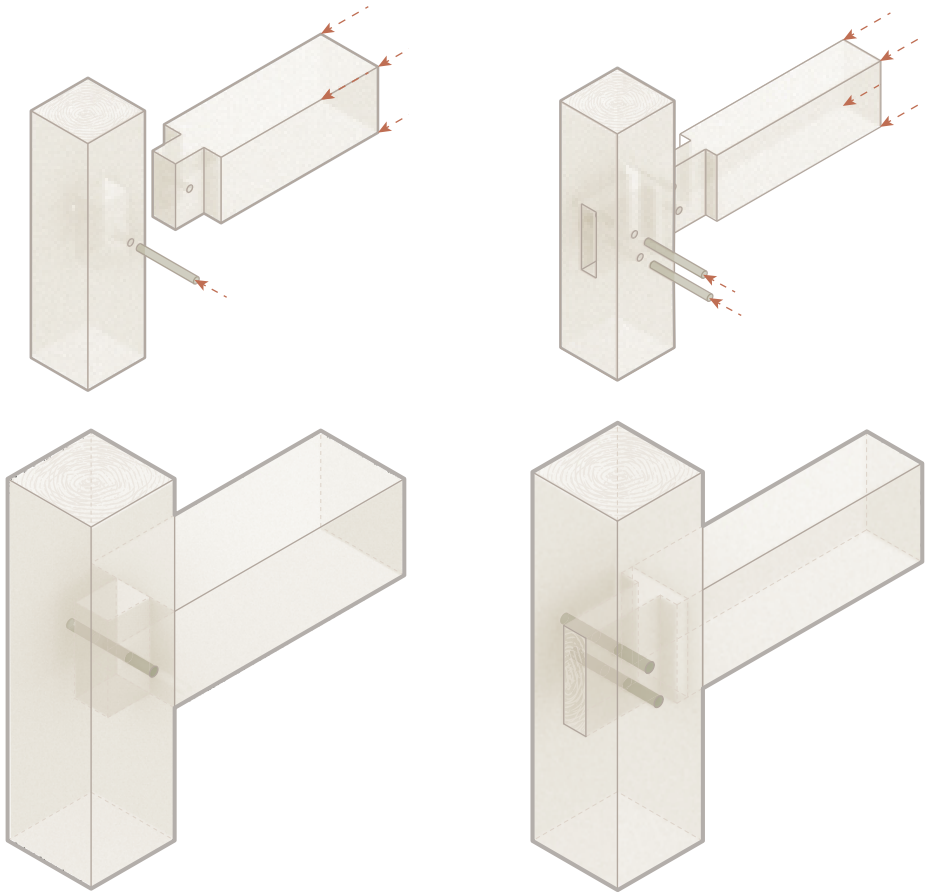

Figure 3. *Pinned tenon and mortise joints.*

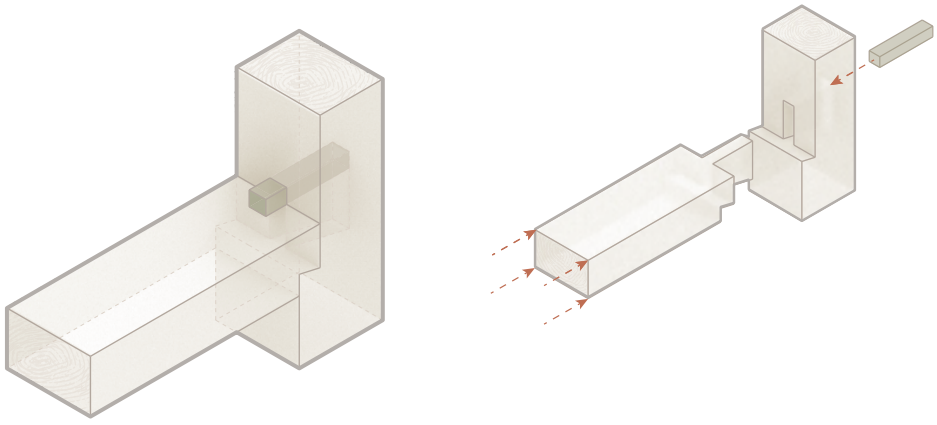

Figure 4. *Wedged dovetail joint with a cut-out angeled top notch.*

Lap joints

In the full lap joint no material is removed to create the joint. In a half-lap joint material is removed so that the resulting thickness of the joint is that of one of the members. The half-lap can be made with additional cogs. In the full lap joint no material is removed to create the joint. In a half-lap joint material is removed so that the resulting thickness of the joint is that of one of the members *(Branco, 2015)*. The half-lap can be made with additional cogs. The two last connections shown can be seen as both lap joints or tenon and mortise joints and the last is also a form of notched joint. The dovetail lap joint is a way to reinforce the joints tensile strength.

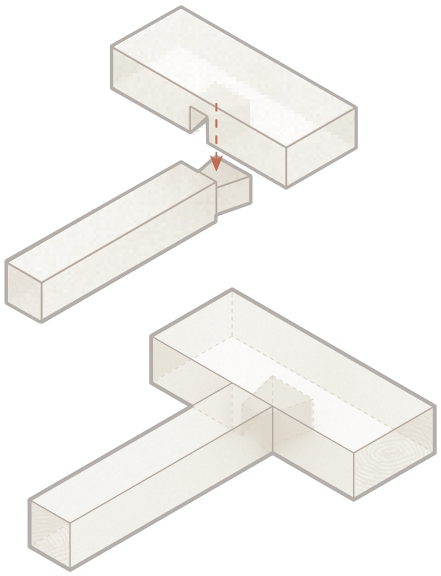

Figure 6. *Dovetail lap joint.*

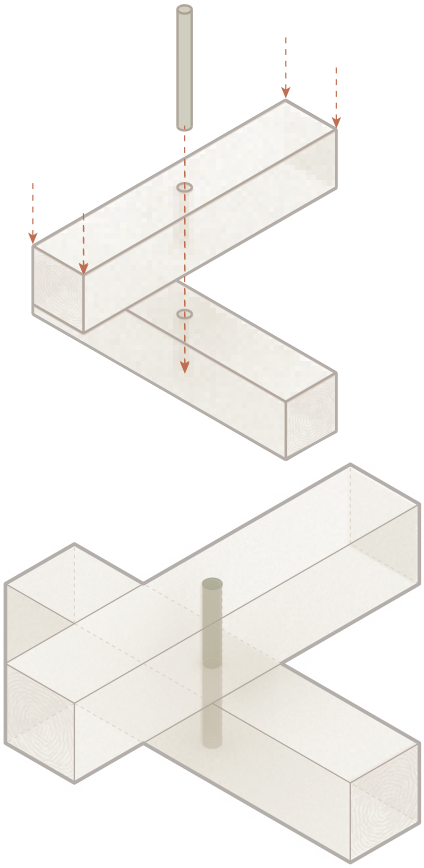

Figure 5. *Pinned full lap joint.*

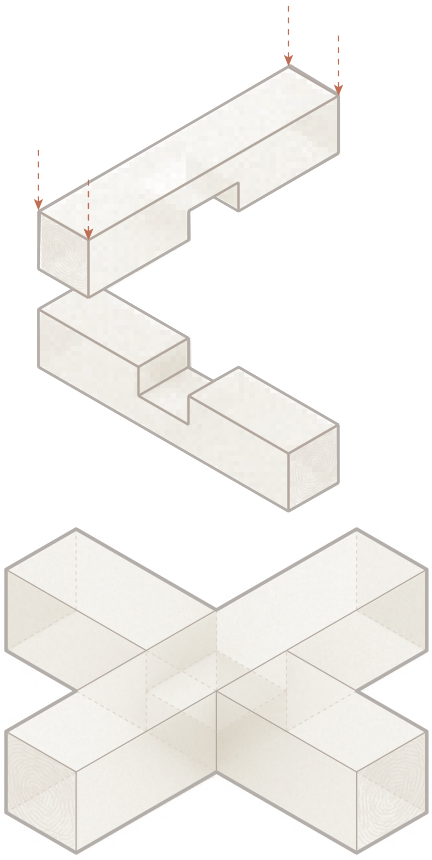

Figure 7. *Half lap joint.*

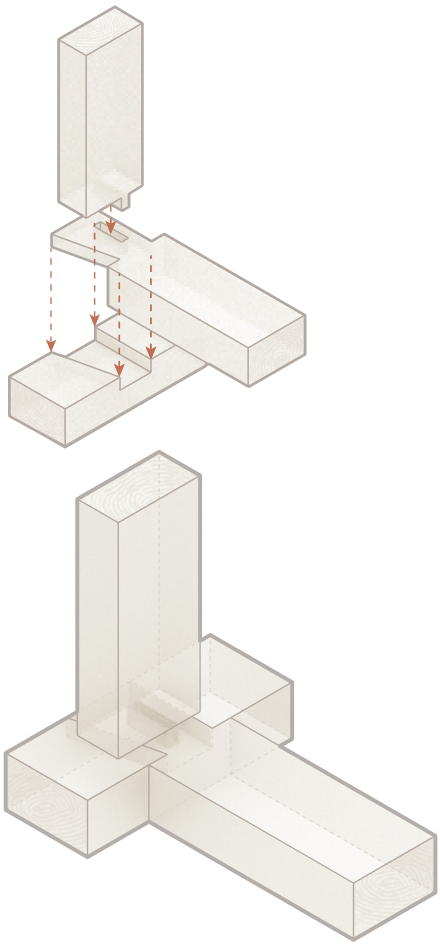

Figure 8. *Full lap joint with a vertical locking.*

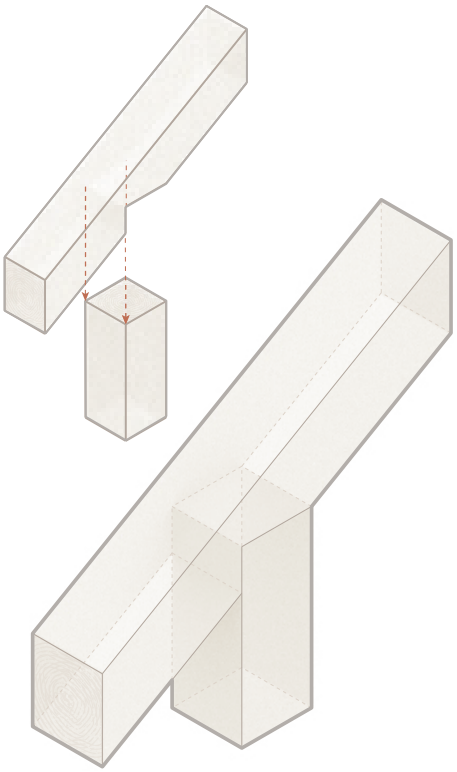

Figure 9. *Birdsmouth joint.*

Notched joints

This type of joint is connected to the development of king post-like frames. In order for these joints to work they need appropriate joinery at multiple locations for example tenons or pegs and pins.

A notch is a V shaped groove most commonly cut perpendicular from the beam *(Branco, 2015)*. A notch like this is usually called a birdsmouth joint. The joints shown below can more commonly be rounded or notched out with a diagonal to reduce the number of sharp corners and the stress extremes in these points.

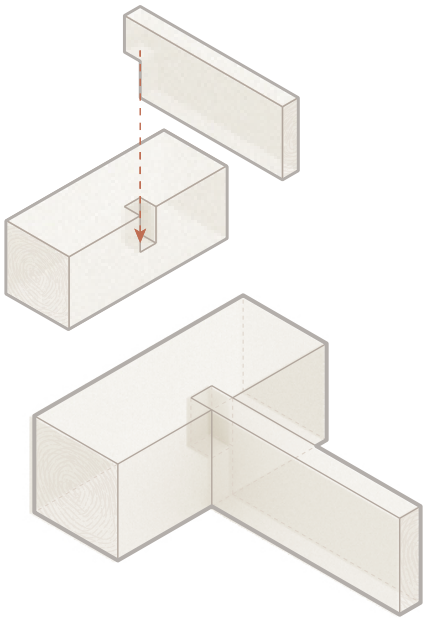

Figure 10. *Notched joint.*

Scarf joints

Scarf joints allow connection of two members at the end to, for example, extend the length of a post or beam. The scarf joints are more efficient when used with a "key" which is a wedge, or several wedges used to lock the joint that is usually made of hardwood *(Branco, 2015)*.

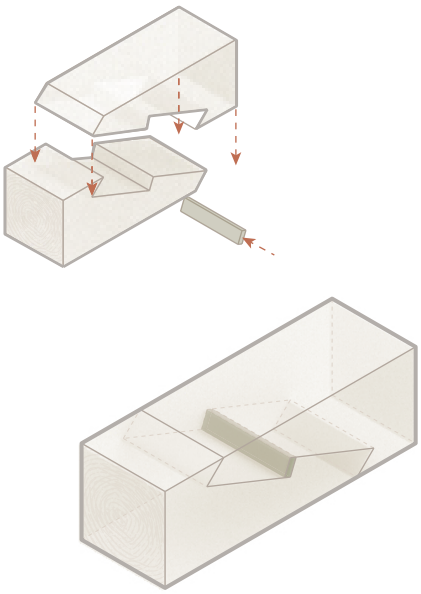

Figure 11. *Wedged scarf joint.*

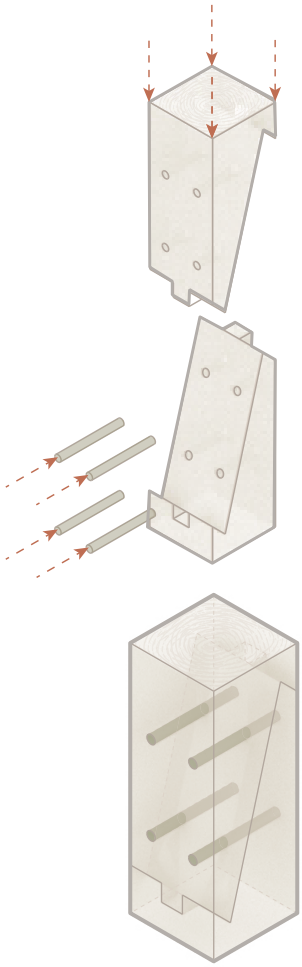

Figure 13. *Pinned scarf joint.*

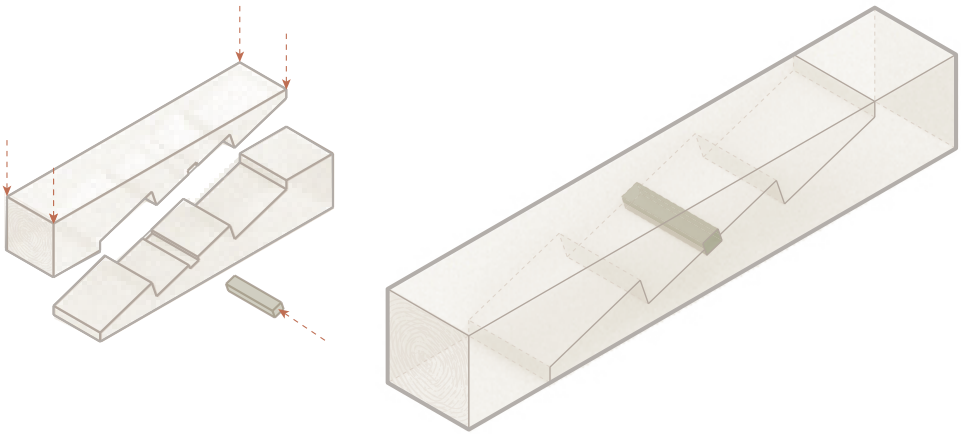

Figure 12. *Wedged scarf joints with steps.*

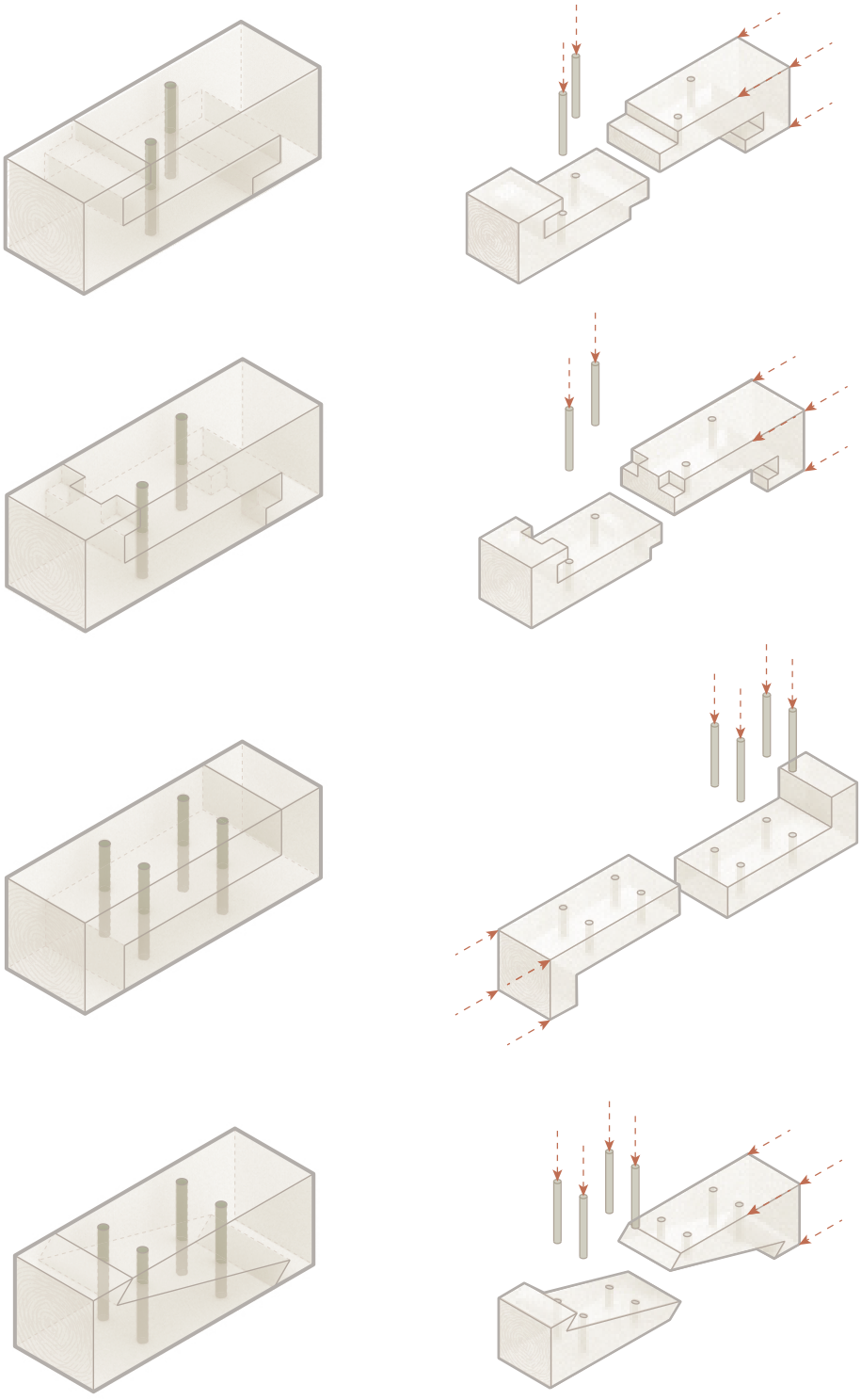

Figure 14. *Illustrations of different types of wedged or pinned scarf joints.*

APPENDIX A2

CONNECTION TABLES

C1

Table 1. *Connections divided into degrees of freedom*

	Translation - 2-way	Translation - 1-way	Translation - Locked
Rotation - 2-way	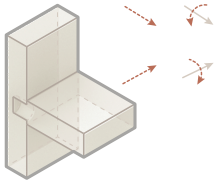 Depending on the horizontal loading, rotation is allowed in two directions	X 2-way rotation is not really possible due to the geometry	X 2-way rotation is not really possible due to the geometry
Rotation - 1-way	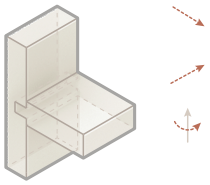 Depending on the horizontal loads, rotation is allowed in one direction 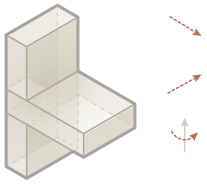	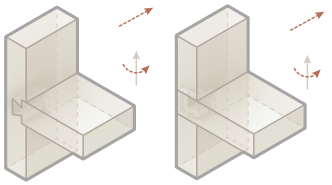 Depending on the depth of the dove, the slight tilting, rotation in all directions are locked 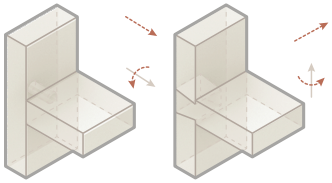	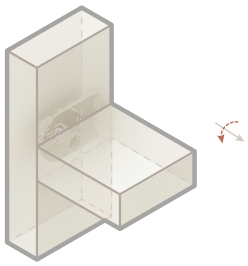
Rotation - Locked	X	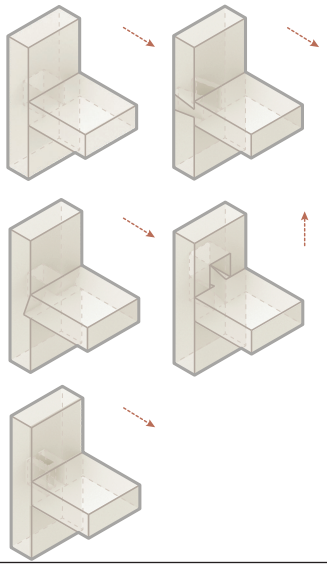	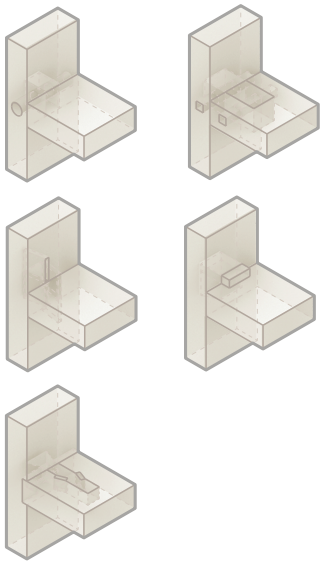

C2

Table 2. *Connections divided into degrees of freedom*

	Translation - 2-way	Translation - 1-way	Translation - Locked
Rotation - 2-way		X 2-way rotation is not really possible due to the geometry.	X 2-way rotation is not really possible due to the geometry.
Rotation - 1-way	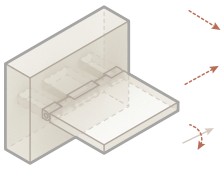 The translation in this case would make the connection fail 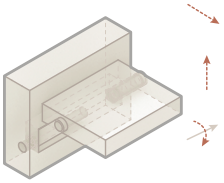	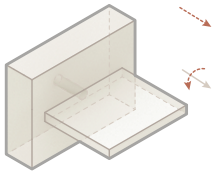 The translation in this case would make the connection fail 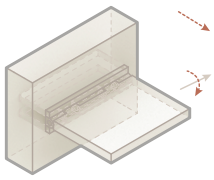	
Rotation - Locked	X	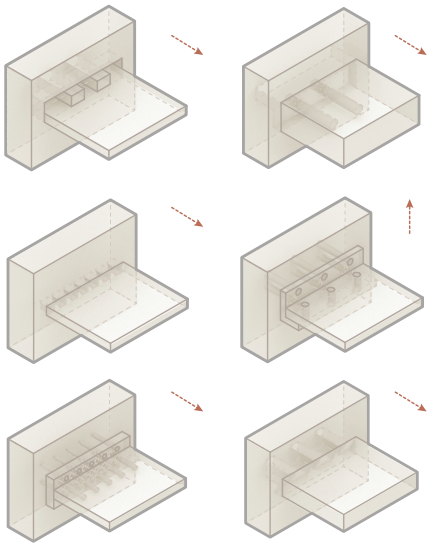	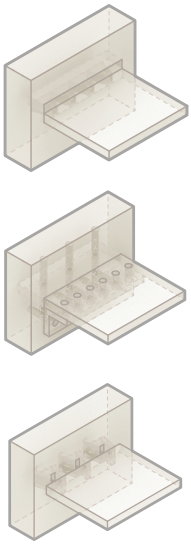

APPENDIX A3

CONNECTION TREES

C1

Table 1. *Small advancements of the connections, staggered from simple to more sophisticated design*

CENTERED INSERTION

Part cross-section

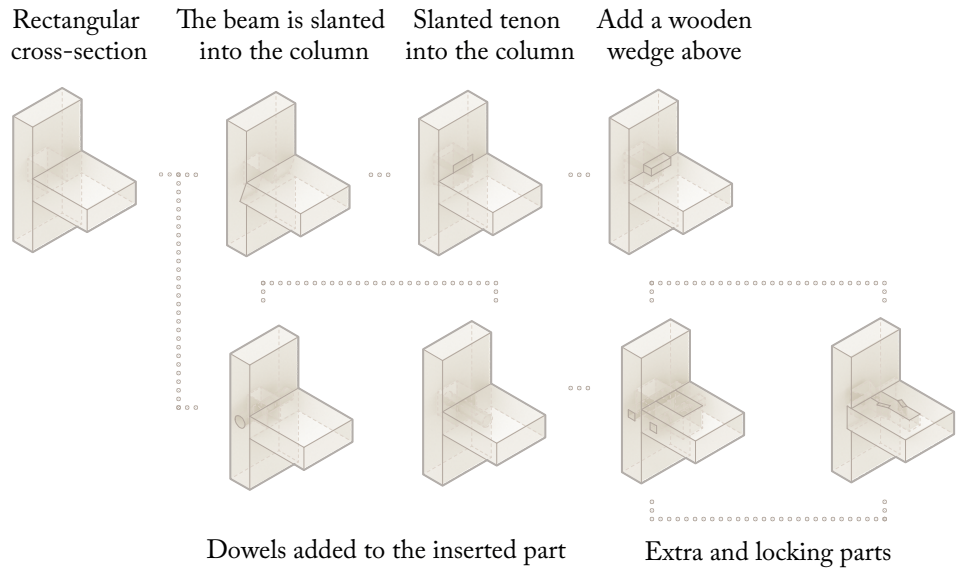

Dovetail tenon

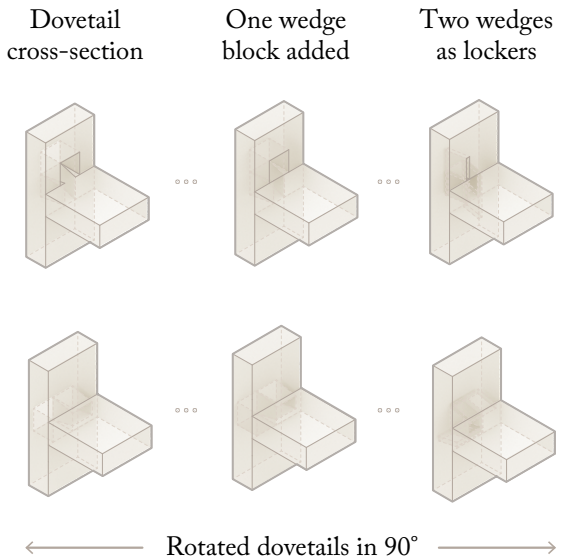

SIDE INSERTION

Part cross-section

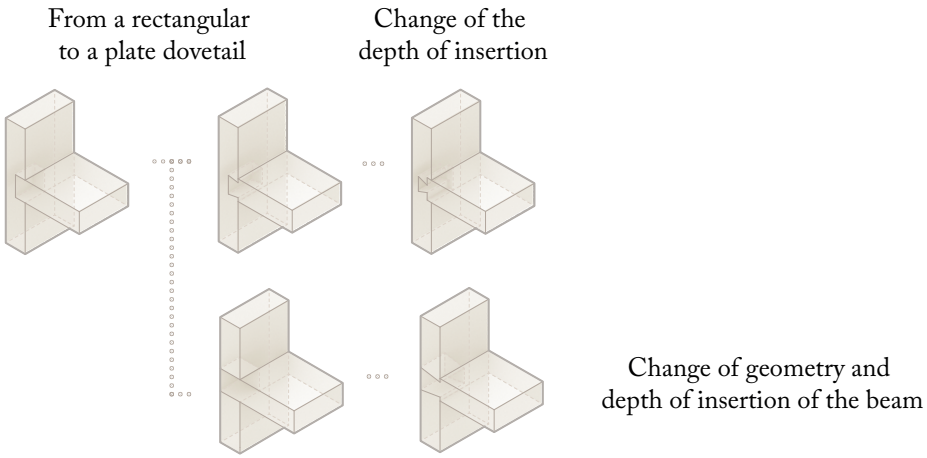

Full cross-section

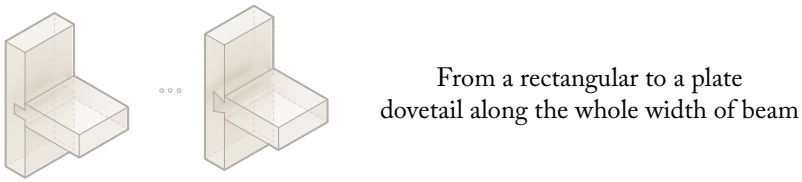

C2

Table 2. *Small advancements of the connections, staggered from simple to more sophisticated design.*

Part cross-section

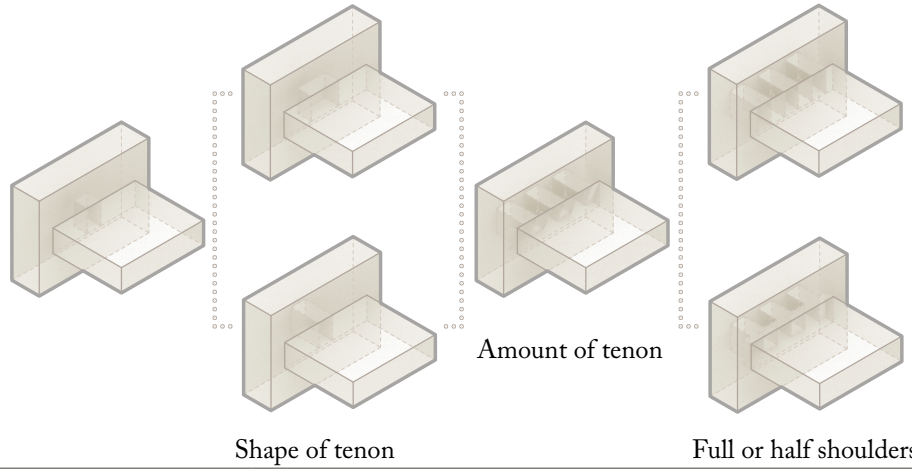

Full cross-section

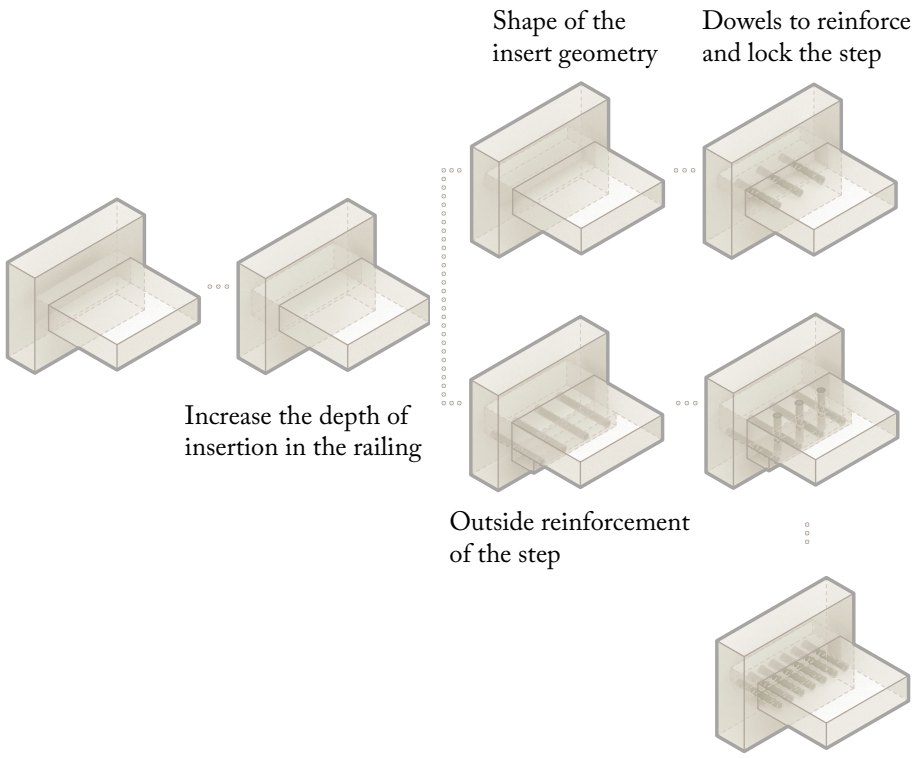

Dovetail tenon

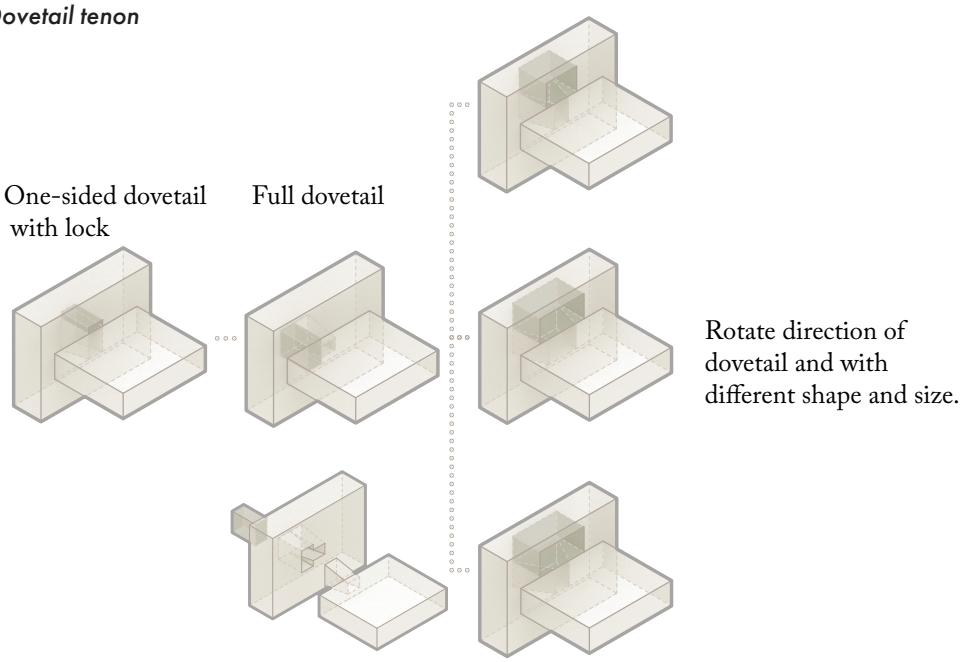

APPENDIX A4

GRADING TABLES

C1

Table 1. *Grading C1*

TYPE OF CONNECTION	MANU-FACTURING	ASSEMBLY	FIRE AND ACOUSTICS	STRUCTURE	ARCHI. QUALITIES	APPLICA-BILITY
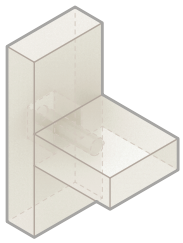	●●○	●○○	●●○	●●○	●●○	●○○
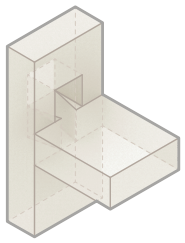	●●○	●○○	●●○	●●●	●●○	●○○
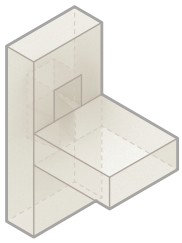	●○○	●○○	●●○	●●●	●●○	●○○
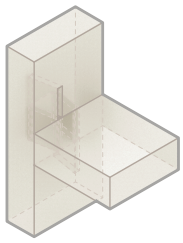	●○○	●○○	●●○	●●○	●●●	●○○

TYPE OF CONNECTION	MANU-FACTURING	ASSEMBLY	FIRE AND ACOUSTICS	STRUCTURE	ARCHI. QUALITIES	APPLICA-BILITY
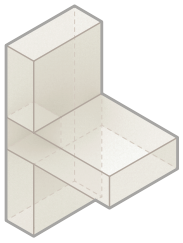	●●●	●●●	●○○	●●○	●●●	●●●
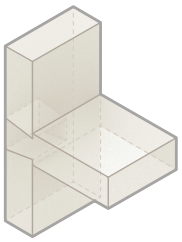	●●○	●●●	●○○	●●○	●●●	●●○
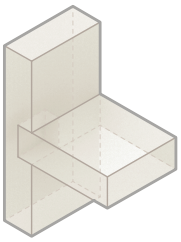	●●●	●●●	●●○	●●○	●●○	●●●
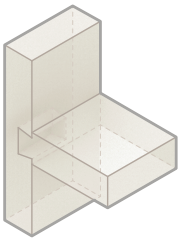	●●○	●●●	●●○	●●○	●●○	●●○
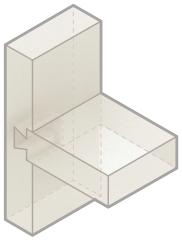	●○○	●●●	●●○	●●○	●●●	●●○
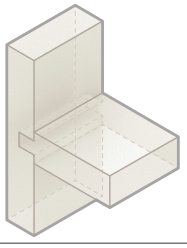	●●●	●●●	●○○	●●○	●○○	●○○

TYPE OF CONNECTION	MANU-FACTURING	ASSEMBLY	FIRE AND ACOUSTICS	STRUCTURE	ARCHI. QUALITIES	APPLICA-BILITY
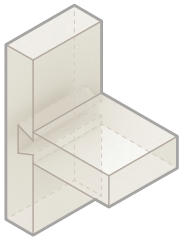	●●●	●●●	●○○	●●○	●●●	●●●
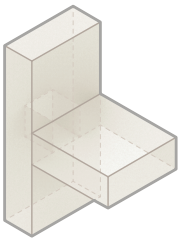	●●●	●●○	●●○	●●●	●●○	●●●
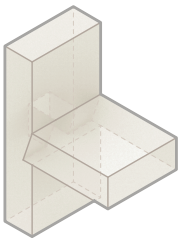	●●○	●●○	●●○	●○○	●●●	●○○
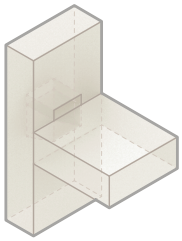	●●○	●●○	●●○	●●●	●●○	●●○
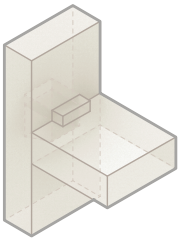	●○○	●○○	●○○	●●●	●●●	●○○
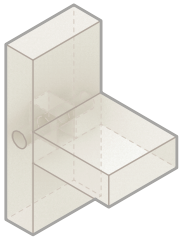	●●○	●○○	●●○	●●●	●●●	●●○

C2

Table 2. *Grading C2*

TYPE OF CONNECTION	MANU-FACTURING	ASSEMBLY	FIRE AND ACOUSTICS	STRUCTURE	ARCHI. QUALITIES	APPLICA-BILITY
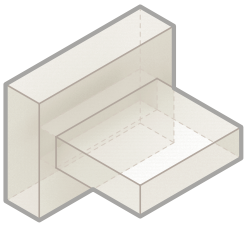	●●●	●●●	●●●	●●●	●○○	●●●
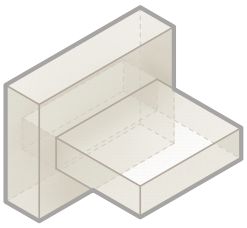	●●●	●●●	●●○	●●○	●○○	●●○
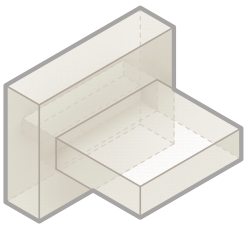	●●●	●●●	●●○	●○○	●●●	●●●
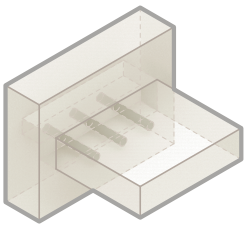	●●○	●●○	●●○	●○○	●●●	●●○
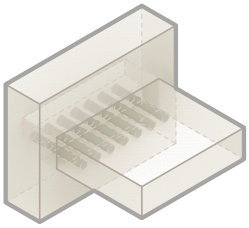	●○○	●○○	●○○	●○○	●●○	●○○

TYPE OF CONNECTION	MANU-FACTURING	ASSEMBLY	FIRE AND ACOUSTICS	STRUCTURE	ARCHI. QUALITIES	APPLICA-BILITY
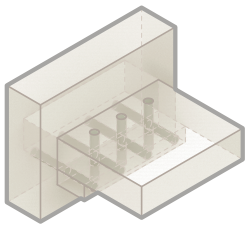	●○○	●○○	●○○	●●○	●●●	●○○
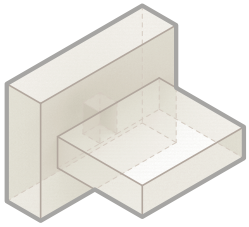	●●●	●●●	●●○	●●○	●○○	●●○
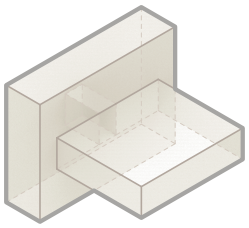	●●●	●●●	●●○	●●○	●●○	●●●
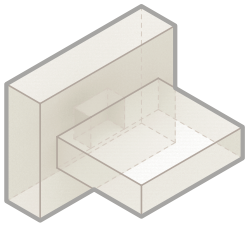	●●●	●●●	●●○	●●○	●●○	●●●
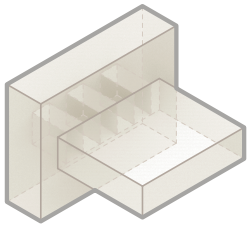	●●○	●●●	●○○	●●○	●●●	●●○
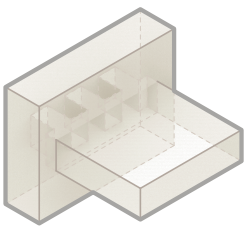	●○○	●●●	●○○	●○○	●●●	●○○

TYPE OF CONNECTION	MANU-FACTURING	ASSEMBLY	FIRE AND ACOUSTICS	STRUCTURE	ARCHI. QUALITIES	APPLICA-BILITY
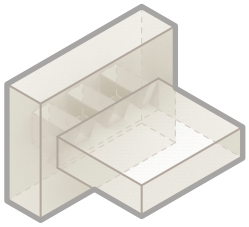	●○○	●●●	●●○	●○○	●●●	●○○
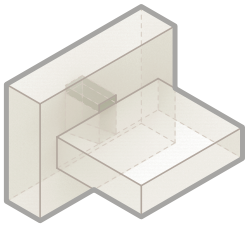	●●○	●●○	●●○	●●○	●●●	●●○
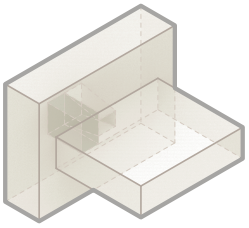	●●○	●●○	●●○	●●○	●●●	●●●
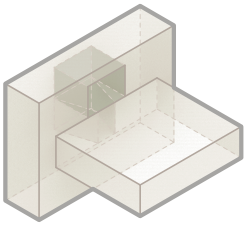	●●○	●●○	●●○	●●●	●●●	●●●
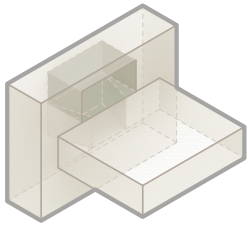	●●○	●●○	●●○	●●○	●●●	●●○
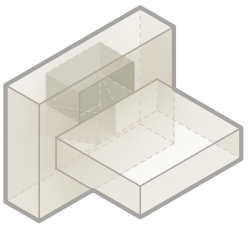	●●○	●●○	●○○	●●○	●●●	●●○

TYPE OF CONNECTION	MANU-FACTURING	ASSEMBLY	FIRE AND ACOUSTICS	STRUCTURE	ARCHI. QUALITIES	APPLICA-BILITY
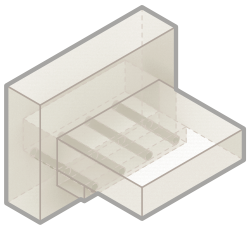	●○○	●●○	●○○	●●○	●●●	●○○

APPENDIX B

Appendix B includes all hand calculations
and verifications for the design process.

APPENDIX B1

LOAD CALCULATIONS C1

Indata

Self-weight

Given from Sweco Structures Calculation sheets for the building.

$g_{roof} := 1.23 \frac{kN}{m^2}$: This load is used to calculate to Euler cracking of the pillar.

$g_{outer,\ wall} := 0.90 \frac{kN}{m^2}$: This load is used to calculate to Euler cracking of the pillar.

$g_{glulam} := 4.3 \frac{kN}{m^3}$: Self wieght of glulam *(Martinsons)*

Snow load

Roof angle is 30 degrees. This load is also given from weco Structures Calculation sheets for the building.

$s_{k,\ max} := 2.64 \frac{kN}{m^2}$: This load is used to calculate to Euler cracking of the pillar.

Wind load

Borlänge, terrain type II *(Given in the Sweco Calculation Sheet)*

$v_b := 22 \frac{m}{s}$:

$q_p := 0.68 \frac{kN}{m^2}$:

The pressure coefficients for the relevant parts of Volume B is calculated for each load case.

Assumptions

The beam is for hand calculations simplified as a simply supported beam with two moment free supports.

Load case 1 (LC1)

The loads are calculated for the wind on Volume B, for a special verification of the window raster in Volume C a special load case need to be checked but for the design verification of C1 it is enough to check the load case for Volume B.

Wind direction: 0 degrees

Volume B Geometry

Geometric data is taken from given drawings form Volume B.

$h_B := 11.5\ \text{m}$:

$b_{B1} := 21.4\ \text{m}$: (b is the cross wind dimension)

$d_{B1} := 13.7\ \text{m}$:

$e := \min\left(b_{B1}, 2 \cdot h_B\right) = 21.4\ \text{m}$

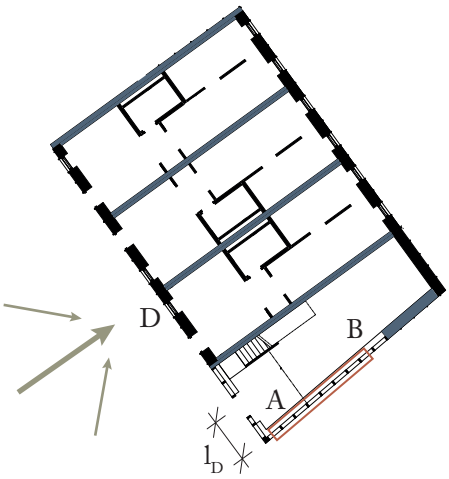

The red area marks the window raster area used to calculate the forces out of the two sides.

Geometry Glulam

$d_{glulam} := 225\,\text{mm}$:

$w_{glulam} := 90\,\text{mm}$:

$c_{pillar} := 1000\,\text{mm}$:

$c_{beam} := 1790\ \text{mm}$:

Wind load

Internal pressure coefficents:

$c_{pip} := 0.2$: $c_{pin} := -0.3$:

For each load case the internal pressure coefficents are applied to find the most critical load case.

$$w_{i,p} := q_p \cdot c_{pip} = 0.136 \ \frac{\text{kN}}{\text{m}^2}$$

$$w_{i,n} := q_p \cdot c_{pin} = -0.204 \ \frac{\text{kN}}{\text{m}^2}$$

External pressure coefficents:

$$z_e := \text{if}\left(\frac{h_B}{\text{m}} \leq \frac{b_{B1}}{\text{m}}, h_B, 0\right) = 11.5 \ \text{m}$$

The wind load on the wall perpendicular to the load bearing wall is divided 50 % - 50 % between the two walls so that half the load on this wall area is applied as an axial force on the window raster.

$$\frac{h_B}{d_{B1}} \ 0.839$$

$$c_{pe,1,A} := -1.4 : \qquad c_{pe,1,B} := -1.1 : \qquad c_{pe,1,D} := 1.0 :$$

In-plane wind load:

$$l_D := 2755.9\text{mm} = 2.76 \ \text{m}$$

This is the 50 % length of the wind load that goes to the window raster from wall D.

$$q_{wind,D,pos} := \left(c_{pe,1,D} - c_{pip}\right) \cdot q_p \cdot l_D = 1.499 \ \frac{\text{kN}}{\text{m}}$$

$$q_{wind,D,neg} := \left(c_{pe,1,D} - c_{pin}\right) \cdot q_p \cdot l_D = 2.436 \ \frac{\text{kN}}{\text{m}}$$

Abaqus load: this is simulated as a pressure on the side of the modelled pillar with the value: $q_{wind,IP,A} := \frac{q_{wind,D,neg}}{d_{glulam}} = 0.011 \ \text{MPa}$

Hand calculation load is applied on the connection as an axial point load on the beam with the value: $q_{wind,IP,H} := q_{wind,D,neg} \cdot c_{beam} = 4.361 \ \text{kN}$

Out-of-plane wind load:

Since the outer wind pressure creates suction on these walls the worst case is when the internal pressure is positive. To calculate the maximum load on the beams the wind pressure for wall A is used as this becomes the dimensioning value.

$$q_{wind,A} := \left(c_{pe,1,A} - c_{pip}\right) \cdot q_p = -1.088 \ \frac{\text{kN}}{\text{m}^2}$$

Assuming an even distribution of the horizontal loads between beams and pillars.

It is more likely that the pillars will take more load since the load is transfered directly from these to the supports but for simplicity 50 % - 50 % is used and this also gives a worse case for loads on the beams.

For the applied load in Abaqus the load is applied is applied as a pressure over the surface over the beam and pillars, the highest value of q.w for the beam and pillar is used.

$$q_{w,A,beam} := \frac{q_{wind,A} \cdot \frac{c_{beam}}{2}}{w_{glulam}} \quad -0.011 \text{ MPa}$$

$$q_{w,A,pillar} := \frac{q_{wind,A} \cdot \left(\frac{c_{pillar} \cdot 2}{2} \right)}{w_{glulam}} = -0.012 \text{ MPa}$$

$$q_{wind,OP,A} := \min\left(q_{w,A,beam}, q_{w,A,pillar}\right) = -0.012 \text{ MPa}$$

For the hand calculations this load is applied as a horizontal line load with the magnitude:

$$q_{wind,OP,H} := q_{wind,OP,A} \cdot w_{glulam} \quad -1.088 \ \frac{\text{kN}}{\text{m}}$$

Self weight

$$q_{glulam} := g_{glulam} \cdot w_{glulam} \cdot d_{glulam} = 0.0871 \ \frac{\text{kN}}{\text{m}}$$

Summary of loads

LOAD	
Self weight, q_{glulam} :	$0.0871 \frac{\text{kN}}{\text{m}}$:
Horizontal axial load, $q_{wind,IP,H}$:	4.36 kN :
Horizontal line load, $q_{wind,OP,H}$:	$-1.088 \frac{\text{kN}}{\text{m}}$:

Table 1: Summary of loads - Load case 1

Reaction forces

Vertical loads

$$R_{C1,v} := \frac{q_{glulam} \cdot c_{pillar}}{2} = 0.044 \text{ kN}$$

$$M_v(x) := R_{C1,v} \cdot x - \frac{q_{glulam} \cdot x^2}{2} :$$

$$V_v(x) := R_{C1,v} - q_{glulam} \cdot x :$$

Horizontal loads

The axial horizontal load does not entail any further reaction force calculations since it simply reacts to the axial load applied.

$$R_{C1,h} := \frac{-q_{wind,OP,H} \cdot c_{pillar}}{2} = 0.544 \text{ kN}$$

$$M_h(x) := R_{C1,h} \cdot x - \frac{q_{wind,OP,H} \cdot x^2}{2} :$$

$$V_h(x) := R_{C1,h} - q_{wind,OP,H} \cdot x :$$

Load case 2 (LC2)

For load case 2 the wind load is applied in a 90 degree angle from load case 1.

Wind direction: 90 degrees

Volume B Geometry

Geometric data is taken from given drawings form Volume B.

$h_B := 11.5 \text{ m} :$

$b_{B2} := 13.7 \text{ m} :$ b is the cross wind dimension

$d_{B2} := 21.4 \text{ m} :$

$e := \min\left(b_{B2}, 2 \cdot h_B\right) = 13.7 \text{ m}$

Geometry Glulam

Same as in LC1.

Wind load

Internal pressure coefficents:

The internal pressure coefficents are the same as in LC1.

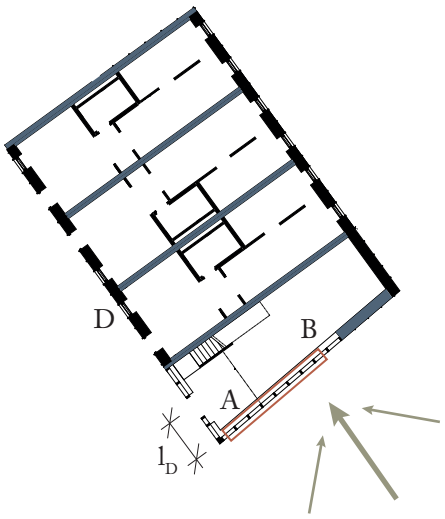

External pressure coefficents:

$$z_e := \text{if}\left(\frac{h_B}{\text{m}} \leq \frac{b_{B2}}{\text{m}}, h_B, 0\right) = 11.5\ \text{m}$$

The in-plane wind load on the wall perpendicular to the wind is divided 50 % - 50 % between the two walls so that half the load on this wall area is applied as an axial force on the window raster.

$$\frac{h_B}{d_{B2}} = 0.537$$

$c_{pe,1,A} := -1.4$: $\qquad$ $c_{pe,1,D} := 1.0$:

In-plane wind load:

$l_A := 2755.9\,\text{mm} = 2.76\ \text{m}$

This is the 50 % length of the wind load that goes to the window raster from wall A.

$$q_{wind,A,pos} := \left(c_{pe,1,A} - c_{pip}\right) \cdot q_p \cdot l_A = -2.998\ \frac{\text{kN}}{\text{m}}$$

$$q_{wind,A,neg} := \left(c_{pe,1,A} - c_{pin}\right) \cdot q_p \cdot l_A = -2.061\ \frac{\text{kN}}{\text{m}}$$

Abaqus load: this is simulated as a pressure on the side of the modelled pillar with the value: $q_{wind,\,IP,\,A} := \frac{q_{wind,\,A,\,pos}}{d_{glulam}} = -0.013\ \text{MPa}$

Hand calculation load is applied on the connection as an axial point load on the beam with the value: $q_{wind,\,IP,\,H} := q_{wind,\,A,\,pos} \cdot c_{beam} = -5.367\ \text{kN}$

Out-of-plane wind load:
Since the outer wind creates pressure on these walls the worst case is when the internal pressure is negative.

$$q_{wind,\,\mathrm{D}} := \left(c_{pe,\,1,\,\mathrm{D}} - c_{pin}\right) \cdot q_p = 0.884\ \frac{\text{kN}}{\text{m}^2}$$

Assuming an even distribution of the horizontal loads between beams and pillars.

It is more likely that the pillars will take more load since the load is transfered directly from these to the supports but for simplicity 50 % - 50 % is used and this also gives a worse case for loads on the beams.

For the applied load in Abaqus the load is applied is applied as a pressure over the surface over the beam and pillars, the highest value of q.w for the beam and pillar is used.

$$q_{w,\,\mathrm{D},\,beam} := \frac{q_{wind,\,\mathrm{D}} \cdot \frac{c_{beam}}{2}}{w_{glulam}} = 0.0088\ \text{MPa}$$

$$q_{w,\,\mathrm{D},\,pillar} := \frac{q_{wind,\,\mathrm{D}} \cdot \left(\frac{c_{pillar} \cdot 2}{2}\right)}{w_{glulam}} = 0.0098\ \text{MPa}$$

$$q_{wind,\,OP,\,A} := \max\left(q_{w,\,\mathrm{D},\,beam},\, q_{w,\,\mathrm{D},\,pillar}\right) = 0.0098\ \text{MPa}$$

For the hand calculations this load is applied as a horizontal line load with the magnitude:

$$q_{wind,\,OP,\,H} := q_{wind,\,OP,\,A} \cdot w_{glulam} = 0.884\ \frac{\text{kN}}{\text{m}}$$

Summary of loads

LOAD	
Self weight, q_{glulam} :	$0.0871 \frac{\text{kN}}{\text{m}}$:
Horizontal axial load, $q_{wind,IP,H}$:	-5.37 kN :
Horizontal line load, $q_{wind,OP,H}$:	$0.884 \frac{\text{kN}}{\text{m}}$:

Table 2: Summary of loads - Load case 2

Reaction forces

Vertical loads:

$$R_{C2,v} := \frac{q_{glulam} \cdot c_{pillar}}{2} = 0.0435 \text{ kN}$$

$$M_v(x) := R_{C2,v} \cdot x - \frac{q_{glulam} \cdot x^2}{2} :$$

$$V_v(x) := R_{C2,v} - q_{glulam} \cdot x :$$

Horizontal loads:

The axial horizontal load does not entail any further reaction force calculations since it simply reacts to the axial load applied.

$$R_{C1,h} := \frac{q_{wind,OP,H} \cdot c_{pillar}}{2} = 0.442 \text{ kN}$$

$$M_h(x) := R_{C1,h} \cdot x - \frac{q_{wind,OP,H} \cdot x^2}{2} :$$

$$V_h(x) := R_{C1,h} - q_{wind,OP,H} \cdot x :$$

Comparison reaction forces

FORCE	L1	L2	L1/L2
Vertical maximum shear force, $V_v(x)$:	0.044 kN	0.044 kN	100 %
Horizontal axial force, Q_{Axial} :	4.36 kN	-5.37 kN	81 %
Horizontal maximum shear force, $V_h(x)$:	0.544 kN	0.442 kN	123 %

Table 3: Force comparisson

Bibliography

Swedish Standards Institute. (2008). *Eurocode 1: Actions on Structures – Part 1-4: General actions – Wind actions* (Standards No. SS-EN 1991-1-4:2005).

APPENDIX B2

LOAD CALCULATIONS C2

Indata

Stair geometry

$w_{step} := 300 \text{ mm} :$

$l_{step} := 1.0 \text{ m} :$

$A_{step} := w_{step} \cdot l_{step} :$

$t_{1,step} := 40 \text{ mm} :$ $t_{2,step} := 40 \text{ mm} :$ $t_{3,step} := 40 \text{ mm} :$

$t_{step} := t_{1,step} + t_{2,step} + t_{3,step} :$

$V_{step} := A_{step} \cdot t_{step} :$

GEOMETRY	(mm)
THICKNESS	120
WIDTH	300
LENGTH	1000

Table 1: Geometry - Stair Step

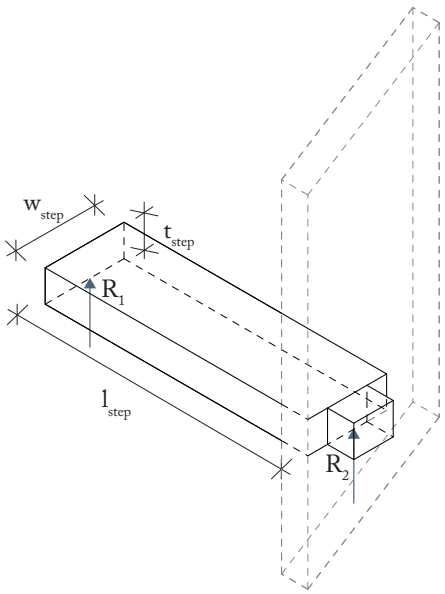

Self-weight

Gravity

$g := 9.82 \ \frac{\text{m}}{\text{s}^2} :$

Type: C24-C14-C24

$54 \ \frac{\text{kg}}{\text{m}^2} :$ *(Martinsons, 2020)*

Self-weight: $\frac{54\ \frac{\mathrm{kg}}{\mathrm{m}^2}}{t_{step}} = 450\ \frac{\mathrm{kg}}{\mathrm{m}^3}$

$Q_{step} := 450\ \frac{\mathrm{kg}}{\mathrm{m}^3} \cdot V_{step} \cdot g = 159.08\ \mathrm{N}$

Since the stair step is 1 meter long. The distributed load per m is the same:

$Q_{step,\,m} := \frac{159.0840000\ \mathrm{N}}{1\,\mathrm{m}} = 159.08\ \frac{\mathrm{N}}{\mathrm{m}}$

In Abaqus the self-weight is applied as a body load of magnitude:

$Q_{step,\,A} := 450\ \frac{\mathrm{kg}}{\mathrm{m}^3} \cdot g = 4.42\ \frac{\mathrm{kN}}{\mathrm{m}^3}$

Imposed loads

$P_{step} = Q_k$: from *(SIS, 2009)*.

$P_{step} := 2000\ \mathrm{N}$:

There is also an imposed load that is in the horizontal direction of the step. This is a line load.

$q_{k,\,h} := 0.5\ \frac{\mathrm{kN}}{\mathrm{m}}$:

In Abaqus the imposed point load is applied in 4 different points to first and foremost check which location of the point load that gives the most critical load case and to check the influence of the location of the pointload depthwise of the step. The four points will distribute the point load on different areas depending if it's in the centre, on the side or at the corner. These pressure loads are calculated below.

$P_{step,\,A,\,CC} := \frac{P_{step}}{(100\,\mathrm{mm} \cdot 100\,\mathrm{mm})} = 0.20\ \mathrm{MPa}$

$P_{step,\,A,\,CS,\,SC} := \frac{P_{step}}{(50\,\mathrm{mm} \cdot 100\,\mathrm{mm})} = 0.40\ \mathrm{MPa}$

$P_{step,\,A,\,CC} := \frac{P_{step}}{(50\,\mathrm{mm} \cdot 50\,\mathrm{mm})} = 0.80\ \mathrm{MPa}$

The horizontal line load is applied in abaqus as a pressure or suction over an area, this line load is therefore divided by the height of the step.

$$q_{k,h,A} := \frac{q_{k,h}}{t_{step}} = 0.0042 \text{ MPa}$$

Assumptions

For this case hinged supports are assumed for the railing and the wall.

R_1 : = reaction force from wall support and R_2 : = reaction force from railing support

The depth of the step and the position of the point load is not taken into consideration as simple FEM models have been analysed which showed the most critical load case where the point load is centered on the step in depth. In hand calculations this is also a simplification so that the supports will be moment free and hinged. With the point load applied with an exentricity from the support a console case would be created and the connection would have needed to be dimensioned for a moment.

Load case 1 (LC1) - Point load on railing

Equilibrium for moment around railing support (positive clockwise): l_{step} : = at support 2.

$\overset{\frown}{R_2}$: Global equilibrium gives the following equations:

$$M(l_{step}) := R_1 \cdot l_{step} - \frac{Q_{step,m} \cdot l_{step} \cdot l_{step}}{2} = 0 : \qquad R_1 := \frac{Q_{step,m} \cdot l_{step} \cdot l_{step}}{2 \cdot l_{step}} = 79.54 \text{ N}$$

Vertical force balance:

$$-R_1 + P_{step} + Q_{step,m} \cdot l_{step} - R_2 = 0 :$$

Reaction force for the railing support, R_2 :

$$R_2 := -R_1 + P_{step} + Q_{step,m} \cdot l_{step} = 2.08 \text{ kN}$$

Load case 2 (LC2) - Point load on the centre of the step

Equilibrium for moment around (positive clockwise): l_{step} : = at support 2.

$$M(l_{step}) := + R_1 \cdot l_{step} - \frac{Q_{step,m} \cdot l_{step} \cdot l_{step}}{2} - \frac{P_{step} \cdot l_{step}}{2} = 0 :$$

$$R_1 := \frac{\left(\frac{Q_{step,m} \cdot l_{step} \cdot l_{step}}{2} + P_{step} \cdot \frac{l_{step}}{2} \right)}{l_{step}} = 1.08 \text{ kN}$$

Vertical force balance:

$-R_1 + P_{step} + Q_{step,m} \cdot 1_{step} - R_2 = 0$:

Reaction force for the railing support, C2:

$R_2 := -R_1 + P_{step} + Q_{step,m} \cdot l_{step} = 1.08$ kN

Horizontal load case

The horizontal load case also gives reaction forces in the supports in the horizontal direction. Because the supports are counted as hinged.
The horizontal load is applied in both in-plane directions which will result in one axial force at the connection as well.

$Q_{h,Axial} := q_{k,h} \cdot w_{step} = 0.15$ kN

$R_h := \frac{q_{k,h} \cdot l_{step}}{2} = 0.25$ kN

Summary of reaction forces

RESULT	(kN)
LC1, R_2 :	2.08
LC2, R_2 :	1.08
Horizontal load case, Q_{Axial} :	0.15
Horizontal load case, R_h :	0.25

Table 2: Reaction forces at the railing

APPENDIX B3

VERIFICATIONS, CONNECTION C1

1. Loads

$V_{Ed,V} := 0.044\ \text{kN}$:

$V_{Ed,H} := 0.544\ \text{kN}$:

$Q_{Ed} := 4.36\,\text{kN}$:

2. Material properties

The chosen material for this connection is Glulam GL30c with the values according to Gustafsson et al. *(2019)*.

2.1. Correction and modification factors

$\gamma_M := 1.25$:

$k_{\mathbf{mod}} := 0.90$: (for climate class 1 and short duration load as dimensioning)

$k_{cr} := \frac{2.5\,\text{MPa}}{3.2\,\text{MPa}} = 0.78$ (according to eq. (2))

$k_n := 6.5$: (according to eq. (3))

$k_{c,90} := 1.75$: (according to eq. (5))

2.2. Design values for material properties

	Characteristic strength		Design strength	
Compressive strength ⊥ to the grain	$f_{c,90,k}$:	2.5 MPa	$f_{c,90,d}$:	1.80 MPa
Tension strength ∥ to the grain	$f_{t,0,k}$:	19.5 MPa	$f_{t,0,d}$:	14.04 MPa
Tension strength ⊥ to the grain	$f_{t,90,k}$:	0.5 MPa	$f_{t,90,d}$:	0.36 MPa
Panel shear	$f_{v,k}$:	3.2 MPa	$f_{v,d}$:	2.30 MPa
Rolling shear	$f_{Rv,k}$:	1.2 MPa	$f_{Rv,d}$:	0.86 MPa

Material Properties - glulam, GL30c

$f_{c,90,d} := k_{\mathbf{mod}} \cdot \frac{2.5\,\text{MPa}}{\gamma_M} = 1.80\ \text{MPa}$

$f_{t,0,d} := k_{\mathbf{mod}} \cdot \frac{19.5\,\text{MPa}}{\gamma_M} = 14.04\ \text{MPa}$

$$f_{t,90,d} := k_{\mathbf{mod}} \cdot \frac{0.5\,\mathrm{MPa}}{\gamma_M} = 0.36\ \mathrm{MPa}$$

$$f_{v,d} := k_{\mathbf{mod}} \cdot \frac{3.2\,\mathrm{MPa}}{\gamma_M} = 2.30\ \mathrm{MPa}$$

$$f_{Rv,d} := k_{\mathbf{mod}} \cdot \frac{1.2\,\mathrm{MPa}}{\gamma_M} = 0.86\ \mathrm{MPa}$$

3. Geometry

Four different geometries are evaluated with the relevant indata below. The geometries of two of these can be seen in Figure 1 and 2. The other two geometries are similar, compared to Figure 1 the second dovetail portrudes the full width of the pillar and compared to Figure 2 the fourth geometry has a slightly smaller peg. The geometrical data is stated in the table below.

PD1	PD2	P1	P2
Tenon			
$b_{N,1} := 60\,\mathrm{mm}$:	$b_{N,2} := 60\,\mathrm{mm}$:	$b_{N,3} := 90\,\mathrm{mm}$:	= P1
$b_1 := \frac{b_{N,1}}{0.8}$:	$b_2 := \frac{b_{N,2}}{0.8}$:	$b_3 := b_{N,3}$:	= P1
$h_1 := 225\,\mathrm{mm}$:	$h_2 := 225\,\mathrm{mm}$:	$h_3 := 225\,\mathrm{mm}$:	= P1
$h_{N,1} := 112.5\,\mathrm{mm}$:	$h_{N,2} := 112.5\,\mathrm{mm}$:	$h_{N,3} := 142.5\,\mathrm{mm}$:	= P1
-	-	$h_{T,3} := 60\,\mathrm{mm}$:	= P1
$l_{z,1} := 45\,\mathrm{mm}$:	$l_{z,2} := 90\,\mathrm{mm}$:	$l_{z,3} := 90\,\mathrm{mm}$:	= P1
$i := 0$:	$i := 0$:	$i := 0$:	= P1
Header			
$b_{H,1} := 90\,\mathrm{mm}$:	$b_{H,2} := 90\,\mathrm{mm}$:	$b_{H,3} := 90\,\mathrm{mm}$:	= P1
$h_{H,1} := 225\,\mathrm{mm}$:	$h_{H,2} := 225\,\mathrm{mm}$:	$h_{H,3} := 225\,\mathrm{mm}$:	= P1
$h_{H,u,1} := 112.5\,\mathrm{mm}$:	$h_{H,u,2} := h_{H,u,1}$:	$h_{H,u,3} := 82.5\,\mathrm{mm}$:	= P1
Peg			
		$d_3 := 40\,\mathrm{mm}$:	$d_4 := 20\,\mathrm{mm}$:

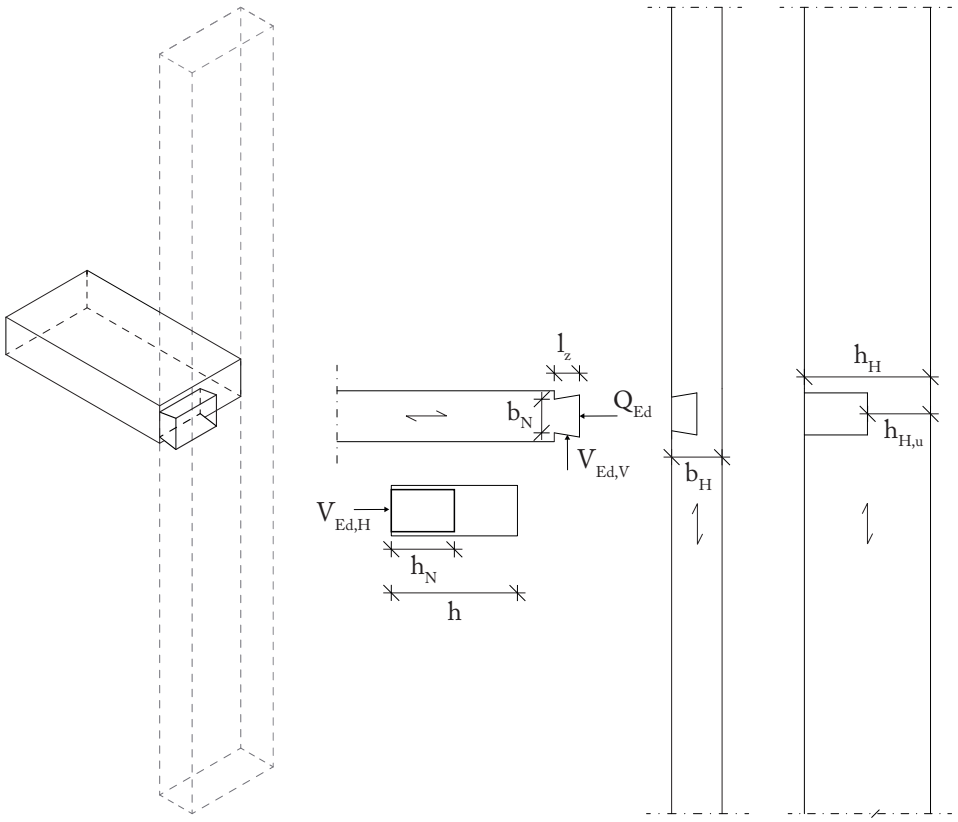

Figure 1. *Geometry for PD1. PD2 is the same but with the dovetail protruding fully through the pillar.*

4. Verifications

4.1 Joist member

4.1.1 Failure in shear and tension at the notch corner

4.1.1.1 Vertical loads

Verified for PD1 and PD2 according to eq. (24) for a dovetail type IV.

$$\alpha_{V,1} := \frac{b_{N,1}}{b_1} = 0.80 \qquad \alpha_{V,2} := \frac{b_{N,2}}{b_2} = 0.80$$

$$x_1 := \frac{l_{z,1}}{2} = 22.50\ \text{mm} \qquad x_2 := \frac{l_{z,2}}{2} = 45\ \text{mm}$$

$$k_{v,V,1} := \min\left(1.0,\ \frac{k_n \cdot \left(1 + \frac{1.1 \cdot i^{1.5}}{\sqrt{b_1}}\right) \cdot \sqrt{\text{mm}}}{\sqrt{b_1} \cdot \left(\sqrt{\alpha_{V,1} - \alpha_{V,1}^2} + 0.8 \cdot \frac{x_1}{b_1} \cdot \sqrt{\frac{1}{\alpha_{V,1}} - \alpha_{V,1}^2}\right)}\right) = 1.0$$

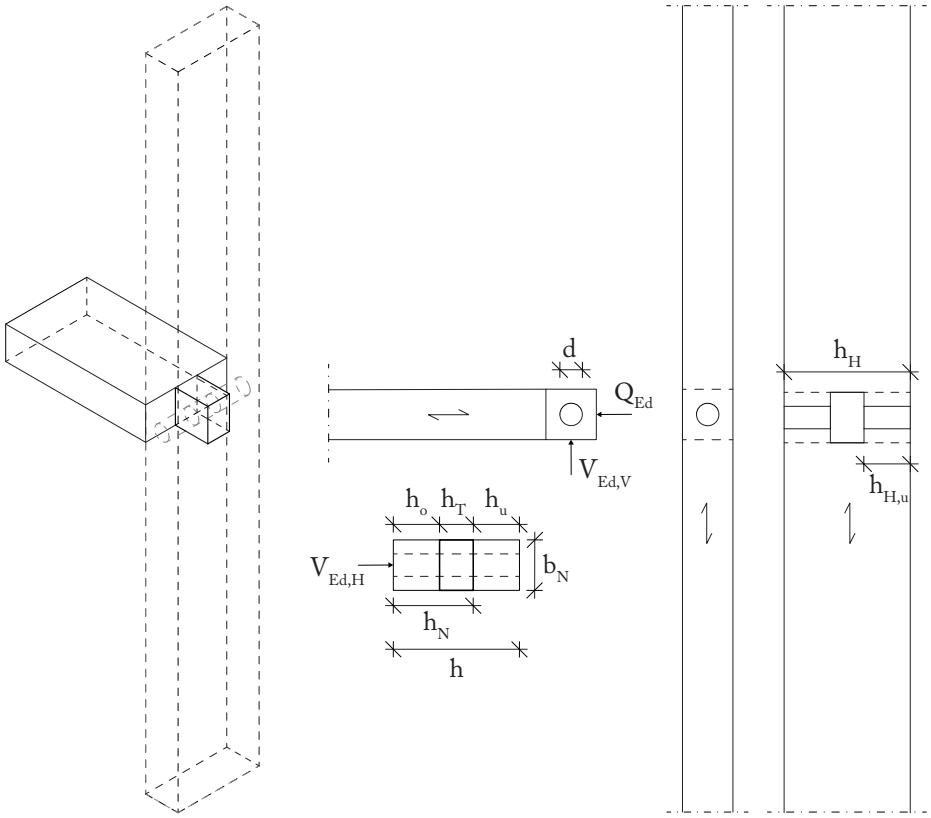

Figure 2. *Geometry for P1. P2 is the same but with a smaller peg.*

$$k_{v,V,2} := \min\left(1.0,\ \frac{k_n \cdot \left(1 + \frac{1.1 \cdot i^{1.5}}{\sqrt{b_2}}\right) \cdot \sqrt{\text{mm}}}{\sqrt{b_2} \cdot \left(\sqrt{\alpha_{V,2} - \alpha_{V,2}^2} + 0.8 \cdot \frac{x_2}{b_2} \cdot \sqrt{\frac{1}{\alpha_{V,2}} - \alpha_{V,2}^2}\right)}\right) = 0.97$$

$$F_{v,Rd,V,1} := \frac{2}{3} \cdot b_{N,1} \cdot h_{N,1} \cdot k_{v,V,1} \cdot f_{v,d} = 10.37\ \text{kN}$$

$$F_{v,Rd,V,2} := \frac{2}{3} \cdot b_{N,2} \cdot h_{N,2} \cdot k_{v,V,2} \cdot f_{v,d} = 10.04\ \text{kN}$$

	PD1	PD2
$F_{v, Rd, V}$	10.37 kN	10.04 kN
$V_{Ed, V}$	0.044 kN	0.044 kN
Utilization ratio	0.42 %	0.44 %
	OK!	**OK!**

Failure mode 1, Vertical loads

4.1.1.2 Horizontal loads

PD1 and PD2 are verified as dovetail type III and the other two as tenon and mortise joints. Verified according to eq. (6)

$$\alpha_{H,1} := \frac{h_{N,1}}{h_1} = 0.50 \qquad \alpha_{H,2} := \frac{h_{N,2}}{h_2} = 0.50$$

$$b_{ef,1} := k_{cr} \cdot b_{N,1} = 46.9 \text{ mm} \qquad b_{ef,2} := k_{cr} \cdot b_{N,2} = 46.9 \text{ mm}$$

$$k_{v,H,1} := \min\left(1.0, \frac{k_n \cdot \left(1 + \frac{1.1 \cdot i^{1.5}}{\sqrt{h_1}}\right) \cdot \sqrt{\text{mm}}}{\sqrt{h_1} \cdot \left(\sqrt{\alpha_{H,1} - \alpha_{H,1}^2} + 0.8 \cdot \frac{x_1}{h_1} \cdot \sqrt{\frac{1}{\alpha_{H,1}} - \alpha_{H,1}^2}\right)}\right) = 0.72$$

$$k_{v,H,2} := \min\left(1.0, \frac{k_n \cdot \left(1 + \frac{1.1 \cdot i^{1.5}}{\sqrt{h_2}}\right) \cdot \sqrt{\text{mm}}}{\sqrt{h_2} \cdot \left(\sqrt{\alpha_{H,2} - \alpha_{H,2}^2} + 0.8 \cdot \frac{x_2}{h_2} \cdot \sqrt{\frac{1}{\alpha_{H,2}} - \alpha_{H,2}^2}\right)}\right) = 0.61$$

$$\tau_{d,H,2} := \frac{3}{2} \cdot \frac{V_{Ed,H}}{\alpha_{H,2} \cdot h_2 \cdot b_{ef,2}} \cdot \frac{1}{k_{v,H,2}} = 0.25 \text{ MPa}$$

$$\tau_{d,H,1} := \frac{3}{2} \cdot \frac{V_{Ed,H}}{\alpha_{H,1} \cdot h_1 \cdot b_{ef,1}} \cdot \frac{1}{k_{v,H,1}} = 0.22 \text{ MPa}$$

P1 and P2 has the same geometry for the tenon and therefore only one need to be verified. Due to symmetry and placement of the tenon $z_{0,T} = z_0$: and therefore the strength is calculated according to eq. (20b)

$\alpha_{H,3} := \frac{h_{N,3}}{h_3} = 0.63$ $x_3 := \frac{l_{z,3}}{2} = 45$ mm $b_{ef,3} := k_{cr} \cdot b_{N,3} =$ 70.3 mm

$$k_{v,H,3} := \min\left(1.0, \frac{k_n \cdot \left(1 + \frac{1.1 \cdot i^{1.5}}{\sqrt{h_3}}\right) \cdot \sqrt{\text{mm}}}{\sqrt{h_3} \cdot \left(\sqrt{\alpha_{H,3} - \alpha_{H,3}^2} + 0.8 \cdot \frac{x_3}{h_3} \cdot \sqrt{\frac{1}{\alpha_{H,3}} - \alpha_{H,3}^2}\right)}\right) = 0.66$$

$$k_{z,3} := \frac{h_{T,3}}{h_{N,3}} \cdot \left(1 + 2 \cdot \left(1 - \frac{h_{T,3}}{h_{N,3}}\right)^2\right) \cdot \left(2 - \frac{h_{N,3}}{h_3}\right) = 0.96$$

$$F_{v,Rd,H,3} := \frac{4}{9} \cdot b_{ef,3} \cdot h_{N,3} \cdot k_{z,3} \cdot k_{v,H,3} \cdot f_{v,d} = 6.52 \text{ kN}$$

	PD1	PD2	P1	P2
$\tau_{d,H}$ / $V_{\text{Ed},H}$	0.25 MPa	0.22 MPa	0.54 kN	0.54 kN
$f_{v,d}$ / $F_{v,Rd,H}$	2.30 MPa	2.30 MPa	6.52 kN	6.52 kN
Utilization ratio	10.9 %	9.6 %	8.3 %	8.3 %
	OK!	**OK!**	**OK!**	**OK!**

Failure mode 1, Horizontal loads

4.1.2 Compression failure at the bottom of the notch

Verified according to eq. (13).

4.1.2.1 Vertical loads

PD1 and PD2

$l_{z,ef,1} := \min\left(l_{z,1} + 30\text{mm}, 2 \cdot l_{z,1}\right) = 75$ mm

$l_{z,ef,2} := \min\left(l_{z,2} + 30\text{mm}, 2 \cdot l_{z,2}\right) = 120$ mm

$\sigma_{c,90,d,V,1} := \frac{V_{Ed,V}}{h_{N,1} \cdot l_{z,ef,1}} \cdot \frac{1}{k_{c,90}} = 0.0030$ MPa

$\sigma_{c,90,d,V,2} := \frac{V_{Ed,V}}{h_{N,2} \cdot l_{z,ef,2}} \cdot \frac{1}{k_{c,90}} = 0.0019$ MPa

P1 and P2

$$l_{z,ef,3} := \min\left(l_{z,3} + 30\,\text{mm}, 2 \cdot l_{z,3}\right) = 120\ \text{mm}$$

$$\sigma_{c,90,d,V,3} := \frac{V_{Ed,V}}{b_{T,3} \cdot l_{z,ef,3}} \cdot \frac{1}{k_{c,90}} = 0.0035\ \text{MPa}$$

	PD1	PD2	P1	P2
$\sigma_{c,90,d,V}$	0.003 MPa	0.002 MPa	0.003 MPa	0.003 MPa
$f_{c,90,d}$	1.80 MPa	1.80 MPa	1.80 MPa	1.80 MPa
Utilization ratio	0.2 %	0.1 %	0.2 %	0.2 %
	OK!	**OK!**	**OK!**	**OK!**

Failure mode 2, Vertical loads

4.1.2.2 Horizontal loads

PD1 and PD2

$$\sigma_{c,90,d,H,1} := \frac{V_{Ed,H}}{b_{N,1} \cdot l_{z,ef,1}} \cdot \frac{1}{k_{c,90}} = 0.069\ \text{MPa}$$

$$\sigma_{c,90,d,H,2} := \frac{V_{Ed,H}}{b_{N,2} \cdot l_{z,ef,2}} \cdot \frac{1}{k_{c,90}} = 0.043\ \text{MPa}$$

P1 and P2

$$\sigma_{c,90,d,H,3} := \frac{V_{Ed,H}}{b_{N,3} \cdot l_{z,ef,3}} \cdot \frac{1}{k_{c,90}} = 0.029\ \text{MPa}$$

	PD1	PD2	P1	P2
$\sigma_{c,90,d,H}$	0.069 MPa	0.043 MPa	0.029 MPa	0.029 MPa
$f_{c,90,d}$	1.80 MPa	1.80 MPa	1.80 MPa	1.80 MPa
Utilization ratio	3.8 %	2.4 %	1.6 %	1.6 %
	OK!	**OK!**	**OK!**	**OK!**

Failure mode 2, Horizontal loads

4.2 Header member

The header need not to be verified for the vertical loads as the grain is then parallel to the reaction forces.

4.2.1 Failure in shear and tension perpendicular to the grain

PD1 and PD2 are verified as dovetail type III according to eq. (18)

$b_{H,ef,1} := k_{cr} \cdot b_{H,1} = 70.31 \text{ mm}$ $\quad b_{H,ef,2} := b_{H,ef,1}$:

$\tau_{d,H,1} := \frac{3}{4} \cdot \frac{V_{Ed,H}}{b_{H,ef,1} \cdot b_{H,u,1}} = 0.052 \text{ MPa}$ $\quad \tau_{d,H,2} := \tau_{d,H,1}$:

P1 and P2 are verified similarly.

$b_{H,ef,3} := k_{cr} \cdot b_{H,3} = 70.31 \text{ mm}$

$\tau_{d,H,3} := \frac{3}{4} \cdot \frac{V_{Ed,H}}{b_{H,ef,3} \cdot b_{H,u,3}} = 0.070 \text{ MPa}$

	PD1	PD2	P1	P2
$\tau_{d,H}$	0.052 MPa	0.052 MPa	0.070 MPa	0.070 MPa
$f_{v,d}$	2.30 MPa	2.30 MPa	2.30 MPa	2.30 MPa
Utilization ratio	2.3 %	2.3 %	3.0 %	3.0 %
	OK!	**OK!**	**OK!**	**OK!**

Failure mode 4, Horizontal loads

4.2.2 Failure in compression perpendicular to the grain

No interaction in compression zones occur as $l_1 := 1790\text{mm}$:

Calculated similarly as for the joist.

$l_{z,ef,1} := \min\left(b_{N,1} + 60\text{mm}, 2 \cdot b_{N,1}\right) = 120 \text{ mm}$

$l_{z,ef,2} := \min\left(b_{N,2} + 60\text{mm}, 2 \cdot b_{N,2}\right) = 120 \text{ mm}$

$l_{z,ef,3} := \min\left(b_{N,3} + 60\text{mm}, 2 \cdot b_{N,3}\right) = 150 \text{ mm}$

$b_{N,1} := l_{z,1}$: $\quad b_{N,2} := l_{z,2}$: $\quad b_{N,3} := l_{z,3}$:

$$\sigma_{c,90,d,H,H,1} := \frac{V_{Ed,H}}{b_{N,1} \cdot l_{z,ef,1}} \cdot \frac{1}{k_{c,90}} = 0.058 \text{ MPa}$$

$$\sigma_{c,90,d,H,H,2} := \frac{V_{Ed,H}}{b_{N,2} \cdot l_{z,ef,2}} \cdot \frac{1}{k_{c,90}} = 0.029 \text{ MPa}$$

$$\sigma_{c,90,d,H,H,3} := \frac{V_{Ed,H}}{b_{N,3} \cdot l_{z,ef,3}} \cdot \frac{1}{k_{c,90}} = 0.023 \text{ MPa}$$

	PD1	PD2	P1	P2
$\sigma_{c,90,d,H,H}$	0.058 MPa	0.029 MPa	0.023 MPa	0.023 MPa
$f_{c,90,d}$	1.80 MPa	1.80 MPa	1.80 MPa	1.80 MPa
Utilization ratio	3.2 %	1.6 %	1.3 %	1.3 %
	OK!	**OK!**	**OK!**	**OK!**

Failure mode 5, Horizontal loads

4.2.3 Failure in compression perpendicular to the grain due to an axial compression force on the joist

This is verified according to eq. (19)

$$A_B := 225\,\text{mm} \cdot 90\,\text{mm} = 20250 \text{ mm}^2$$

$$A_{N,1} := b_{N,1} \cdot h_{N,1}: \qquad A_{B,ef,1} := A_B - A_{N,1} = 13500.0 \text{ mm}^2$$

$$A_{N,2} := b_{N,2} \cdot h_{N,2}: \qquad A_{B,ef,2} := A_B - A_{N,2} = 13500.0 \text{ mm}^2$$

$$A_{N,3} := b_{N,3} \cdot h_{N,3}: \qquad A_{B,ef,3} := A_B - A_{N,3} = 7425.0 \text{ mm}^2$$

$$\sigma_{c,90,d,Q,1} := \frac{Q_{Ed}}{A_{B,ef,1}} \cdot \frac{1}{k_{c,90}} = 0.18 \text{ MPa}$$

$$\sigma_{c,90,d,Q,2} := \frac{Q_{Ed}}{A_{B,ef,2}} \cdot \frac{1}{k_{c,90}} = 0.18 \text{ MPa}$$

$$\sigma_{c,90,d,Q,3} := \frac{Q_{Ed}}{A_{B,ef,3}} \cdot \frac{1}{k_{c,90}} = 0.34 \text{ MPa}$$

	PD1	PD2	P1	P2
$\sigma_{c,90,d,Q}$	0.18 MPa	0.18 MPa	0.34 MPa	0.34 MPa
$f_{c,90,d}$	1.80 MPa	1.80 MPa	1.80 MPa	1.80 MPa
Utilization ratio	10 %	10 %	19%	19 %
	OK!	**OK!**	**OK!**	**OK!**

Failure mode 6, Axial load

4.2.4 Failure in tension perpendicular to the grain due to an axial force on the joist

This failure mode is only valid for the dovetail joints and in this case only PD1 since PD2 protrudes the full header and therefore this failure mode cannot occur.

$$h_{H,ef,1} := k_{cr} \cdot h_{H,1} = 175.78 \text{ mm}$$

$$\tau_{d,Q,1} := \frac{3}{4} \cdot \frac{Q_{Ed}}{h_{H,ef,1} \cdot l_{z,1}} = 0.41 \text{ MPa}$$

	PD1
$\tau_{d,Q,1}$	0.41 MPa
$f_{v,d}$	2.30 MPa
Utilization ratio	18 %
	OK!

Failure mode 7, Axial load

4.3 Peg

4.3.1. Shear failure of a laterally loaded peg joint

This failure mode is verified according to eq. (25).

Where: $n := 1$:

$$F_{v,Rd,P,3} := \frac{9.5\text{MPa} \cdot n \cdot d_3{}^2 \cdot k_{\text{mod}}}{\gamma_M} = 10.94 \text{ kN}$$

$$F_{v,Rd,P,4} := \frac{9.5\text{MPa} \cdot n \cdot d_4{}^2 \cdot k_{mod}}{\gamma_M} = 2.74 \text{ kN}$$

	P1	P2
$F_{v, Rd, P}$	10.94 kN	2.74 kN
Q_{Ed}	4.36 kN	4.36 kN
Utilization ratio	40 %	160 %
	OK!	**NOT OK!**

Failure mode 8, Axial load

4.3.2. Tension failure perpendicular to the grain

Verified according to eq. (26) where:

$b_S := h_{H,3} - h_{T,3} = 165$ mm

$h_S := b_{H,3} = 90$ mm

$d_S := \frac{h_S}{2} = 45$ mm

$$F_{90, Rd} := 14\text{MPa} \cdot b_S \cdot \sqrt{\frac{d_S}{\left(1 - \frac{d_S}{h_S}\right)}} \cdot \frac{\text{mm}}{\sqrt{\text{mm}}} \cdot \frac{k_{\text{mod}}}{\gamma_M} = 4.99 \sqrt{10.00}\ \text{kN}$$

$evalf\left(F_{90, Rd}\right) = 15.78$ kN

	P1 and P2
$F_{90, Rd}$	15.78 kN
Q_{Ed}	4.36 kN
Utilization ratio	28 %
	OK!

Failure mode 9, Axial load

APPENDIX B4

VERIFICATIONS, CONNECTION C2

1. Loads

$V_{Ed,V} := 2.08\ \text{kN}$:

$V_{Ed,H} := 0.25\ \text{kN}$:

$Q_{Ed} := 0.15\,\text{kN}$:

2. Material properties

The chosen material for this connection is CLT from the products of Martinsons with the values according to Gustafsson et al. *(2019)*.

2.1. Correction and modification factors

$\gamma_M := 1.25$:

$k_{\mathbf{mod}} := 0.80$: (for climate class 1 and average duration load as dimensioning)

$k_{cr} := 0.67$: (according to eq. (2))

$k_n := 6.5$: (according to eq. (3))

$k_{c,90} := 1.5$: (according to eq. (5))

2.2. Design values for material properties

C24-C14-C24	Characteristic strength		Design strength	
Compressive strength ⊥ to the grain	$f_{c,90,k}$:	2.7 MPa	$f_{c,90,d}$:	1.73 MPa
Tension strength ⊥ to the grain	$f_{t,90,k}$:	0.4 MPa	$f_{t,90,d}$:	0.26 MPa
Panel shear	$f_{v,k}$:	4.0 MPa	$f_{v,d}$:	2.56 MPa
Rolling shear	$f_{Rv,k}$:	3.0 MPa	$f_{Rv,d}$:	1.92 MPa

Material Properties - CLT, 3-layer panel

$$f_{c,90,d} := k_{\mathbf{mod}} \cdot \frac{2.7\text{MPa}}{\gamma_M} = 1.73\ \text{MPa} \qquad f_{v,d} := k_{\mathbf{mod}} \cdot \frac{4.0\text{MPa}}{\gamma_M} = 2.56\ \text{MPa}$$

$$f_{t,90,d} := k_{\mathbf{mod}} \cdot \frac{0.4\text{MPa}}{\gamma_M} = 0.26\ \text{MPa} \qquad f_{Rv,d} := k_{\mathbf{mod}} \cdot \frac{3.0\text{MPa}}{\gamma_M} = 1.92\ \text{MPa}$$

	Characteristic strength		Design strength	
(Values in MPa)	C24	C14	C24	C14
Compressive strength ⊥ to the grain, $f_{c,\,90}$	2.5	2.0	1.6	1.28
Tension strength ∥ to the grain, $f_{t,\,0}$	14.5	7.2	9.28	4.61
Tension strength ⊥ to the grain, $f_{t,\,90}$	0.4	0.4	0.26	0.26
Panel shear, f_v	4.0	3.0	2.56	1.92
Elasticity module, E_0	11000	7000		
Elasticity module, E_{90}	370	230		

Material Properties - CLT, Internal layers

$E_{0,\,C24} := 11000\,\text{MPa}$:

$E_{90,\,C14} := 230\,\text{MPa}$:

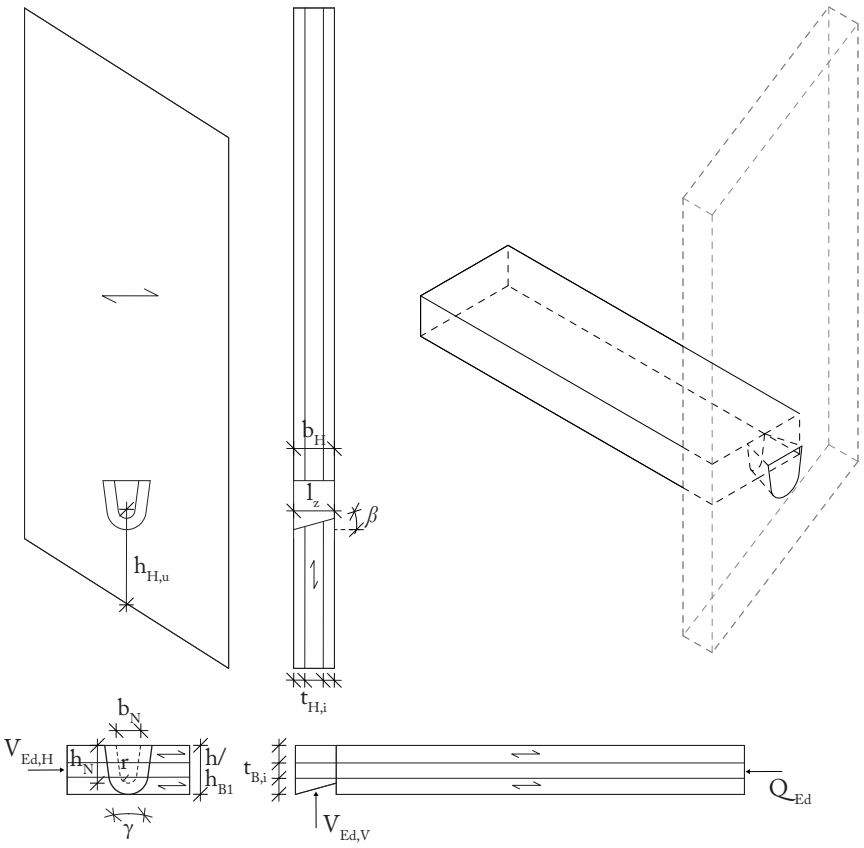

Figure 1. *Geometry for RD.*

3. Geometry

Three different geometries are evaluated with the relevant indata below. The geometries can be seen in Figure 1, 2 and 3. The geometrical data is stated in the table below.

RD1	TM1	N2
Tenon		
$b_{N,RD} := 55.6\,\text{mm}$:	$b_{N,TM} := b_{RD}$:	$b_{N,N} := 300\,\text{mm}$:
$b_{RD} := \frac{b_{N,RD}}{0.8}$:	-	-
$t_{B1} := 40\,\text{mm}$:	$t_{B1} := 40\,\text{mm}$:	$t_{B1} := 40\,\text{mm}$:
$t_{B2} := t_{B1}$:	$t_{B2} := t_{B1}$:	$t_{B2} := t_{B1}$:
$t_{B3} := t_{B1}$:	$t_{B3} := t_{B1}$:	$t_{B3} := t_{B1}$:
$h_{RD} := t_{B1} + t_{B2} + t_{B3} = 120\ \text{mm}$	$h_{TM} := 300\,\text{mm}$:	$h_N := h_{RD}$:
$h_{N,RD} := 93.2\,\text{mm}$:	$h_{N,TM} := 225\,\text{mm}$:	$h_{N,N} := 60\,\text{mm}$:
-	$h_T := 150\,\text{mm}$:	-
$h_{B1} := h_{RD}$:	-	-
$l := 100\,\text{mm}$:	$l_{z,TM} := 100\ \text{mm}$:	$l_{z,N} := 100\,\text{mm}$:
$r := 20\,\text{mm}$:	-	-
$\gamma_{RD} := \frac{12}{360} \cdot 2\pi = \frac{1}{15}\ \pi$	-	-
$i := 0$:	$i := 0$:	$i := 0$:
Header		
$t_{H1} := 30\,\text{mm}$:	$t_{H1} := 30\,\text{mm}$:	$t_{H1} := 30\,\text{mm}$:
$t_{H2} := 40\,\text{mm}$:	$t_{H2} := 40\,\text{mm}$:	$t_{H2} := 40\,\text{mm}$:
$t_{H3} := 30\,\text{mm}$:	$t_{H3} := 30\,\text{mm}$:	$t_{H3} := 30\,\text{mm}$:
$b_H := 100\,\text{mm}$:	$b_H := 100\,\text{mm}$:	$b_H := 100\,\text{mm}$:
$h_{H,u,RD} := 220\,\text{mm}$:	$h_{H,u,TM} := 180\,\text{mm}$:	$h_{H,u,N} := 180\,\text{mm}$:

4. Verifications

4.1 Joist member

4.1.1 Failure in shear and tension at the notch corner

4.1.1.1 Vertical loads

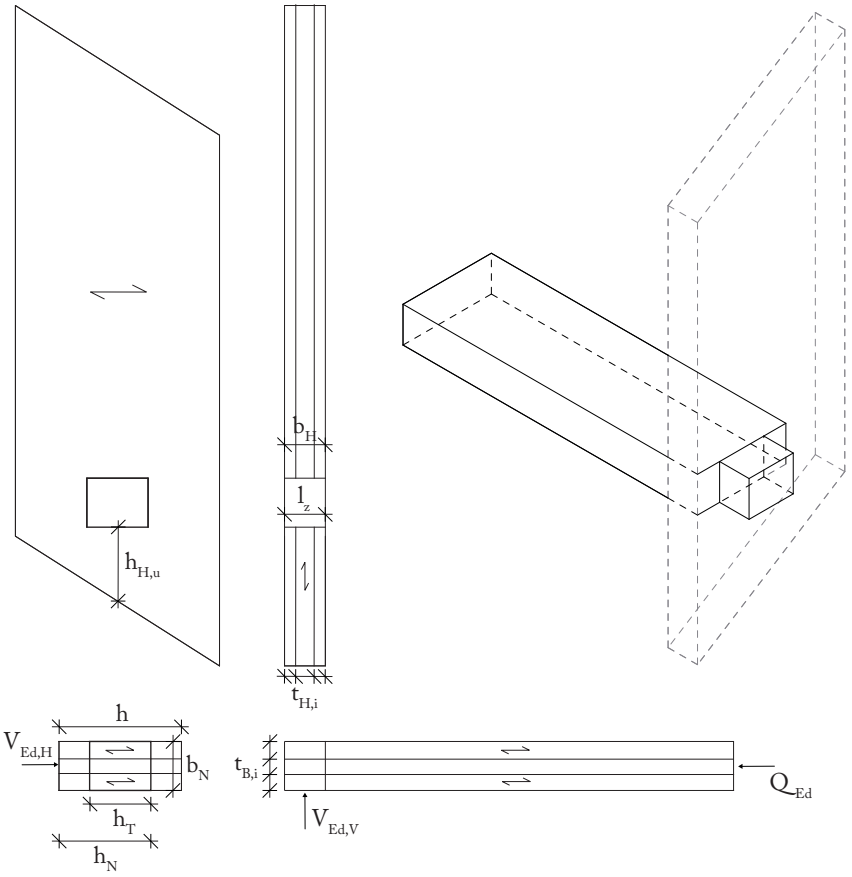

Figure 2. *Geometry for TM.*

Verified for RD1 and N2. The TM1 joist for the vertical load is a simple rectangular beam with a reduced cross-section.

The dovetail is verified according to eq. (23) and the notch according to eq. (6).

RD1

As the crack seem to appear in a perpendicular layer to the crack propagation the height in this formula is reduced. The height h_{B1} is reduced by the distance from the crack to the nearest layer with grain parallel to the crack according to the modifications for CLT for this geometry.

$$F_{v,Rd} = \frac{2}{3} \cdot \left(b_{B1} \cdot \left(h_{B1} - r\right)\right) \cdot k_v \cdot f_{v,d} \qquad \rightarrow F_{v,Rd} = \frac{2}{3} \cdot b_{B1} \cdot t_{B1} \cdot k_v \cdot f_{v,d}$$

$$b_{B1} := evalf\left(\cos\left(\frac{\gamma_{RD}}{2}\right) \cdot r \cdot 2\right) = 39.78 \text{ mm}$$

$red := 33.2\text{mm}$:

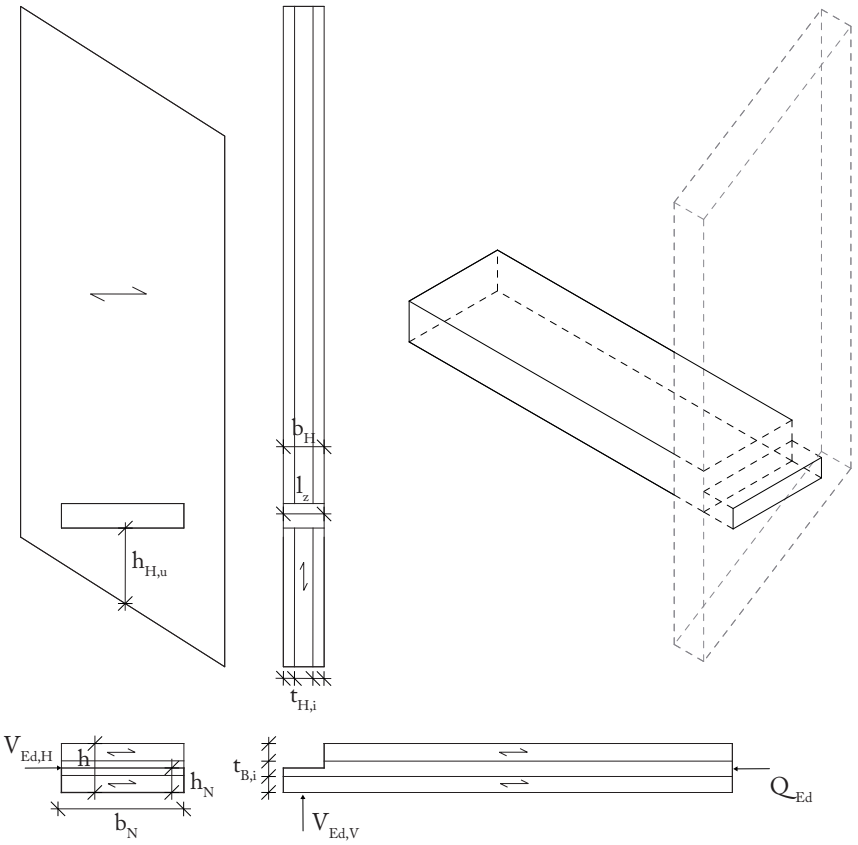

Figure 2. *Geometry for N.*

$$h_{B1,\,red} := h_{B1} - red = 86.8 \text{ mm}$$

$$k_{v,\,V,\,RD} := \left(\frac{h_{B1,\,red}}{h_{RD}} \right)^2 = 0.52$$

$$F_{v,\,Rd,\,V,\,RD} := \frac{2}{3} \cdot b_{B1} \cdot \left(h_{B1,\,red} - r \right) \cdot k_{v,\,V,\,RD} \cdot f_{v,d} = 2.37 \text{ kN}$$

N2

For the notch the crack appear in a perpendicular layer as well. Since the notch is on the opposite side as the support $k_{v,\,V,\,N} := 1$:

$$\alpha_{V,\,N} := \frac{t_{B3}}{h_N} = 0.33 \qquad b_{ef,\,V,\,N} := k_{cr} \cdot b_{N,\,N} = 201.00 \text{ mm}$$

$$\tau_{d,\,V,\,N} := \frac{3}{2} \cdot \frac{V_{Ed,\,V}}{\alpha_{V,\,N} \cdot h_N \cdot b_{ef,\,V,\,N}} = 0.39 \text{ MPa}$$

	RD1	N2
$F_{v, Rd, V}$ / $f_{v, d}$	2.37 kN	2.56 MPa
$V_{Ed, V}$ / $\tau_{d,V}$	2.08 kN	0.39 MPa
Utilization ratio	88 %	15 %
	OK!	**OK!**

Failure mode 1, Vertical loads

RD1 is verified as dovetail type II and then TM1 is verified. Verification according to eq. (24) and eq. (20b). Both of these are modified for CLT because the centre layer act as reinforcement against this crack.

RD1

$$b_{N, ef, RD} := evalf\left(b_{N, RD} - h_{N, RD} \cdot \tan\left(\frac{\gamma_{RD}}{2}\right)\right) = 45.80 \text{ mm}$$

$$\alpha_{H, RD} := \frac{0.5 \cdot \left(b_{N, RD} + b_{N, ef, RD}\right)}{b_{RD}} = 0.73 \qquad x_{RD} := \frac{l_{z, RD}}{2} = 50 \text{ mm}$$

$$k_{v, H, RD} := \min\left(1.0, \frac{k_n \cdot \left(1 + \frac{1.1 \cdot i^{1.5}}{\sqrt{b_{RD}}}\right) \cdot \sqrt{\text{mm}}}{\sqrt{b_{RD}} \cdot \left(\sqrt{\alpha_{H, RD} - \alpha_{H, RD}^2} + 0.8 \cdot \frac{x_{RD}}{b_{RD}} \cdot \sqrt{\frac{1}{\alpha_{H, RD}} - \alpha_{H, RD}^2}\right)}\right) = 0.80$$

$$F_{v, Rd, H, RD} := \frac{2}{3} \cdot b_{N, ef, RD} \cdot \left(h_{N, RD} - t_{B2}\right) \cdot k_{v, H, RD} \cdot f_{v,d} = 3.34 \text{ kN}$$

TM1

$$b_{ef, TM} := k_{cr} \cdot \left(b_{N, TM} - t_{B2}\right) = 53.60 \text{ mm}$$

$$k_{z,H} := \frac{h_T}{h_{N,TM}} \cdot \left(1 + 2 \cdot \left(1 - \frac{h_T}{h_{N,TM}}\right)^2\right) \cdot \left(2 - \frac{h_{N,TM}}{h_{TM}}\right) = 1.02$$

$$\alpha_{H, TM} := \frac{h_{N, TM}}{h_{TM}} = 0.75 \qquad x_{TM} := \frac{l_{z, TM}}{2} = 50 \text{ mm}$$

$$k_{v,H,TM} := evalf\left(\min\left(1.0, \frac{k_n \cdot \left(1 + \frac{1.1 \cdot i^{1.5}}{\sqrt{h_{TM}}}\right) \cdot \sqrt{\text{mm}}}{\sqrt{h_{TM}} \cdot \left(\sqrt{\alpha_{H,TM} - \alpha_{H,TM}^2} + 0.8 \cdot \frac{x_{TM}}{h_{TM}} \cdot \sqrt{\frac{1}{\alpha_{H,TM}} - \alpha_{H,TM}^2}\right)}\right)\right) = 0.68$$

$$F_{v,Rd,H,TM} := \frac{4}{9} \cdot b_{ef,TM} \cdot h_{N,TM} \cdot k_{z,H} \cdot k_{v,H,TM} \cdot f_{v,d} = 9.53 \text{ kN}$$

	RD1	TM1
$F_{v,Rd,H}$	3.34 kN	9.53 kN
$V_{Ed,H}$	0.25 kN	0.25 kN
Utilization ratio	7.5 %	2.6 %
	OK!	**OK!**

Failure mode 1, Horizontal loads

As the reduced cross-section still gives a capacity that is well above the dimensioning load no verification of the reinforcement layer is needed.

4.1.2 Compression failure at the bottom of the notch

Verified according to eq. (13).

4.1.2.1 Vertical loads

$l_{z,ef,V} := \min\left(l_{z,RD} + 30\text{mm}, 2 \cdot l_{z,RD}\right) = 130$ mm (The same for all three connections)

$$\sigma_{c,90,d,V,RD} := \frac{V_{Ed,V}}{b_{N,RD} \cdot l_{z,ef,V}} \cdot \frac{1}{k_{c,90}} = 0.1918 \text{ MPa}$$

$$\sigma_{c,90,d,V,TM} := \frac{V_{Ed,V}}{b_T \cdot l_{z,ef,V}} \cdot \frac{1}{k_{c,90}} = 0.0711 \text{ MPa}$$

$$\sigma_{c,90,d,V,N} := \frac{V_{Ed,V}}{b_{N,N} \cdot l_{z,ef,V}} \cdot \frac{1}{k_{c,90}} = 0.0356 \text{ MPa}$$

	RD1	TM1	N2
$\sigma_{c,90,d,V}$	0.19 MPa	0.07 MPa	0.04 MPa
$f_{c,90,d}$	1.73 MPa	1.73 MPa	1.73 MPa
Utilization ratio	11 %	4 %	2 %
	OK!	**OK!**	**OK!**

Failure mode 2, Vertical loads

4.1.2.2 Horizontal loads

This failure mode is not relevant in this direction as not all layers have fibres perendicular to the load.

4.1.3 Rolling shear failure of the notch (only for CLT)

Verified according to eq. (14) for the vertical force case. For the horizontal force the orientation of the layers doesn't give a rolling shear case.

The dovetail is approximated as shown in Chapter 6.1.4.1. in the general calculation method.

4.1.3.1 Calculation of the first moment of inertia for rolling shear

RD1

$t_{R,1,RD} := t_{B1}$: $t_{R,2,RD} := t_{B2}$: $t_{R,3,RD} := h_{N,RD} - (t_{B1} + t_{B2}) =$ 13.2 mm

$a_{S,1,RD} := \frac{t_{R,1,RD}}{2} = 20$ mm $a_{S,2,RD} := t_{R,1,RD} + \frac{t_{R,2,RD}}{2} = 60$ mm

$a_{S,3,RD} := t_{R,1,RD} + t_{R,2,RD} + \frac{t_{R,3,RD}}{2} = 86.60$ mm

$b_{R,3,RD} := b_{B1,RD} = 39.78$ mm

$b_{R,2,RD} := evalf\left(b_{R,3,RD} + \tan\left(\frac{\gamma_{RD}}{2}\right) \cdot t_{R,3,RD} \cdot 2\right) = 42.56$ mm

$b_{R,1,RD} := evalf\left(b_{R,2,RD} + \tan\left(\frac{\gamma_{RD}}{2}\right) \cdot t_{R,2,RD} \cdot 2\right) = = 50.96$ mm

$$z_{0,RD} := \left(b_{R,1,RD} \cdot t_{R,1,RD} \cdot a_{S,1,RD} + \frac{E_{90,C14}}{E_{0,C24}} \cdot b_{R,2,RD} \cdot t_{R,2,RD} \cdot a_{S,2,RD} + b_{R,3,RD} \cdot t_{R,3,RD} \cdot a_{S,3,RD} \right) \Big/ \left(b_{R,1,RD} \cdot t_{R,1,RD} + \frac{E_{90,C14}}{E_{0,C24}} \cdot b_{R,2,RD} \cdot t_{R,2,RD} + b_{R,3,RD} \cdot t_{R,3,RD} \right)$$

$= 34.00$ mm

The rolling shear layer is only to one side of the centre of gravity.

$$z_{B,2,RD} := t_{R,1,RD} - z_{0,RD} = 6.00 \text{ mm}$$

$$z_{T,2,RD} := z_{B,2,RD} + t_{R,2,RD} = 46.00 \text{ mm}$$

$$S_{R,x,RD} := \frac{E_{90,C14}}{E_{0,C24}} \cdot b_{R,2,RD} \cdot \left(\frac{z_{T,2,RD}^2}{2} - \frac{z_{B,2,RD}^2}{2} \right) = 925.31 \text{ mm}^3$$

TM1

Symmetrical cross-section where all layers have the same width and height hence:

$$z_{0,TM} := \frac{b_{N,TM}}{2} = 60 \text{ mm} \qquad z_{B,TM} := 0\text{mm} : \qquad z_{T,TM} := \frac{t_{B2}}{2} = 20 \text{ mm}$$

$$S_{R,x,TM} := \frac{E_{90,C14}}{E_{0,C24}} \cdot b_T \cdot \left(\frac{z_{T,TM}^2}{2} - \frac{z_{B,TM}^2}{2} \right) = 627.27 \text{ mm}^3$$

N2

All layers have the same width.

$$t_{2,N} := 20\text{mm} : \qquad t_{3,N} := t_{B3} :$$

$$a_{S,2,N} := \frac{t_{2,N}}{2} = 10 \text{ mm} \qquad a_{S,3,N} := t_{2,N} + \frac{t_{3,N}}{2} = 40 \text{ mm}$$

$$z_{0,N} := \frac{\frac{E_{90,C14}}{E_{0,C24}} \cdot b_{N,N} \cdot t_{2,N} \cdot a_{S,2,N} + b_{N,N} \cdot t_{3,N} \cdot a_{S,3,N}}{\frac{E_{90,C14}}{E_{0,C24}} \cdot b_{N,N} \cdot t_{2,N} + b_{N,N} \cdot t_{3,N}} = 39.69 \text{ mm}$$

$$z_{B,N} := z_{0,N} - t_{2,N} = 19.69 \text{ mm}$$

$$z_{T,N} := z_{0,N} = = 39.69 \text{ mm}$$

$$S_{R,x,N} := \frac{E_{90,C14}}{E_{0,C24}} \cdot b_{N,N} \cdot \left(\frac{z_{T,N}^2}{2} - \frac{z_{B,N}^2}{2} \right) = 3724.70 \text{ mm}^3$$

4.1.3.2 Calculation of the second moment of inertia for rolling shear

RD1

$$a_{I,1,RD} := z_{0,RD} - a_{S,1,RD} = 14.00 \text{ mm} \qquad a_{I,2,RD} := \left| z_{0,RD} - a_{S,2,RD} \right| = 26.00 \text{ mm}$$

$$a_{I,3,RD} := \left| z_{0,RD} - a_{S,3,RD} \right| = 52.60 \text{ mm}$$

$$I_{x,net,RD} := \left(\frac{b_{R,1,RD} \cdot t_{R,1,RD}^3}{12} + b_{R,1,RD} \cdot t_{R,1,RD} \cdot a_{I,1,RD}^2 \right) + \left(\frac{E_{90,C14}}{E_{0,C24}} \left(\frac{b_{R,2,RD} \cdot t_{R,2,RD}^3}{12} + b_{R,2,RD} \cdot t_{R,2,RD} \cdot a_{I,2,RD}^2 \right) \right) + \left(\frac{b_{R,3,RD} \cdot t_{R,3,RD}^3}{12} + b_{R,3,RD} \cdot t_{R,3,RD} \cdot a_{I,3,RD}^2 \right)$$
$$= 1548100.10 \text{ mm}^4$$

TM1

$$a_{I,1,TM} := 40\text{mm} : \qquad a_{I,2,TM} := 0\text{mm} :$$

$$a_{I,3,TM} := a_{I,1,TM} = 40.00 \text{ mm}$$

$$I_{x,net,TM} := \left(\frac{h_T \cdot t_{B1}^3}{12} + h_T \cdot t_{B1} \cdot a_{I,1,TM}^2 \right) + \left(\frac{E_{90,C14}}{E_{0,C24}} \left(\frac{h_T \cdot t_{B2}^3}{12} + h_T \cdot t_{B2} \cdot a_{I,2,TM}^2 \right) \right) + \left(\frac{h_T \cdot t_{B3}^3}{12} + h_T \cdot t_{B3} \cdot a_{I,3,TM}^2 \right)$$
$$= 20816727.27 \text{ mm}^4$$

N2

$$a_{I,2,N} := \left| z_{0,N} - a_{S,2,N} \right| = 29.69 \text{ mm}$$

$$a_{I,3,N} := \left| z_{0,N} - a_{S,3,N} \right| = 0.31 \text{ mm}$$

$$I_{x,net,N} := \left(\frac{E_{90,C14}}{E_{0,C24}} \left(\frac{b_{N,N} \cdot t_{2,N}^3}{12} + b_{N,N} \cdot t_{2,N} \cdot a_{I,2,N}^2 \right) \right) + \left(\frac{b_{N,N} \cdot t_{3,N}^3}{12} + b_{N,N} \cdot t_{3,N} \cdot a_{I,3,N}^2 \right)$$
$$= 1715922.71 \text{ mm}^4$$

4.1.3.3 Calculation of the rolling shear stress

RD1

$$b_{ef,V,RD} := k_{cr} \cdot b_{B1,RD} = 26.65 \text{ mm}$$

$$\tau_{Rd,V,RD} := \frac{V_{Ed,V} \cdot S_{R,x,RD}}{I_{x,net,RD} \cdot b_{ef,V,RD}} = 0.033 \text{ MPa}$$

TM1

$$b_{ef,V,TM} := k_{cr} \cdot b_{T} = 100.50 \text{ mm}$$

$$\tau_{Rd,V,TM} := \frac{V_{Ed,V} \cdot S_{R,x,TM}}{I_{x,net,TM} \cdot b_{ef,V,TM}} = 0.004 \text{ MPa}$$

N2

$$b_{ef,V,N} := k_{cr} \cdot b_{N,N} = 201.00 \text{ mm}$$

$$\tau_{Rd,V,TM} := \frac{V_{Ed,V} \cdot S_{R,x,N}}{I_{x,net,N} \cdot b_{ef,V,N}} = 0.022 \text{ MPa}$$

	RD1	TM1	N2
$\tau_{Rd,V}$	0.033 MPa	0.004 MPa	0.022 MPa
$f_{Rv,d}$	1.92 MPa	1.92 MPa	1.92 MPa
Utilization ratio	1.7 %	0.2 %	1.1 %
	OK!	**OK!**	**OK!**

Failure mode 3, Vertical loads

4.2 Header member

For the header the grain direction is, for simplification, assumed to be orthogonal to the loads with the two outer layers having a horizontal grain direction and the centre layer a vertical grain direction.

4.2.1 Failure in shear and tension perpendicular to the grain

4.2.1.1 Vertical loads

The width is modifies to only include the layers with grain parallel to the crack propagation according to Chapter 4.2.2.1. of the general calculation method.

Verified according to eq. (18).

$$b_{H,ef} := k_{cr} \cdot \left(t_{H1} + t_{H3}\right) = 40.20 \text{ mm}$$

$$\tau_{d,V,RD} := \frac{3}{4} \cdot \frac{V_{Ed,V}}{b_{H,ef} \cdot h_{H,u,RD}} = 0.18 \text{ MPa}$$

$$\tau_{d,V,TM} := \frac{3}{4} \cdot \frac{V_{Ed,V}}{b_{H,ef} \cdot h_{H,u,TM}} = 0.22 \text{ MPa}$$

$$\tau_{d,V,N} := \frac{3}{4} \cdot \frac{V_{Ed,V}}{b_{H,ef} \cdot h_{H,u,N}} = 0.22 \text{ MPa}$$

	RD1	TM1	N2
$\tau_{Rd,V}$	0.18 MPa	0.22 MPa	0.22 MPa
$f_{v,d}$	2.56 MPa	2.56 MPa	2.56 MPa
Utilization ratio	7.3 %	8.6 %	8.6 %
	OK!	**OK!**	**OK!**

Failure mode 4, Vertical loads

As the reduced cross-section still gives stresses much lower than what the material can handle it is not necessary to verify the reinforcement layer.

4.2.1.1 Horizontal loads

With regards to the horizontal loads the width from the edge is so far and the reinforcement layers are more than the layers for the crack propagation that this failure is not deemed necessary.

4.2.2 Failure in compression perpendicular to the grain

Since not all layers have grain perpendicular to the load in either the case of the vertical or horizontal load this is not a relevant failure mode for the railing.

4.2.3 Failure in compression perpendicular to the grain due to an axial compression force on the joist

This is verified according to eq. (19)

$$A_B := 300\text{mm} \cdot 120\text{mm} = 36000 \text{ mm}^2$$

$$A_{N,RD} := b_{N,RD} \cdot h_{N,RD}: \qquad A_{B,ef,RD} := A_B - A_{N,RD} = 30818.08 \text{ mm}^2$$

$A_{N,\,TM} := b_{N,\,TM} \cdot h_T$: $\quad A_{B,\,ef,\,TM} := A_B - A_{N,\,TM} = 18000\ \text{mm}^2$

$A_{N,\,N} := b_{N,\,N} \cdot h_{N,\,N}$: $\quad A_{B,\,ef,\,N} := A_B - A_{N,\,N} = 18000\ \text{mm}^2$

$$\sigma_{c,\,90,\,d,\,Q,\,RD} := \frac{Q_{Ed}}{A_{B,\,ef,\,RD}} \cdot \frac{1}{k_{c,\,90}} = 0.003\ \text{MPa}$$

$$\sigma_{c,\,90,\,d,\,Q,\,TM} := \frac{Q_{Ed}}{A_{B,\,ef,\,TM}} \cdot \frac{1}{k_{c,\,90}} = 0.006\ \text{MPa}$$

$$\sigma_{c,\,90,\,d,\,Q,\,N} := \frac{Q_{Ed}}{A_{B,\,ef,\,N}} \cdot \frac{1}{k_{c,\,90}} = 0.006\ \text{MPa}$$

	RD1	TM1	N2
$\sigma_{c,\,90,\,d,\,Q}$	0.003 MPa	0.006 MPa	0.006 MPa
$f_{c,\,90,\,d}$	1.73 MPa	1.73 MPa	1.73 MPa
Utilization ratio	0.2 %	0.4 %	0.4 %
	OK!	**OK!**	**OK!**

Failure mode 6, Axial load

4.2.4 Failure in tension perpendicular to the grain due to an axial force on the joist

This failure mode is only valid for the dovetail joint but not in this case since the dovetail protrudes the full cross-section of the header.

APPENDIX C

Appendix C consists of stress graphs for all FE models from Abaqus.

APPENDIX C1

BENDING STRESS FOR C1 - PD1, PD2, P1 & P2, LC1

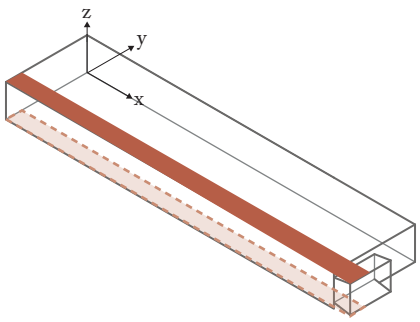

Figure 1. *Paths to consider bending stress for PD1.*

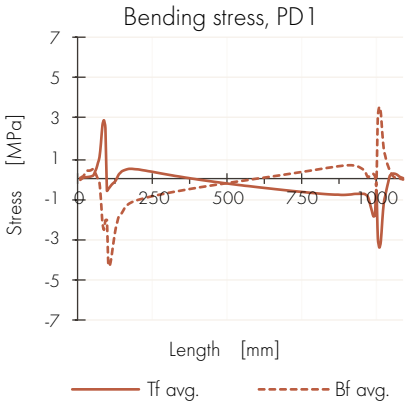

Figure 2. *Bending stress, tf and bf for PD1.*

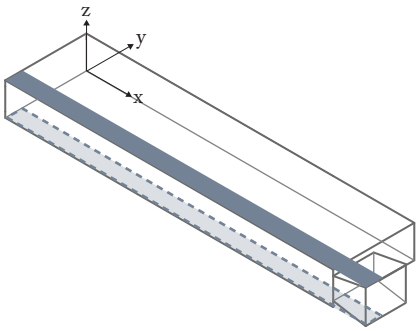

Figure 3. *Paths to consider bending stress for PD2.*

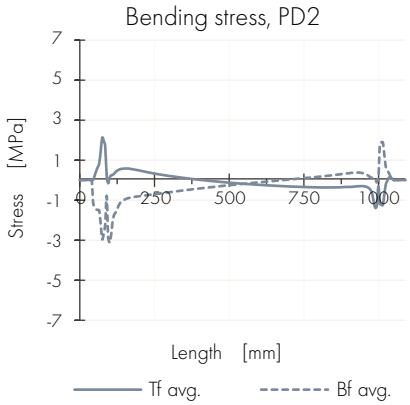

Figure 4. *Bending stress, tf and bf for PD2.*

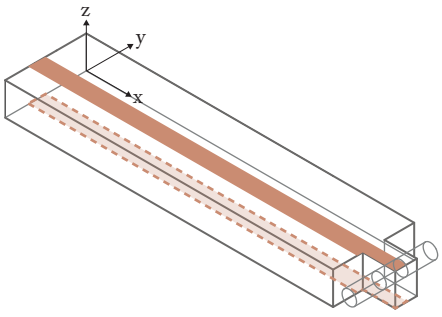

Figure 5. *Paths to consider bending stress for P1.*

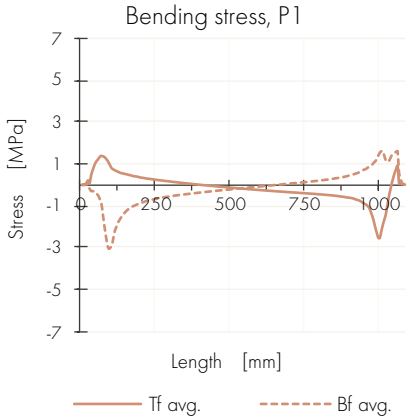

Figure 6. *Bending stress, tf and bf for P1.*

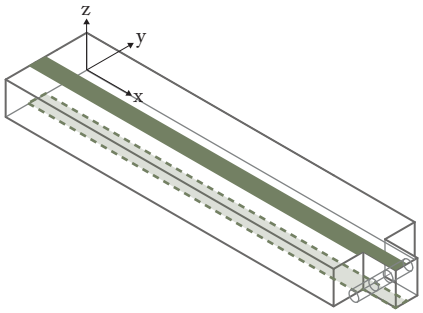

Figure 7. *Paths to consider bending stress for P2.*

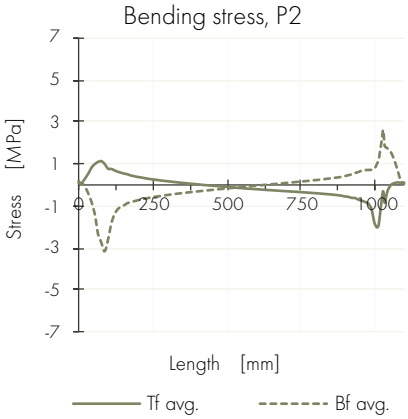

Figure 8. *Bending stress, tf and bf for P2.*

BENDING STRESS FOR C1 - P1 & P2, LC2

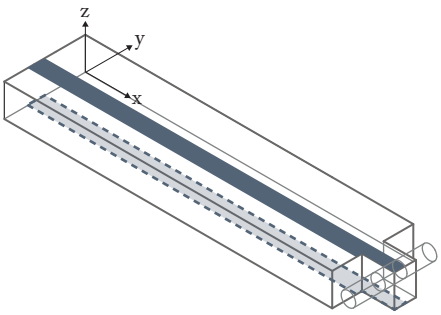

Figure 9. *Paths to consider bending stress for P1, LC2.*

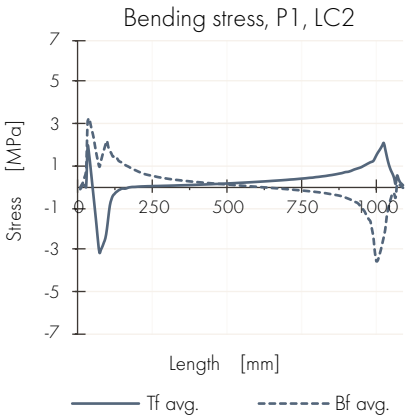

Figure 10. *Bending stress, tf and bf for P1, LC2.*

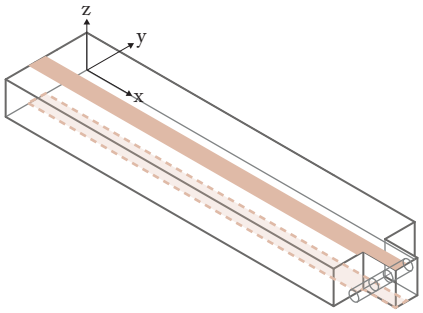

Figure 11. *Paths to consider bending stress for P2, LC2.*

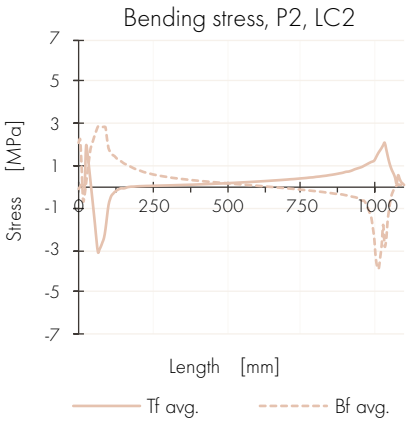

Figure 12. *Bending stress, tf and bf for P2, LC2.*

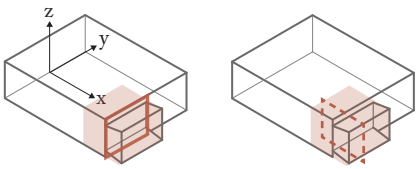

Figure 13. *Paths to consider shear, tension and compression stress for PD1.*

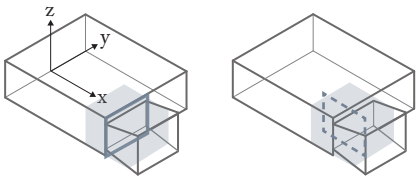

Figure 15. *Paths to consider shear, tension and compression stress for PD2.*

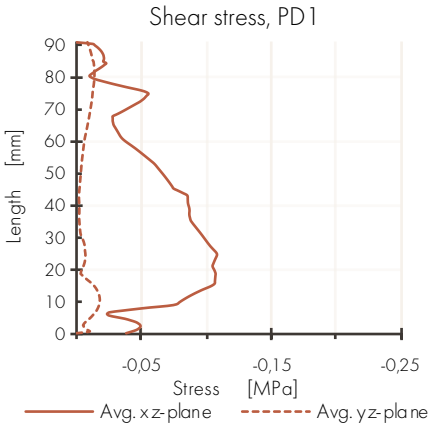

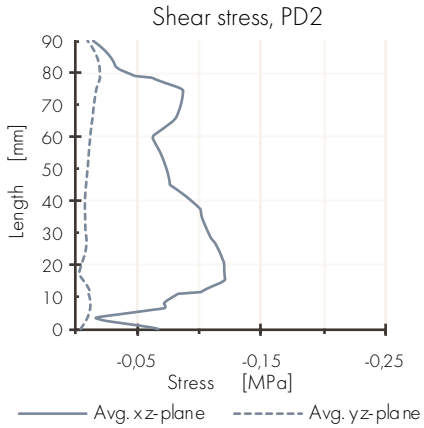

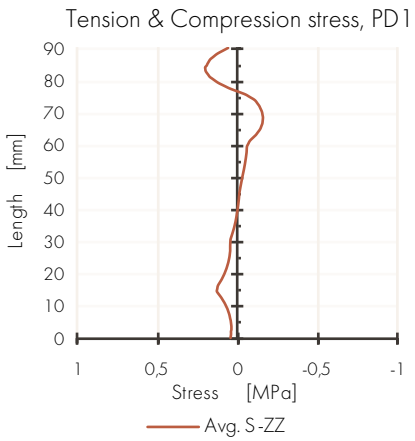

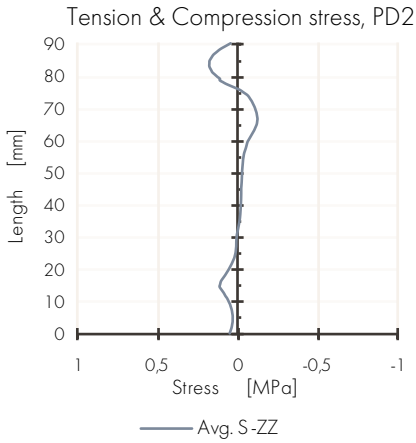

Figure 14. *Average shear, tension and compression stress for PD1.*

Figure 16. *Average shear, tension and compression stress for PD2.*

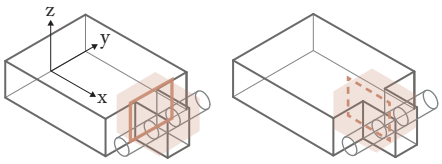

Figure 17 *Paths to consider shear, tension and compression stress for P1.*

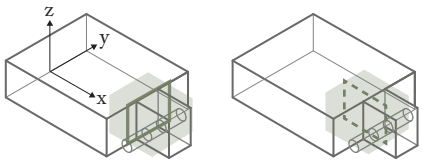

Figure 19. *Paths to consider shear, tension and compression stress for P2.*

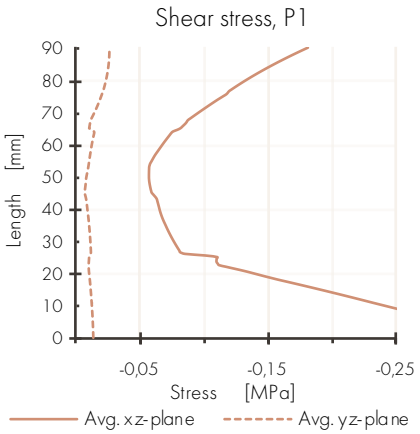

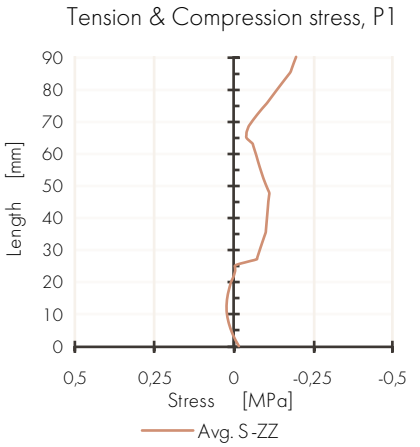

Figure 18. *Average shear, tension and compression stress for P1.*

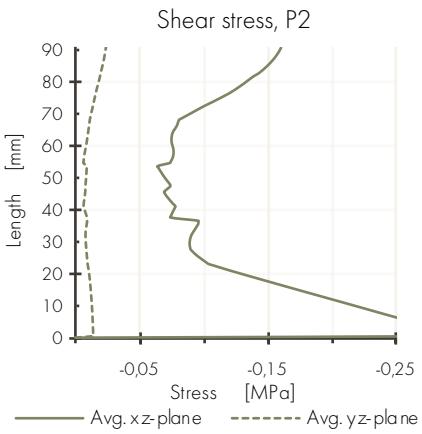

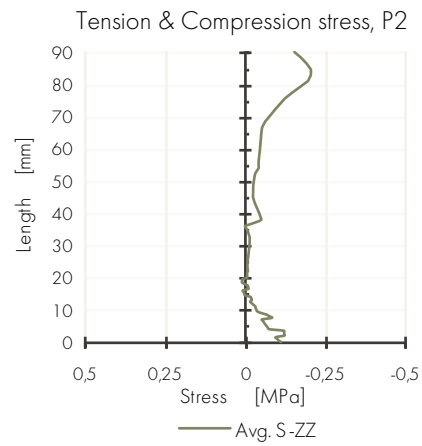

Figure 20. *Average shear, tension and compression stress for P2.*

SHEAR, COMPRESSION AND TENSION
STRESS FOR C1 - P1 & P2 LC2

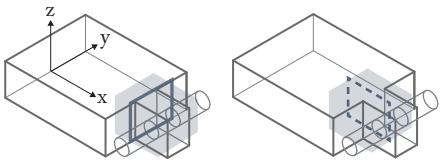

Figure 21. *Paths to consider shear, tension and compression stress for P1.*

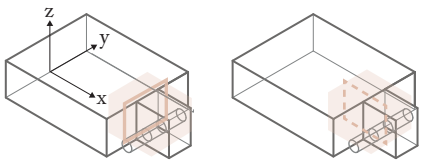

Figure 23. *Paths to consider shear, tension and compression stress for P2.*

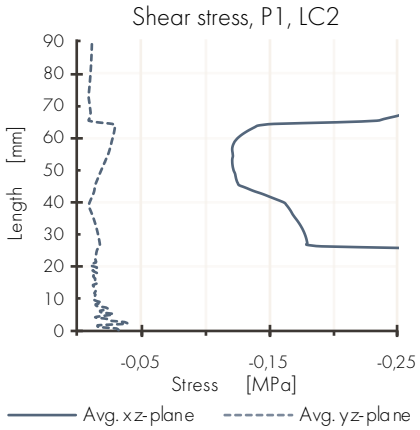

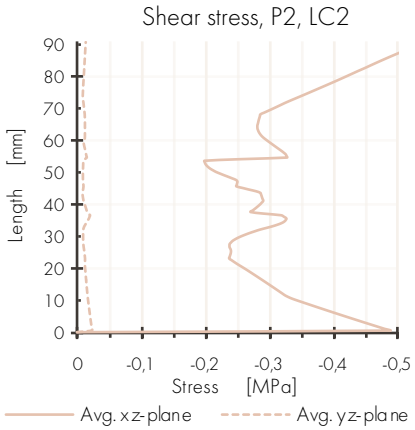

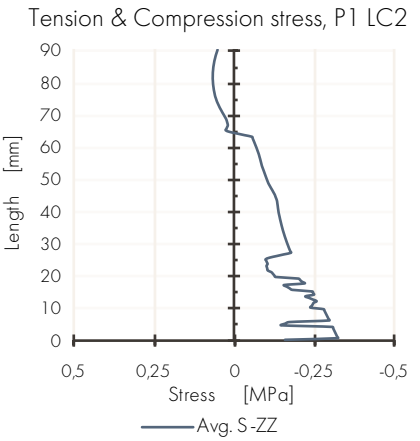

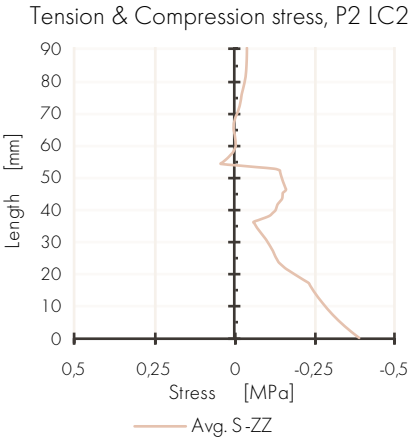

Figure 22. *Average shear, tension and compression stress for P1, LC2.*

Figure 24. *Average shear, tension and compression stress for P2, LC2.*

APPENDIX C2

BENDING STRESS FOR C2 - TM1, N1 & N2

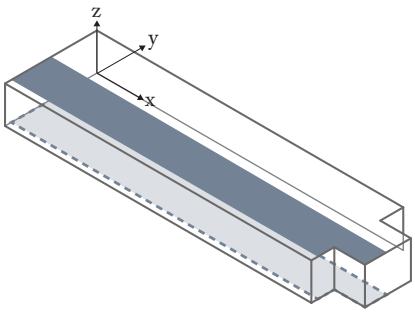

Figure 25. *Paths to consider bending stress for TM1.*

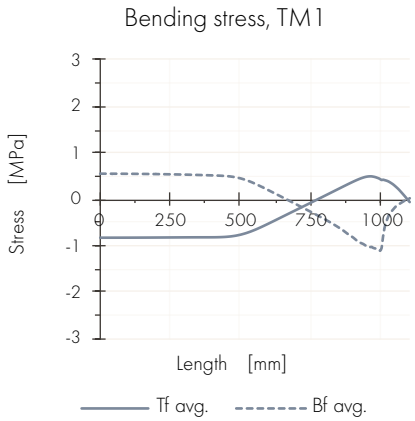

Figure 26. *Bending stress for tenon and mortise, top and bottom fibres, TM1.*

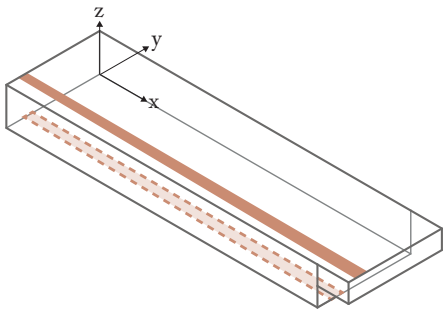

Figure 27. *Paths to consider bending stress for N1.*

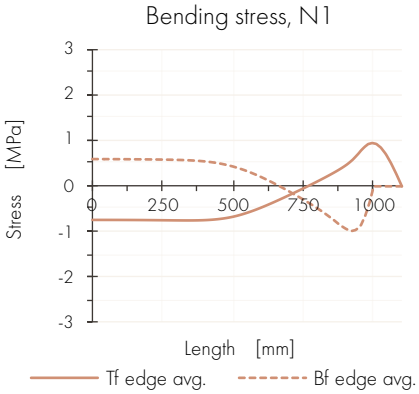

Figure 28. *Bending stress for a top notch, top and bottom fibres, N1.*

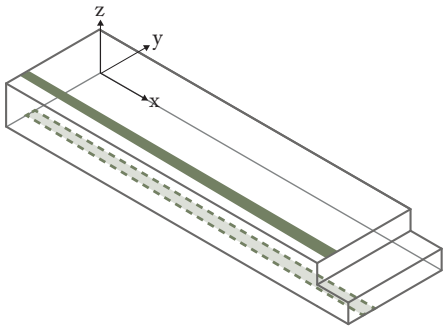

Figure 29. *Paths to consider bending stress for N2.*

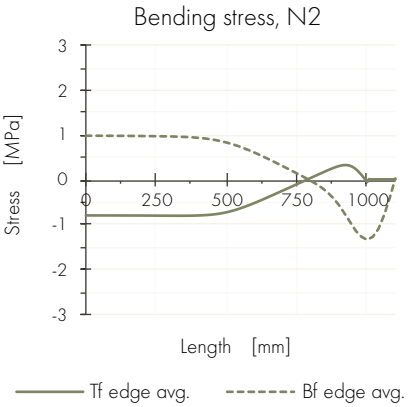

Figure 30. *Bending stress for bottom notch, top and bottom fibres, N2.*

BENDING STRESS FOR C2 - RD1, RD2, RD3, RD4 & RD5

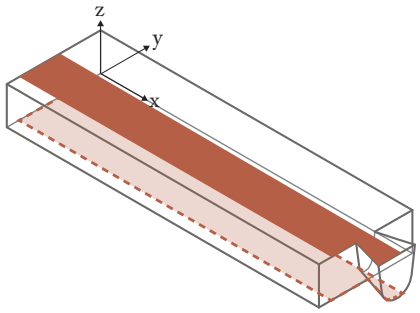

Figure 31. *Paths to consider bending stress for RD1.*

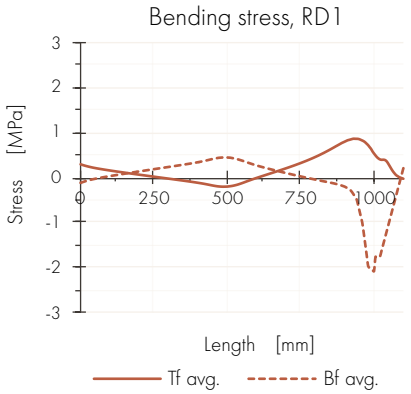

Figure 32. *Bending stress for dovetail joints, top and bottom fibres, RD1.*

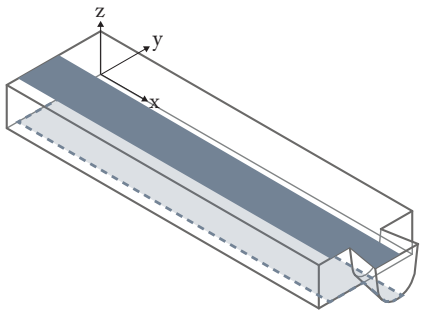

Figure 33. *Paths to consider bending for RD2.*

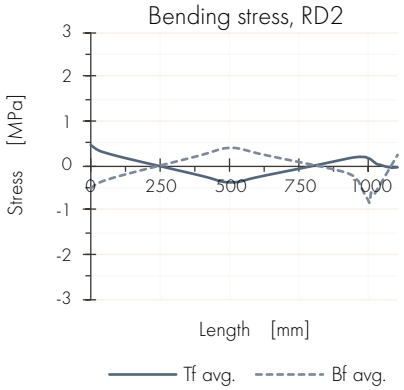

Figure 34. *Bending stress, tf and bf for RD2.*

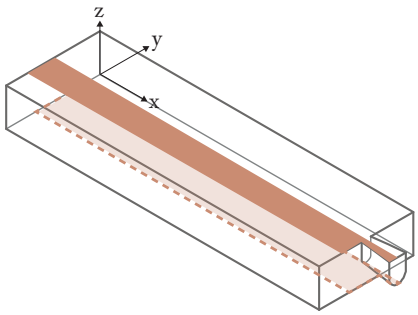

Figure 35. *Paths to consider bending for RD3.*

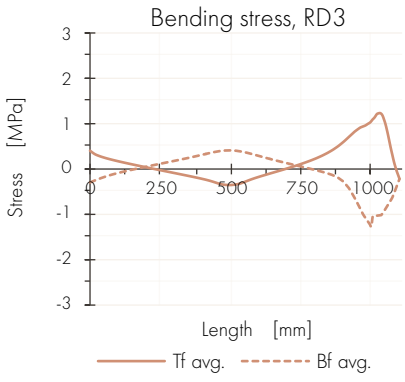

Figure 36. *Bending stress, tf and bf for RD3.*

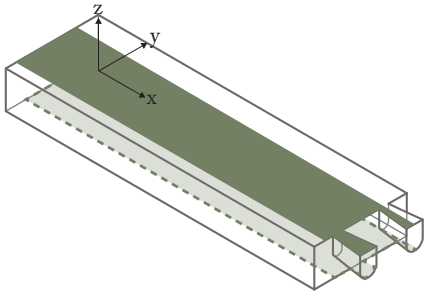

Figure 37. *Paths to consider bending for RD4.*

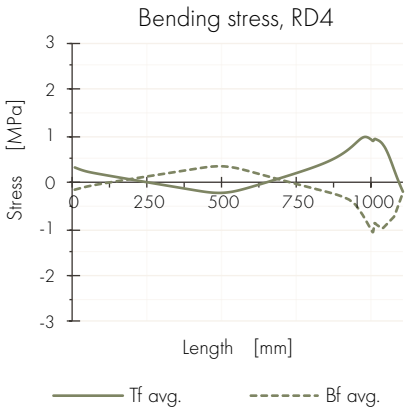

Figure 38. *Bending stress, tf and bf for RD4.*

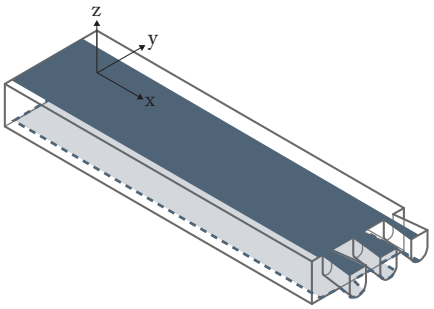

Figure 39. *Paths to consider bending for, RD5.*

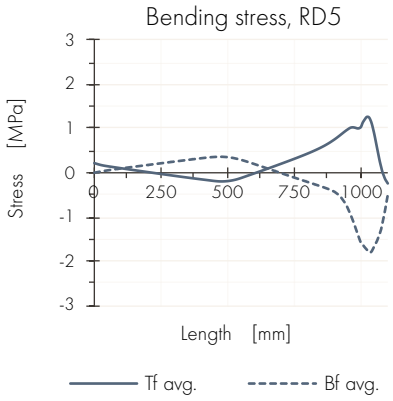

Figure 40. *Bending stress, tf and bf for RD5.*

SHEAR, COMPRESSION AND TENSION
STRESS FOR C2 - TM1, N1, N2 & RD1

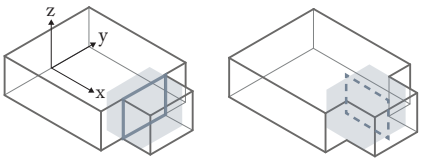

Figure 41. *Path planes to consider shear, tension and compression stress for TM1.*

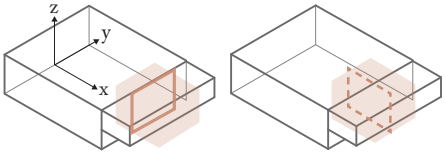

Figure 43. *Paths to consider shear, tension and compression stress for N1.*

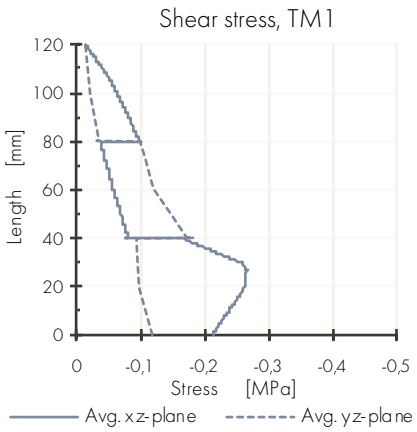

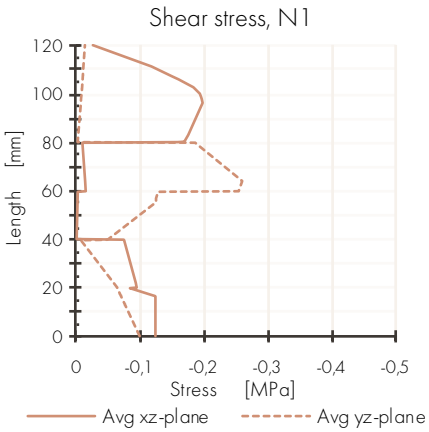

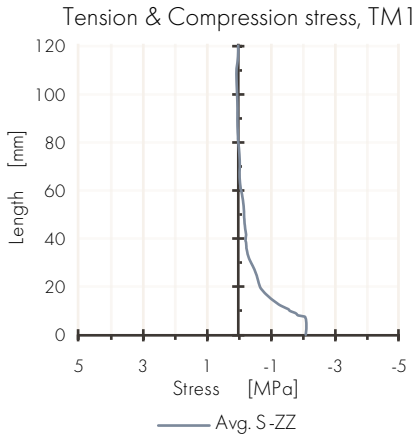

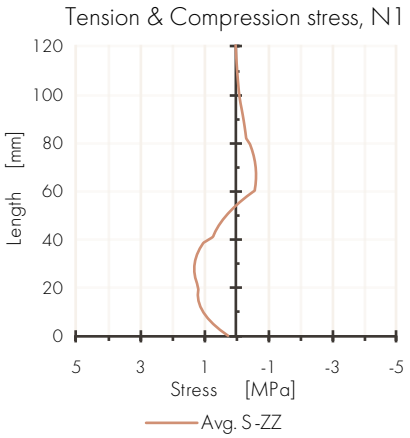

Figure 42. *Average shear, tension and compression stress for TM1.*

Figure 44. *Average shear, tension and compression stress for N1.*

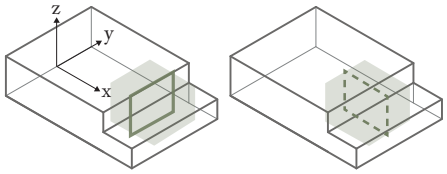

Figure 45. *Paths to consider shear, tension and compression stress for N2.*

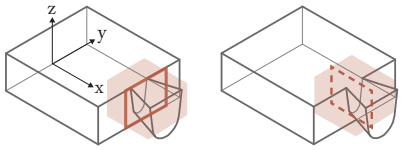

Figure 47. *Paths to consider shear, tension and compression stress for RD1.*

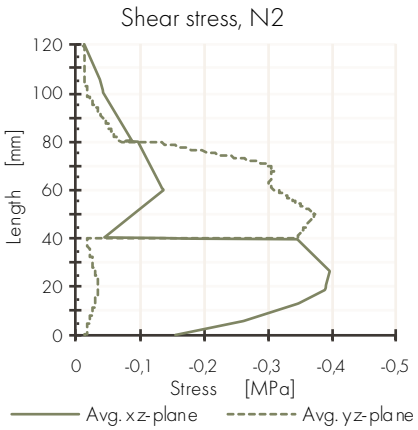

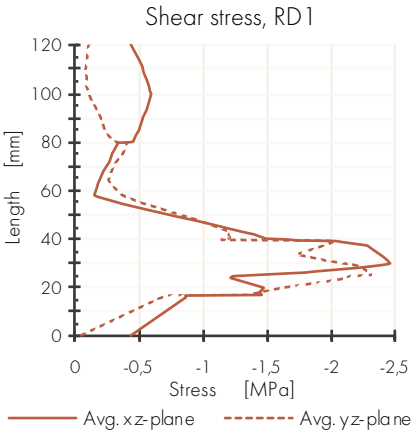

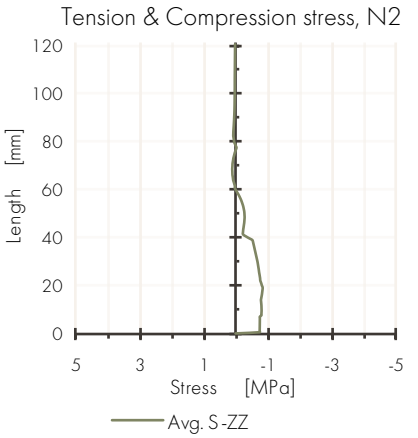

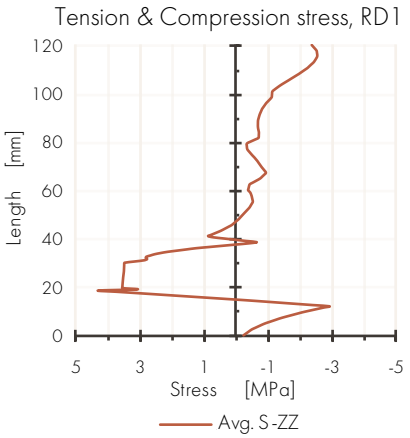

Figure 46. *Average shear, tension and compression stress for N2.*

Figure 48. *Average shear, tension and compression stress for RD1.*

SHEAR STRESS FOR C2 - RD1, RD2, RD3, RD4 & RD5

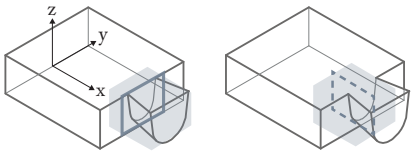

Figure 49. *Paths to consider shear stress for RD2.*

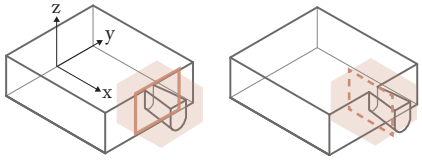

Figure 51. *Paths to consider shear stress for RD3.*

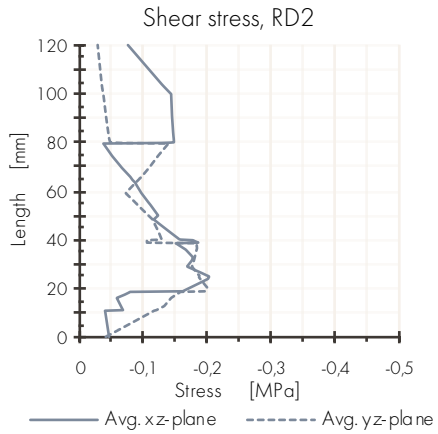

Figure 50. *Average shear stress for RD2.*

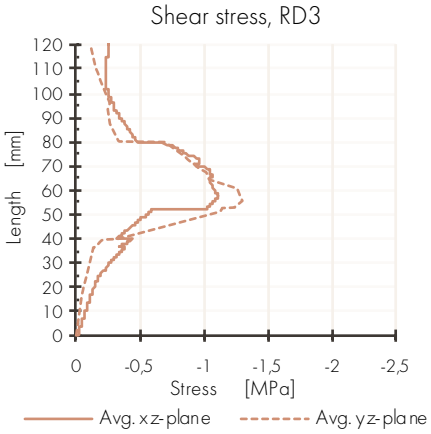

Figure 52. *Average shear stress for RD3.*

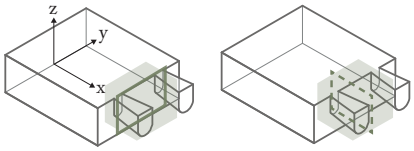

Figure 53. *Paths to consider shear stress for RD4.*

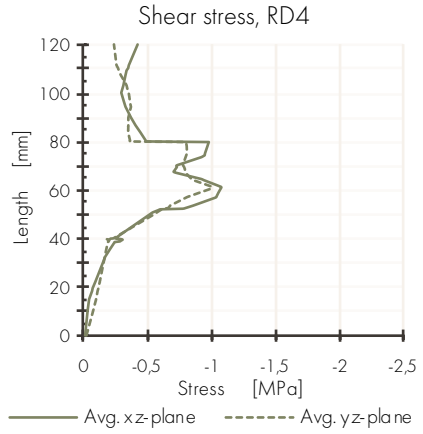

Figure 54. *Average shear stress for RD4.*

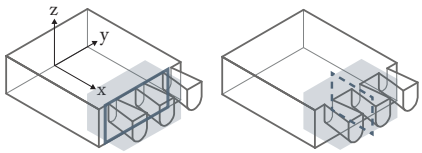

Figure 55. *Paths to consider shear stress for RD5.*

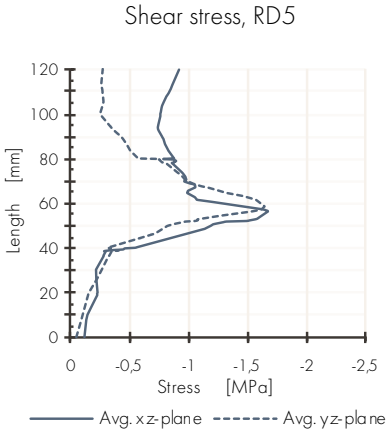

Figure 56. *Average shear stress for RD5.*